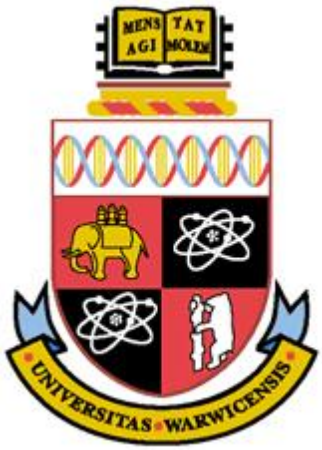

Fabrication and Characterisation of 3 Dimensional Scaffold for Tissue Engineering Application via Microstereolithography Technique

Marina Talib

A thesis submitted to in partial fulfillment of the requirements for the degree of Doctor of Philosophy in Engineering

School of Engineering

University of Warwick

2012

Fabrication and Characterisation of 3 Dimensional Scaffold for Tissue Engineering Application via Microstereolithography Technique

Marina Talib

Doctor of Philosophy

2012

TABLE OF CONTENTS

List of Figures

List of Tables

List of Equation

Summary

Microstereolithography is a method used for rapid prototyping of polymeric and ceramic components. This technique converts a computer-aided design (CAD) to a three dimensional (3D) model, and enables layer-per-layer fabrication curing a liquid resin with UV-light or laser source. However, the use of stereolithography in tissue engineering has not been significantly explored possibly due to the lack of commercially available implantable or biocompatible materials from the SL industry. This thesis seeks to develop a range of new bio-compatible/degradable materials that are compatible with a commercial 3D direct manufacture system (envisionTEC Desktop). Firstly, development and modification of microstereolithography equipments were undertaken in order to allow some understanding on the techniques and the process involved in microstereolithography technique. Secondly, a selection of multifunctional polymer and calcium phosphate were studied in order to formulate biodegradable photopolymer resin for specific tissue engineering applications. A 3D structure was successfully fabricated from the formulated photocurable resins. They were then sintered at high temperature for polymer removal, to obtain a ceramic of the desired porosity. Mechanical properties, morphology and calcium phosphate content of the sintered polymers were characterised and investigated with SEM and XRD, respectively. The addition of calcium phosphate coupled with high temperature sintering, had a significant effect on the mechanical properties exhibited by the bioceramic. The successful fabrication of novel bioceramic polymer composite with MSL technique offers the possibility of designing complex tissue scaffolds with optimum mechanical properties for specific tissue engineering applications.

Acknowledgement

Firstly, I like to thank Allah (S.W.T) for making all this possible and the Department of Public Service, Malaysia for their financial support during the four years of study. I would like to thank my academic supervisor Dr James A. Covington for his support and guidance throughout my PhD. I would also like to thank Dr Andrew Dove, Dr Liam Grover and Dr Alan Smith for their expertise and assistance in samples preparation, hands-on experiences with various laboratory equipments and techniques. I would also like to thank staff members: Mr F. T. Courtney, for his assistance in all mechanical matters. My sincere gratitude extends to my fellow PhD students, Dr. Fauzan Khairi Che Harun, Dr. P.H. King, S. Pattak, C. Pursell, and Dr S. Leigh who have provided me with both technical and moral support throughout my PhD. My sincere gratitude extends to my husband, Mohd Khairy Othman and two daughters; Dayana and Hannah, for the love and constant support during my studies.Last but not least, I would like to acknowledge everyone who has help me in one way or the another, without which this would not have been possible.

Declaration

The work described in this thesis is entirely original and my own, except where otherwise indicated. Parts of this work have been presented at international conferences and published in the scientific literature listed below:

Conference papers/posters

1. M. Talib., J.A. Covington., A. Dove., A. Bolarinwa and L. Grover. "Fabrication and Characterization of Three Dimensional Scaffolds of Bioceramic-Polymer Composite via Microstereolithography Technique". Presented on 8-11th October 2009 in Hannover, Germany.
2. M. Talib., J.A. Covington., A. Dove., A. Bolarinwa and L. Grover. "Fabrication and Characterization of Three Dimensional Scaffolds of Bioceramic-Polymer Composite via Microstereolithography Technique". Tissue Engineering Part A. August 2010, 16(8): A-1-A-2916 Issue 8: August 5, 2010. (Abstract in aJournal).
3. M. Talib., J.A. Covington., A. Dove., A. Bolarinwa and L. Grover. "Fabrication and Characterization of Three Dimensional Scaffolds of Bioceramic-Polymer Composite via Microstereolithography Technique". Presented 31st September – 5th October 2011 at Gordon Research Conference on Biomaterials and Tissue Engineering, Holderness School in Holderness, New Hampshire, USA.

Selected Abbreviations and Acronyms

Term	Definition
ACP	Amorphous calcium phosphate
CAD	Computer Aided Design
CPP	Calcium pyrophosphate
DCP	Dicalcium phosphate
DEF	Diethyl fumarate
DEDGA	Diethylene glycol diacrylate
DMD	Digital Micromirror Device
DPA	Dipentaerrythritol penta/hexa acrylate
DTA	Differential thermal analysis
FDM	Fused Deposition Modelling
GlcAc	Glucopyranoside
HAP	Hydroxyapatite
HDDA	1,6-Hexanediodiacrylate
HDeDA	1,6-Hexanediol ethoxylate diacrylate
LCD	Liquid crystal display
LED	Light emitting diode
LOM	Laminated Object Manufacturing
MSL	Microstereolithography
PCL	Polycaprolactone
PDLLA	poly(D,L-lactide)
PEG	polyethylene glycol
PEGDA	polyethylene glycol diacrylate
PHA	Polyhydroacids
PLA	polylactides acid
PPF	poly(propylene fumarate)
PVA	poly(vinyl alcohol)
RP	Rapid prototyping
SEM	Scanning electron microscopy
SGC	Solid Ground Curing
SLS	Selective laser sintering
SOUP	Solid Object Ultraviolet Laser Printer
TCP	Tricalcium phosphate
TEGDA	Trietyleneglycol diacrylate
TGA	Thermogravimetrical analysis
TMPTA	Trimethylolpropane triacrylate
XRD	X-ray diffraction
a -TCP	a-Tricalcium phosphate
ß-TCP	ß-tricalcium phosphate

CHAPTER 1

1.1 Introduction

The human body is supported by the muscoskeletal system. This system provides form, stability and movement to the human body. It consists of the skeleton (bones), muscles, tendons, ligaments, joints, cartilage and other connective tissues (Figure 1.1).

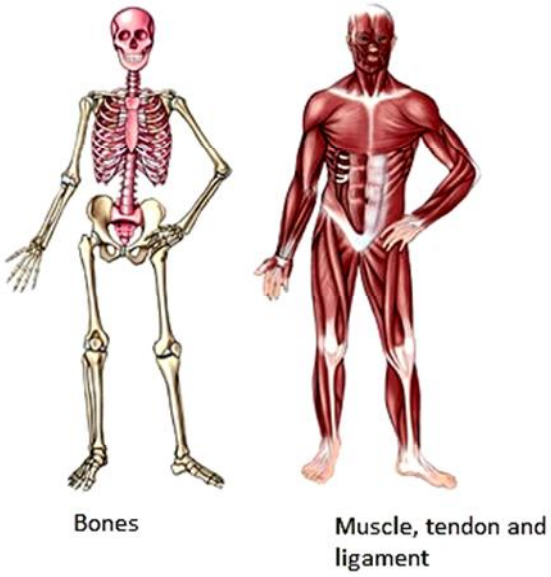

Figure 1.1Muscoskeletal system of a human body (www.oursewareobjects.elsevier.com)

Globally, hundred millions of individuals are affected by musculoskeletal conditions, which make up 2% of the global disease burden and are expected to double by 2020 due to ageing. The primary musculoskeletal dysfunctions include:

i) Osteoarthritis;

ii) Inflammatory arthritis (principally, rheumatoid arthritis);

iii) Back pain;

iv) Musculoskeletal injuries (such as sports injuries);

v) Crystal arthritis (such as gout); and

vi) Metabolic bone disease (principally osteoporosis).

The United Nations (UN) and the World Health Organization (WHO) have emphasized that:

(i) Half of the people aged over 65, affected by chronic conditions, suffer of joint diseases;

(ii) Back pain is the second cause of sick leave;

(iii) The number of osteoporotic fractures has doubled in the last 10 years;

(iv) Severe injuries caused by war and traffic accidents, while increasing the demand of restorative procedures worldwide, are expected to cost 25% of health expenses in developing countries by 2010;

(v) Crippling diseases and deformities still distress the normal development of affected children. The worldwide incidence of bone disorders and conditions are increasing in those societies where population ageing is combined with increased obesity and poor physical activity [1].

Table 1.1: The estimated burden of musculoskeletal condition, by gender and region in 2001 calculated by WHO 2004 [2].

	Number of *DALY (thousand)				
	Total	Males	Females	Developed	Industrial
Osteoarthritis	16,372	6,621	9,750	11,049	5,323
Rheumatoid	4,752	1,353	3,404	3,238	1,520
Other	8,699	5,033	3,638	6,784	1,880
Total	29, 798	13,007	16,792	21,076	8,723

*DALY (disability-adjusted life year) is a composite measure that combines the number of years lived with a disability and the number of years lost to premature death.

This data clearly shows that osteoarthritis has the largest health burden associated with it. Osteoarthritis is a disorder that affects individual joints such as the knee or hip, groups of joints such as the hand or the spine in the neck and back, or combinations of the above. When a joint develops osteoarthritis, some of the cartilage covering the ends of the bones gradually roughens and becomes thin, the joint doesn't move as smoothly and causing pain, stiffness, weakness, joint instability, and reduced range of motion [3].

Osteoarthritis accounts for the largest portion, 52% of the total burden of musculoskeletal conditions in developing countries, and 61% of the total burden of musculoskeletal conditions in industrialized countries. Osteoarthritis is increasing as the world's elderly population grows, and is the sixth leading cause of years lost to disability. In United Kingdom, more than 1 in 50 men aged over 45 years visit their GP at least once each year, and around 1 in 10 in elderly women. The influence of age is shown below [4].

Table 1.2: Group of age consulting GP with osteoarthritis [4].

Group (age)	Percentage consulting	UK estimate
Males:		
45 - 64	2%	146,300
65 - 74	6%	136,600
75+	7%	132,000
Females:		
45 - 64	3%	245,300
65 - 74	9%	225,00
75+	10%	290,100
414,900 males and 760,400 females with OA		

Rheumatoid arthritis is an autoimmune disease that causes chronic inflammation of the tissue around the joint; it affects the limbs more than the spine. The disorder may result in tiredness, fatigue, weight loss, fever, pain, and disability

and deformity of the joints. Rheumatoid arthritis has a prevalence of between 1 and 3 % in most countries.

Back pain is extremely common between the ages of 35 and 55, perhaps due to the nature of occupational hazards in both industrialized and developing countries. It is estimated that half of workers will experience back pain at some point in their lifetime, suffering at least one episode each year. Back pain is an important cause of absence from work, resulting in economic losses. Manual workers are, more likely to have back problems than white-collar workers since their work is more likely to involve occupational risk factors, such as poor lifting behaviours.

Table 1.3: Demography age profile of back pain in United Kingdom [4].

Age group (years)	**Back pain**
25 - 34	12%
35 - 44	17%
45 - 54	18%
55 - 64	19%
65 - 74	15%
≥75	15%
Total population	16%

Osteoporosis is caused by low bone mass and deterioration in the bone structure, which leads to fracture after mild or moderate trauma. The most common fractures occur in the arms, vertebrae, and hips. Fracture risk increases with age and has an important impact on quality of life, mortality, and health care costs in most countries [2].

Nearly three in ten of all those aged over 75 are in chronic pain due to arthritis. Based on annual prevalence report on 2006, chronic pain affects at least 10% of population (population study of 5000 people) across all age of groups as

shown in Table 1.3 [4]. This shows the level of muscoskeletal problem in the adult UK population is alarming.

Arthritis Research UK, a non-government organisation has provided an overview of how musculoskeletal condition affects sufferers and the government in the UK. The overviews are as follow:

- Latest results from Labour Force Survey (LFS) for 2009/2010 indicated that approximately half a million people in the UK suffered from a musculoskeletal condition caused or exacerbated by their current or past. Of these, an estimated 248,000 suffered from a disorder mainly affecting their back, 230,000 from a disorder mainly affecting their upper limbs or neck, and 94,000 mainly affecting their lower limbs [5].

- A study conducted by Lanyor et. has found that more than 650,000 in the UK have painful osteoarthritis in one or both hips, three-quarters of whom are aged over 65 [6].

- There are almost 8.5 million people with X-ray evidence of osteoarthritis of the spine in the UK. Unlike other sites, it is more commonly found in men than women (by a ratio of 3:2)[7].

- A total of 58,952 primary hip replacements were carried out in England and Wales in 2006/7. Of these, 94 per cent were due to osteoarthritis and 60 per cent of these operations were carried out on women [8].

- A total of 62,150 primary knee replacements were performed in England and Wales in 2006/7. Ninety-seven per cent were due to osteoarthritis and 57 per cent were performed on women [9].

- There are around 400,000 adults in the UK with rheumatoid arthritis. Prevalence is more common in women than men by a factor of 3:1[10].

- The cost to the UK of musculoskeletal conditions is £5.7 billion annually [10]. The estimated cost of these operations total £890 million per year (around £430 million for hip replacements and £460 million for knee replacement) [11].

- Arthritis and back problems are the most common condition for which people receive Disability Living Allowance (DLA).Total number of people receiving DLA as a result of arthritis and other musculoskeletal conditions is more than twice that due to heart and chest disease and stroke combined [8, 12].

1.2 Tissue Engineering

For centuries, the loss or failure of a vital organ or tissue is one of the most devastating and challenging problems for physician. Transplantation of tissues and organs from one individual into another is the most fascinating and revolutionary achievement in the medical field of modern era. It is life saving; thus improving the health and life quality for millions of people. Transplantation could be divided into groups; amongst the same species or different species. Figure 1.2 shows the different types of transplantation.

Autograft

Tissue transplanted from one part the body to another in the same individual.

Example: skin graft, vein extraction

Allograft

Tissue/organ transplanted two genetically non-identical members of the same species.

Example: liver transplant, heart transplant

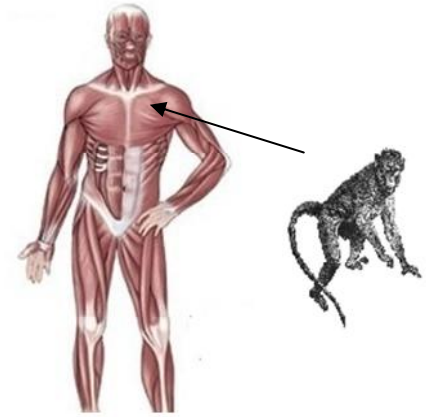

Xenograft

Tissue/organ transplant from one species to an unlike species (or genus or family).

Example: Porcine heart valve transplants, skin graft from baboon

Figure 1.2 Schematic illustrations on types of transplantation

Even though successful transplantations have changed and saved lots of lives, new problems emerge. Autografts, a tissue transplant from one part of the same individual to another part, do not invoke any immune reaction but a few case studies have shown that introducing new tissues on its new location could produce biological changes because of the abnormal interaction between the tissue. Diverting urine into the colon can produce fatal colon cancers 20-30 years later while making oesophageal tubes from the skin can result in skin tumours 30 years later [13].

Allografts, on the other hand, create problems with patients' immune system as it attacks the new transplanted tissue/organ due to genetically dissimilarities to the host, and could result to chronic rejection and destruction over time. All allograft patients need to take immunosuppressant drugs for the rest of their lives and an imbalance of immune surveillance from immunosuppressant can cause new tumour. These constraints demand new solutions that will be able to provide the needed tissues [13, 14].

Globally, millions of patients undergo surgeries of organ/tissue transplant and reconstruction. In the United Kingdom alone, as of 31 March 2010, 10 542 patients were registered for an organ transplant as shown on Figure 1.3 [10, 15].

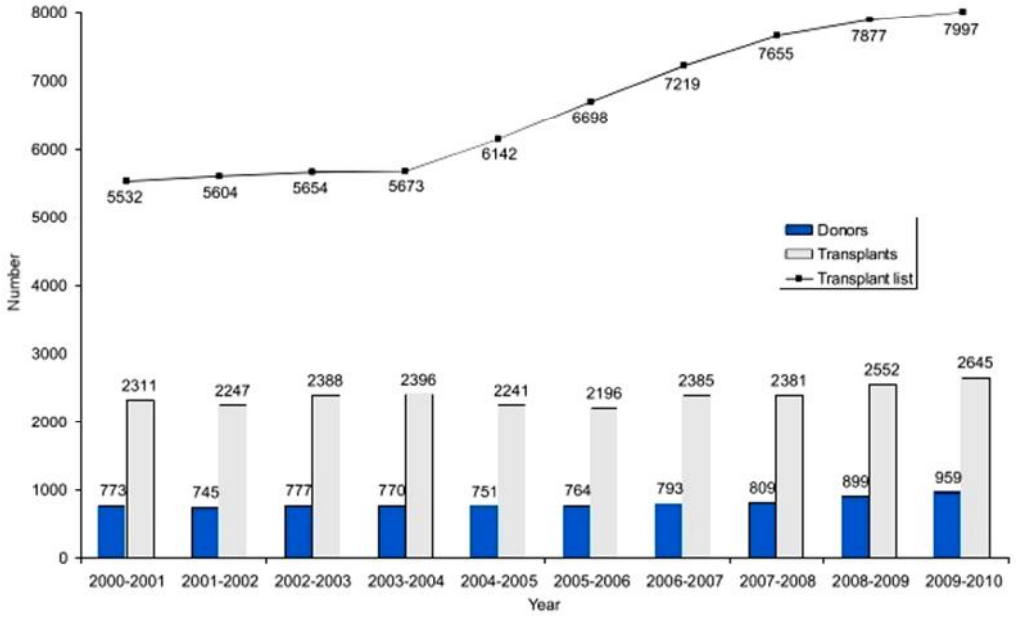

Figure 1.3 Number of deceased donors and transplants in the UK, 1 April 2000 – 31 March 2010, and patients on the active transplant list at 31 March [10, 15].

More than 10 000 people in the UK currently need a transplant. Of these, 1 000 each year – that's three a day - will die waiting as there are not enough organs available. Figure 1.3 shows that the demand of organ/tissue transplantation is more than the supply and the trend that persists. The shortages of replacement tissues or organ transplantations, coupled with the problems of transplantation have resulted in a significant drive, and need for a new revolutionary approach such as the field of tissue engineering.

Tissue engineering is a new multidisciplinary field including biochemistry, cell and molecular biology, genetics, biomedical engineering and materials science. Tissue engineering uses synthetic or naturally derived engineered biomaterials to replace damaged or defective tissues such as bone, skin and even organs. William (2006) has refined the definition of tissue engineering as “the creation (or formation) of new tissue for the therapeutic reconstruction of the human body, by the deliberate

and controlled stimulation of selected target cells through a systematic combination of molecular and mechanical signals" [16].

The fundamental aim of the field is to harvest and seed the donor cell/tissue on scaffolds (artificial extracellular matrix), induce tissue or organs to restore and regenerate themselves [17]. Figure 1.4 shows the diagram explaining the basic principle of tissue engineering.

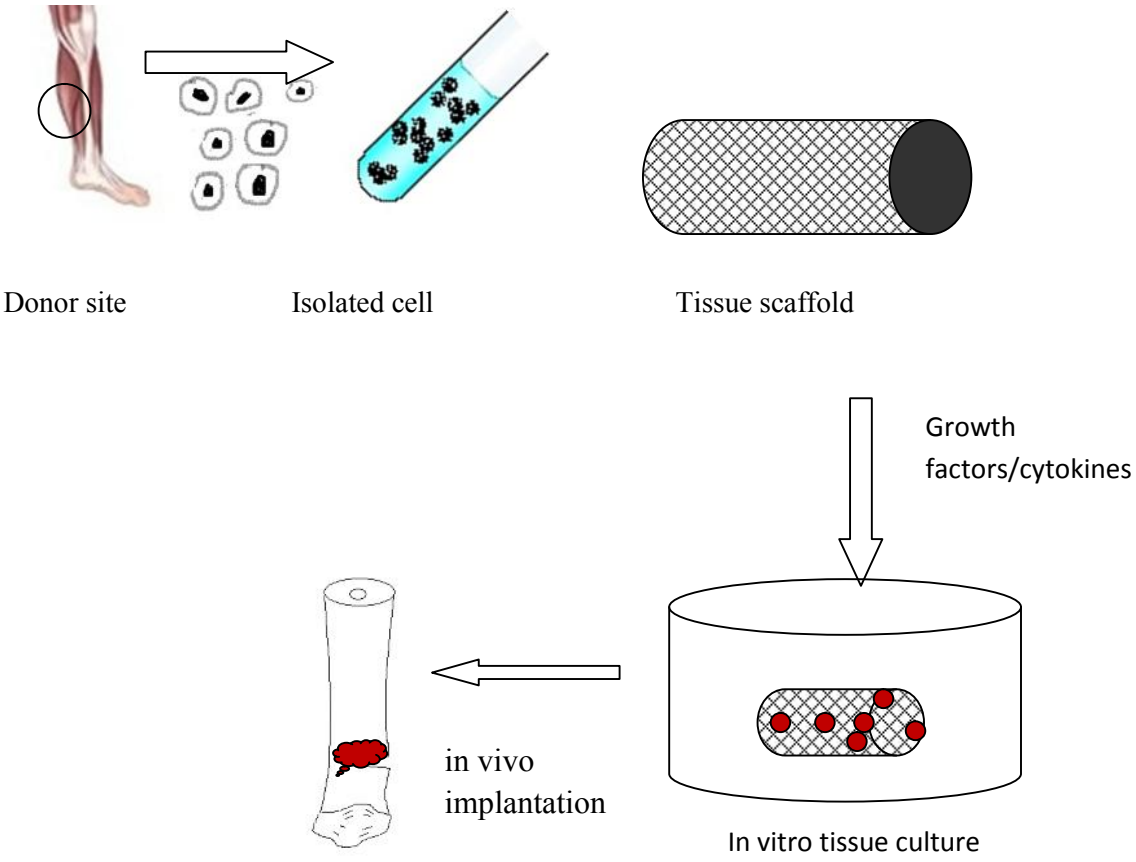

Figure 1.4 Basic principle of tissue engineering

Bone substitutes are often required to help repair or replace damaged or diseased tissues in cases ranging from trauma to congenital and degenerative diseases, to cancer and to cosmetics. Biomaterials as implants or in medical devices in contact with the body, have improved the quality of life of many people that have lost a body

part or its function. Nowadays, restorative therapies of bone and joint conditions are commonly treated with autologous and allogeneic transplantations by using autografts and allografts respectively [18]. However, in treatments using allograft bone, the recovery rate is lower and the infection rate is higher than with autograft bone. What more, allograft bone is in limited supply.

1.3 Tissue Scaffolds

Scaffolds are three dimensional supports that are used as a template at the site injury in guiding cell or tissue growth, in order to regenerate and secrete their own extracellular matrix and thus assisting the body in growing new, functional tissues. Scaffolds work in two way, they either helps direct cell growth or simply provide a shape for the final tissue.

A material that can be used as a scaffold in tissue engineering must satisfy a number of requirements. Important properties in this regard include biocompatibility and biodegradation; it should not elicit severe inflammatory responses, and it should degrade into non-toxic compounds within the time frame required as newly formed tissue is formed. The scaffolds should have suitable porosity for cell in-growth, a surface that balances hydrophilicity and hydrophobicity for cellular attachment, and mechanical properties that are compatible with those of the tissue as well as maintain mechanical strength during most parts of the tissue regeneration process. They can be formulated to contain additives or active agents for more rapid tissue growth or compatibility. For example, a bone implant may contain a form of calcium phosphate or a growth factor such as one of the bone morphogenetic proteins [19].

Both natural and synthetics polymers have been extensively researched for the development of tissue engineering. Chitosan; alginate [20, 21]; collagen [22];

agarose, fibrin and hyaluronic are some examples of naturally-derived polymers [23]. In the recent years, chitosan has been successfully used in oral and nasal deliveries due to their mucoadhesive properties. Collagen has been broadly utilised as gene activated matrices, capable of delivering large quantities of DNA in a direct and localized manner [24]. Although the preliminary results are promising, concern about the feasibility of finding large amounts of materials needed for clinical applications has prompted other researchers to investigate the use of synthetic materials.

Bioceramic scaffolds based on calcium phosphate, are also among the favoured synthetic materials for bone replacement due to the similar chemical compositions to the mineral phase of bone and high mechanical strength [25], [26], [27], [28]. The calcium phosphate family has almost ten members but most materials are composed of either low solubility hydroxyapatite (HA, $Ca_{10}(PO_4)_6(OH)_2$) [29], [29], [30], [31], [32], [33], slowly degradable β-tricalcium phosphate (β-TCP, $Ca_3(PO_4)_2$) [29], [30], or degradable dicalcium phosphate dihydrate (DCPD, brushite, $CaHPO_42H_2O$) [31], [32]. These materials are currently used as a stand- alone materials for bone defect fillers because they do not elicit a foreign body reaction and are compatible with the host tissues. They are claimed to be osteoconductive, where bone ingrowths could occur when placed adjacent to normal host bone, and osteoinductive, meaning they could actively induce the bone formation. However, the amount of induced bone is very limited [29], [30], [31], [32], [33].

Currently, lots of work has been done to make calcium phosphate ceramic more osteoconductive by adding growth factors and/or osteoprogenitor cell to the scaffolds [38], [39]. Although significant research has already been done in these fields, scientists have yet to produce an ideal tissue scaffolds that can mimic the human bone entirely.

The biggest problem faced by scientists is cell attachment to the surface and in growth into scaffold as they are only able to grow a short distance into the scaffold because report stated they cannot migrate more than 500μm from the surface [40]. The depth also contributes to the lack of oxygen and nutrient supply to the more in-depth cells. Botchwey et. al has speculated that high cell density on the exterior of the scaffold may deplete nutrient supply before these nutrients can diffuse to the scaffold interior to support tissue growth [41]. The success and ideal design of the tissue scaffolds is hindered by a few problems listed below; as per reviewed by Chung et. al [42]:

1. Inability to create vascularised tissue constructs
2. Inability to precisely control the spatial and temporal features of the cellular microenvironment.
3. The lack of materials with desired functional properties
4. The lack of suitable source of functional cells that is immunologically compatible with the host.
5. The requirement for large sample volumes, low throughput and slow reaction time.

1.4 Fabrication Technique

The fabrication of scaffolds for better tissue regeneration has attracted a great deal of attention. The fabrication of three-dimensional (3D) scaffolds that mimic the *in vivo* cellular microenvironment is of fundamental importance to the success of tissue engineered constructs. Both scaffold chemistry and architecture can influence the fate and function of engrafted cells [41], [43], [44], [45], [46].

Most scaffolds in tissue engineering have been fabricated by the traditional fabrication methods such as gas foaming/salt leaching [39], [40], and freeze drying [41], [42]. However, these methods do not control the inner/outer architecture, pores, porosity, and interconnectivity. Rapid prototyping technology has been utilised extensively because it has the highest fabrication accuracy and with increased number of material availability, some of the drawback of conventional methods could be overcome.

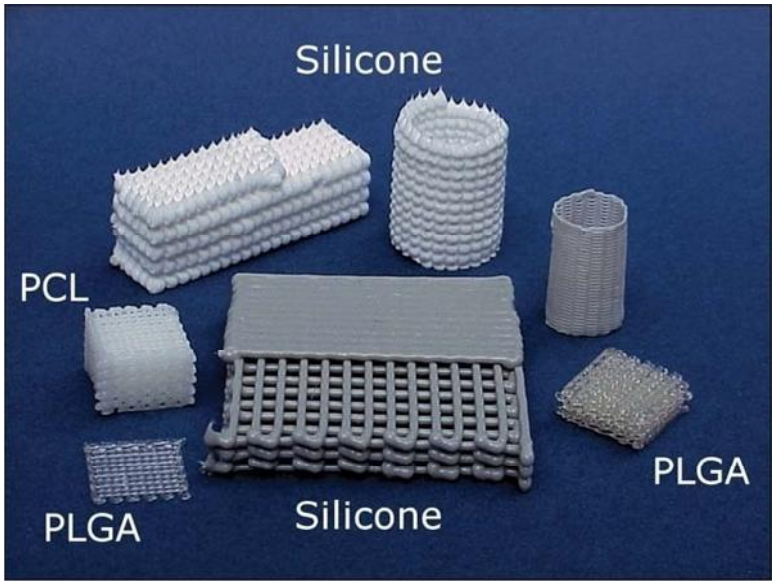

Figure 1.5 Biocompatible scaffold structures built on an Envisiontec 3D-Bioplotter (http://www.deskeng.com/articles/aaawxe.htm, published 1 May 2010).

Rapid manufacture is a group of technologies that build a three dimensional (3D) object in layer-by-layer principle. The system is incorporated of computer-aided design, (CAD) to design a two-dimensional image and transfer to equipment with different types of technology [51], [52]. There are many ways to classify a rapid prototyping (RP) technique, one of the ways is categorised based on the prior form of its materials which are; (1) liquid based, (2) solid based and (3) powder based.

1.4.1 Liquid-based

The starter material for this technique is in liquid form. The liquid is then converted to solid form through a process known as photo curing [53], [54], [55], [56]. The RP system within this category include amongst others:

i) StereolithographyApparatus (SLA)

ii) Solid Ground Curing (SGC)

iii) Solid Object Ultraviolet Laser Printer (SOUP)

iv) Microfabrication,

1.4.2 Solid-based

Solid-based RP systems are meant to encompass all form of materials in the solid state. The solid form can include the shape in the form of a wire, a roll, laminates and pellets [50, 51]. Some of the RP systems that fall in this category are:

i) Laminated Object Manufacturing (LOM)

ii) Paper Lamination Technology (PLT)

iii) Fused Deposition Modelling (FDM)

iv) Slicing Solid Manufacturing (SSM)

RP system i) and ii) use cutting and gluing/joining method whereas system iii) and iv) applied the melting and solidifying/fused method.

1.4.3 Powder-based

Even though powder by itself is in solid state, however, in the RP system it is specially categorised as powder in grain-like form which use the joining/binding method [25], [39], [59], [60], [61]. Below is some of the example of RP system that categorised in this definition:

i) Selective Laser Sintering (SLS)

ii) Three Dimension Printing (3DP)

iii) Electron Beam Melting (EBM)

iv) Direct Metal Deposition (DMD)

In this project, microstereolithography (MSL) has been selected as a means for the 3-dimensional fabrication of a tissue scaffold. It is the most versatile method with the highest accuracy and precision to control the matrix architecture such as size, shape, interconnectivity, branching, geometry and orientation which will yield biomimetic structures varying in design and material composition.

1.5 Challenges and Opportunities

Currently, biopolymers in use are based on polyesters such as polycaprolactone (PCL) or polyhydroacids (PHA), copolymer of lactic and glycolic acid. These materials are not suitable for the fabrication of scaffold by direct or indirect methods using stereolithography because they can only be processed by melt or solution techniques. Generally, only a few monomers, especially acrylic and epoxy-based ones, have the appropriate photoabsorption characteristic to allow affective stereolithography photopolymerization to take place. These polymers were never optimised for medical application *in vivo*.

The use of stereolithography in TE has not been significantly explored, perhaps because of the lack of commercially available implantable or biocompatible materials from the SL industry. On the other hand, polyethylene glycol (PEG) with an acrylate group is a suitable choice for this kind of rapid prototyping technique. PEG has characteristic properties such as high hydrophilicity, good tissue biocompatibility, lack of toxicity and availability of reactive sites for chemical modification whereas acrylate monomers are known for their high reactivity, which polymerise rapidly in the present of photogenerated free radicals.

1.6 Research Aim and Objective

Microstereolithography is chosen as a means for the 3D fabrication as it offers unique ways to precisely control matrix architecture such as size, shape, interconnectivity, branching, geometry and orientation which will yield biomimetic structures varying in design and material composition. The use of stereolithography in tissue engineering

has not been significantly explored, perhaps because of the limitation of commercially available implantable or biocompatible materials from the stereolithography industry.

The purpose of this project is to develop a range of new bio-compatible/degradable materials that are compatible with commercial 3D direct manufacture techniques. There are three stages of development in this project:

1. To develop a stereolithography system for the optimal formulation of biodegradable photopolymer resin to fabricate 3D scaffolds with controlled microstructures specifically for soft tissue engineering applications such as hydrogel.

2. To develop a stereolithography system for the optimal formulation of polymer ceramic resin to fabricate 3D scaffolds with controlled microstructures specifically for hard tissue engineering applications such as bone.

3. Based on the optimal formulation of photopolymer resin in (1) and (2), the fabrication of the 3D scaffold is to be fabricated on the commercial microstereolithography (MSL) apparatus available in the School of Engineering.

It is hoped that we can develop formulations of photopolymer resin that are feasible and versatile for the specific application such as bones implants and, drug delivery system. The scaffold fabricated from the new formulation should support biological cell growth and have a spectrum of mechanical properties. In addition, the findings of this study could broaden the selection of photopolymer resins which is currently limited commercially.

1.7 Thesis Outline

Chapter 1 reviews the research background of the project, such as the materials development, technology available, comparing their differences and similarities. It also discusses the aims and objectives of the thesis are then presented.

Chapter 2 and 3 describes the recent development in biodegradable polymer, ceramic composites, the properties and technology applied during fabrication.

Chapter 4 details the development of the stereolithography system and establishes parameter by using commercially supply photopolymer resin as controlled sample.

Chapter 5 and 6 reports the analysis and characterisation results for the biodegradable polymer and polymer ceramic respectively.

Chapter 7 is a preliminary study on the exploration of fabricating ceramic tissue scaffold via 3D printing. This is to diversify the usage of biomaterials developed during this study.

Chapter 8 concludes the research and the latest developments are presented to highlight possible future enhancements.

CHAPTER 2

Biodegradable Polymer in Tissue Scaffolds

2.1 Introduction

In the recent years, tissue engineering has emerged as an exciting and remarkable field of research. It is a cross-disciplinary field of biochemistry, cell and molecular biology, genetics, biomedical engineering and materials science. Tissue engineering uses synthetic or naturally derived engineered biomaterials to replace damaged or defective tissues such as bones, skin, and even organs. In tissue engineering, scaffolding material is the main highlight of the field. The development of scaffold materials with biodegradable abilities attracts the most attention because they can be absorbed by the surrounding tissue without surgical removal.

2.2 Biodegradable Polymers

Biodegradable polymers may be made from natural polymers such as corn, wood and cellulose. They can also be synthesized by bacteria, or small molecules like butyric acid or valeric acid that provide polyhydroxybutyrate (PHB) and polyhydroxyvalerate (PHV), as examples. With the development of synthesis studies, biodegradable polymers could also be derived from petroleum sources or may be obtained from mixed sources of bio- mass and petroleum [62], [63]. The best known petroleum sourced biodegradable polymers are aliphatic polyesters or aliphatic-aromatic copolyesters. Nevertheless, biodegradable polymers that are made from renewable sources such as polylactides acid (PLA) are demanding the most attention. This is due to its environmentally friendly origin, in contrast to the fully petroleum-based

biodegradable polymers [64]. Traditional scaffolds based on biodegradable polymers such as poly(lactic acid) and poly(lactic acid- co-glycolic acid) are weak and non-osteoconductive [65].

The polymer matrix may represent the device itself, or can be a scaffold for cell growth *in vitro* that is degraded by the growing cells prior to implantation [66]. The device can also be formulated to contain additives or active agents to increase tissue growth or to improve compatibility. For example, a bone implant may contain a form of calcium phosphate or a growth factor such as one of the bone morphogenetic protein. Specific conditions in terms of pH, humidity, oxygenation and the presence of some metals are required to ensure the biodegradation of such polymers [64].

When the damaged or lost tissue has been successfully replaced by new tissue, the scaffold will have been completely reabsorbed or become soluble or metabolised with the by-product eliminated in the body's metabolic pathways. Consequently, this eliminates any adverse effect to the human cell tissue or organ associated with the long-term presence of the foreign material and the need for a second surgery for implant removal.

2.2.1 Natural biodegradable polymer

There are two major classes of natural polymers; polypeptides and polysaccharides. Natural polymers are typically biocompatible and enzymatically biodegradable. Chitosan, alginate, collagen, agarose, fibrin and hyaluronic are some examples of naturally-derived polymers [20], [67-72] as shown in Table 2.1. In the recent years, chitosan has been successfully used in oral and nasal delivery due to their mucoadhesive properties [73-75]. Collagen has been broadly utilised as gene activated matrices, capable of delivering large quantities of DNA in a direct, localized

manner [24]. Although the preliminary results are promising, concern about the feasibility of finding the large amounts of materials needed for clinical applications has prompted other researchers to investigate the use of synthetic materials.

The main advantage for using natural polymers is that they contain bio-functional molecules that aid the attachment, proliferation, and differentiation of cells [23]. Although biodegradable polymers have great potential as scaffolds, some of the enzymatic degradation may inhibit function, and as a result, the rate of this degradation may not be easily controlled. Therefore it may be difficult to determine the lifespan of natural polymers *in vivo* [23]. Natural polymers are often weak in terms of mechanical strength due to their brittleness. In addition, low heat distortion, high gas permeability and low melt viscosity has made the material processing difficult. Fisher & Bousmina has introduced cross-linking to these polymers, which has shown to enhance their structural stability [64].

Table 2.1.Example of biodegradable polymer extensively studied for tissue engineering application [23].

Natural polymer	Synthetic polymer
Agarose	Poly(glycolic acid)
Alginate	Poly(l-lactic acid)
Hyaluronic acid	Poly(d,l-lactic acid-co-glycolic acid)
Chitosan	Poly(caprolactone)
Collagen	Polyorthoester
Gelatin	Polyanhydride
Silk	Polyphosphazene
	Polycarbonate (tyrosine derived)
	Poly(ethylene glycol)/ Polyethylene oxide
	Polyurethane

2.2.2 Synthetic biodegradable polymer

Biodegradable synthetic polymers offer a number of advantages over other materials for developing scaffolds in tissue engineering. The key advantages include the ability to tailor mechanical properties and degradation kinetics. The most common synthetic polymers are polyesters. Other types include polyanhydride, polycarbonates, and polyphos-phazenes.

Biodegradable synthetic polymers such as poly(glycolic acid), poly(lactic acid) and their copolymers, poly(p-dioxanone), and copolymers of trimethylene carbonate and glycolide have been widely used in a number of clinical applications due to their degradability and US Food and Drug Administration (FDA) approval [44], [55], [76-83]. Polyglycolide is widely used for degradable sutures, drug delivery systems and orthopaedic fixation devices such as pins, rods and screws. Since early 1990s, poly(α-hydroxyl acid) polymers such as polylactide, polyglycolide and their copolymers (poly(D,L-lactide-co-glycolide) have been investigated as scaffolds for cartilage tissue engineering [74], [84]. Implants have been fabricated from both polyglycolides and polylactides. Both the polymers are polyesters and possess an ester group in the polymer backbone that can be hydrolysed causing chain scission (Figure 2.1).

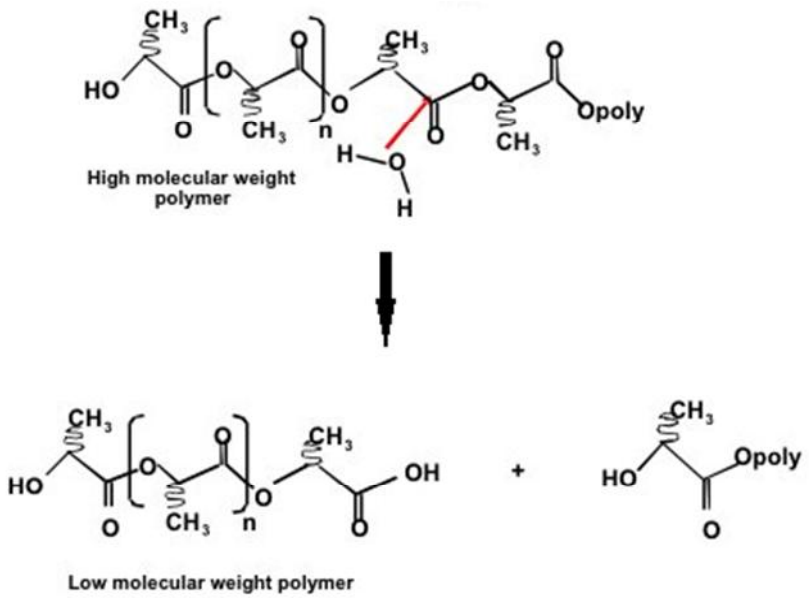

Figure 2.1 Hydrolysis and cleavage of the ester linkage
(http://www.uweb.engr.washington.edu/research/tutorials/plagla.html)

The degradation products of these two polymers are glycolic acid and lactic acid respectively, both of which occur naturally in the body. At high concentrations of these degradation products, local acidity may increase, resulting in adverse responses such as inflammation or fibrous encapsulation which the major drawback in the degradable polymers [85], [86] .

2.3 Mechanism of Degradation

Biodegradable polymers are designed to degrade by two principal ways: (1) passively by hydrolysis, which is the reaction with water to produce –OH bonds, and (2) actively by enzymatic oxidation. After implantation, the biomaterial absorbs water and swells, and degradation will progress from the exterior of the material towards its interior. The attack of water to the biomaterials initiate the hydrolytic scission of polymer backbone to form oligomers and finally monomers. During the hydrolysis, inflammatory cells, particularly leukocytes and macrophages, produce highly reactive

oxygen species such as superoxide (O_2^-), hydrogen peroxide (H_2 O_2), hypochlorous acid (HOCl), nitric oxide (NO) [85], [87], [88], [89]. The oxidative effect of these species may cause polymer chain scission and contribute to their degradation. Acids, bases, salts, or enzymes play a major role in hydrolytic process. As time increases, the molecular weight of degradation products is reduced by further hydrolysis, which allows them to diffuse from the bulk material to the surface and then to the solution, causing significant weight loss [85].

Polymers can be degraded by bulk degradation or surface erosion mechanisms as shown in Figure 2.2. Bulk degradation is characterized by hydrolysis of chemical bonds in the polymer chain at the centre of the material, which typically results in an empty shell but maintains its size for a considerable portion of time. Degradation by surface erosion mechanism is characterized by loss of the material from the surface only, resulting in very predictable mass loss profiles [86], [90-94]. The materials get smaller but keep their original geometric shape. This feature may be beneficial for delivering molecules at a constant rate and maintaining the mechanical and structural integrity of the material with degradation. Poly (anhydrides) and poly(orthoesters) are examples of surface-eroding polymers. All biodegradable polymers contain hydrolysable bonds, such as glycosides, esters, orthoesters, anhydrides, carbonates, amides, urethanes, ureas, etc. Polymers with strong covalent bonds in the backbone (like C-C) and with no hydrolysable groups require longer times to degrade [95].

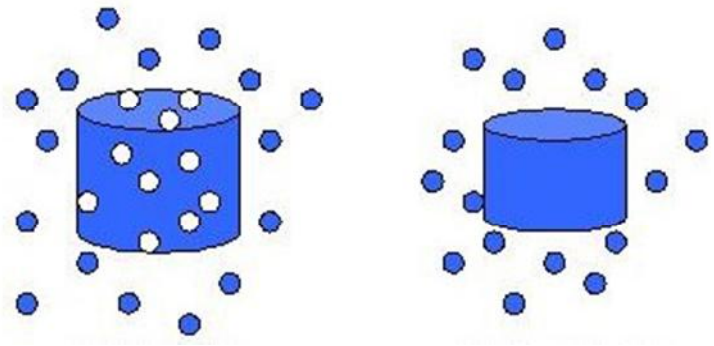

(a) Bulk erosion (b) surface erosion

Figure 2.2 Illustration of biopolymer degradation

There are several factors that influence the velocity of the degradation: type of chemical back bone, pH, copolymer composition and water intake. The most important factor is the water intake. The water absorption is often related to their solubility parameter, their glass transition temperature and their degree of crystalinity. Polyesters based on $(\text{-R-COO-})_n$ are often susceptible to hydrolysis. During hydrolysis of an ester, a carboxylic acid is produced which consequently reduces the pH level during hydrolysis. Esters are hydrolysed at a faster rate under acid and alkaline conditions than they are at neutral pH [96], [97]. If the local pH of the surrounding microenvironment is reduced below that of the natural physiological pH, an immunological response is thus elicited. This acidic effect can cause excessive inflammatory responses, while poor clearance and chronic inflammation associated with high molecular weight polymers may result in tissue necrosis. Autocatalytic degradation also causes rapid loss in mechanical strength [84].

While there are several ways to monitor the degradation rate of the biodegradable polymer, the most important criterion is the molecular weight. Other types of monitoring that could be used to measure are (1) the loss of mechanical

strength and (2) complete degradation into monomers or monomer releases. Attempts to find tissue-engineered solutions as replacement for tissues regeneration have made the development of new polymers that meet a number of demands is a formidable task for material scientists.

2.4 Requirement for Tissue Scaffolds

Scaffold is a three dimensional (3D) porous implant that acts as a temporary template for cell adhesion, proliferation and directs the formation of tissue or organ. A material that can be used as a scaffold in tissue engineering must satisfy a number of properties and requirements. These requirements are fundamental as they affect cell survival, signalling, growth, propagation and reorganization, and also play major roles in influencing cell shape modelling and gene expression that relate to cell growth and the preservation of native phenotypes [98].

2.4.1 Biocompatibility

A tissue scaffold should be biocompatible as it should not initiate or promote any adverse tissue reaction or interrupt other physiological process [99]. These include the ability to support cell growth and proliferation, as well as the requirement of sufficient mechanical integrity and strength to withstand manipulations associated with implantation during tissue regeneration without compromising the scaffold architecture.

Hydroxyapatite (HAP) is well known to be highly biocompatible and widely used as tissue culture scaffolding in regenerative medicine. A study on biocompatibility of ultrathin films of HAP show that the proliferation and differentiation of cells cultured on the thin layer are 2 to 3 times faster than on

titanium, and they also show little risk of inflammatory reaction onsite [100], [101]. This shows that culture times on HAP membranes are shorter than with conventional culture scaffolds. Incompatibility will result in poor cell attachment and inadequate subsequent tissue generation. Therefore a scaffold should be built with surface that balances hydrophilicity and hydrophobicity for cellular attachment [102], [103], [104], [105] .

2.4.2 Biodegradability

The scaffold should be biodegradable and the rate of degradation should be adequate with the rate of new tissue formation for the controlled release of bioactive molecules. The rate of enzymatic degradation will depend both on the number of cleavage sites in the polymer and the amount of available enzymes in the scaffold environment [106], [107]. As a consequence, the by-product should to be non-toxic, non-stimulatory of inflammatory cells, and non-immunogenic, which would be detrimental to tissue regeneration. For example, poly(lactide) acid undergoes hydrolysis scission to produce lactic acid, then further incorporated in the tricarboxylic acid cycle, and then excreted by the lungs as carbon dioxide and water. Poly(glycolide) is degraded by hydrolysis and esterases to glycolic acid. Glycolic acid monomer is either excreted directly in the urine or enters the tricarboxylic acid cycle [108].

Needless to say, it is important to understand and control both the mechanism and the rate by which each material is degraded, and to select the perfect choice for biodegradable polymers with matching mechanical properties, as well as the degradation rate to the needs of the application.

2.4.3 Pore size

Another important requirement is the pore size. It must allow appropriate diffusion of nutrients and metabolites to and from the seeded cell and surrounding tissue. Pore size has contributed to the progression of osteogenesis due to vascularation. Based on the previous studies, many researchers have defined scaffold based on size; either micro for diameters less than 100μm or macro for diameters more than 100μm. The minimum requirement for pore size was considered to be approximately 100μm, due to cell size, migration requirement and transport [40]. If the pore size is too small, pore occlusion can occur in cells, preventing further cell penetration and bone formation [98], [102], [103], [105], [109]. For colonisation of macropores to occur, the minimum pore size in which bone will form is claimed to be approximately 100μm. Other researchers have created scaffolds with pore sizes of between 150-300μm and 500-170μm to promote bone formation [77], [110]. Scaffolds with pore sizes between 20 and 125 μm have been used for regenerating adult mammalian skin and 45–150 μm for regenerating liver tissues [98]. Small pores favour hypoxic conditions and induce osteochondral formation before osteogenesis occurs. In contrast, scaffold architectures with larger pores rapidly become well-vascularised and lead to direct osteogenesis [104], [111].

The tissue-type to be implanted on the scaffolds also influences the selection of pore size. For example scaffolds with pore sizes less than 150μm have been successfully used for regeneration of skin in burnt patients [50]. Past reports show that vascular density near the surface of an implanted synthetic membrane was shown to be highest when membrane pore sizes were between 0.8 and 8.0μm [112]. Whereas studies using porous chitosan scaffolds observed neovascularisation in scaffolds with pore size 90 μm [113].

Research conducted by Chang et.al and Li et. al has shown that osteoblast appears to exhibit greater cellular response when pore sizes of between 200 and 400μm are employed [35], [40]. This suggests that the curvature of the pore may provide optimum compression and tension on the cells' mechanoreceptors and allow them to migrate into the opening of such size [114].

2.4.4 Interconnectivity of the porous structure

Simultaneously, the incorporation of microporosity within the scaffold materials has added advantages with regard to pore size. Interconnectivity is a physical characteristic that aids in the delivery of the physiological nutrients, gases, and the removal of metabolic waste and by-products from cells that have penetrated the scaffold [13, 14]. It provides an open porous network structure allowing for easier vascularisation, which is important for the maintenance of penetrating cells from surrounding tissues and the development of new bone or tissues *in vivo*. The higher the macroporosity, the easier it is for vascularisation to occur. It also ensures the spatially uniform cell distribution, cell survival, proliferation and migration in vitro [115].

In-vitro, lower porosity stimulates osteogenesis by suppressing cell proliferation and forcing cell aggregation. On the other hand, *in vivo*, higher porosity pore size results in greater bone in-growth but previous reports show results in low mechanical properties [116]. Failure to develop an adequate vascular network will mean that only peripheral cells may survive or differentiate, supported by diffusion. The degree of interconnectivity may give a greater influence on osteoconduction instead of the actual size of pores [40].

High internal surface area to volume ratios is essential in order to accommodate the large number of cells required to replace or restore tissue or organ function(s). In addition to the cell attachment, migration and intracellular signalling are also dependent on the morphology and physiochemistry of the scaffold's surface [22], [23].

Taboas et al. successfully incorporated microporosity within a scaffold material (PLA) consisting of interconnected plate structures, yielding 5-11 μm void openings, through an emulsion solvent diffusion technique [117]. A scaffold with adequate microporosity enabled the precondition of bone morphogenetic protein (BMPs), anti-inflammatory drugs (Dexamethosone), and oxygen releasing agents (ORAs) such as perflurocarbons on the scaffold [48].

Porosity requirements exceeding 90% and the degree of pore interconnectivity are fundamental that a scaffold needs to possess a higher degree of interconnectivity in conjunction with a suitable pore size, in order to minimise diffusion limitations and pore occlusion. High internal surface area to volume ratios is essential in order to accommodate the large number of cells required to replace or restore tissue or organ function(s) [98]. Figure 2.3 clearly illustrates the range of pore size, the relationship between macroporosity and microporosity, and the interconnectivity of scaffold made from silk fibron [116].

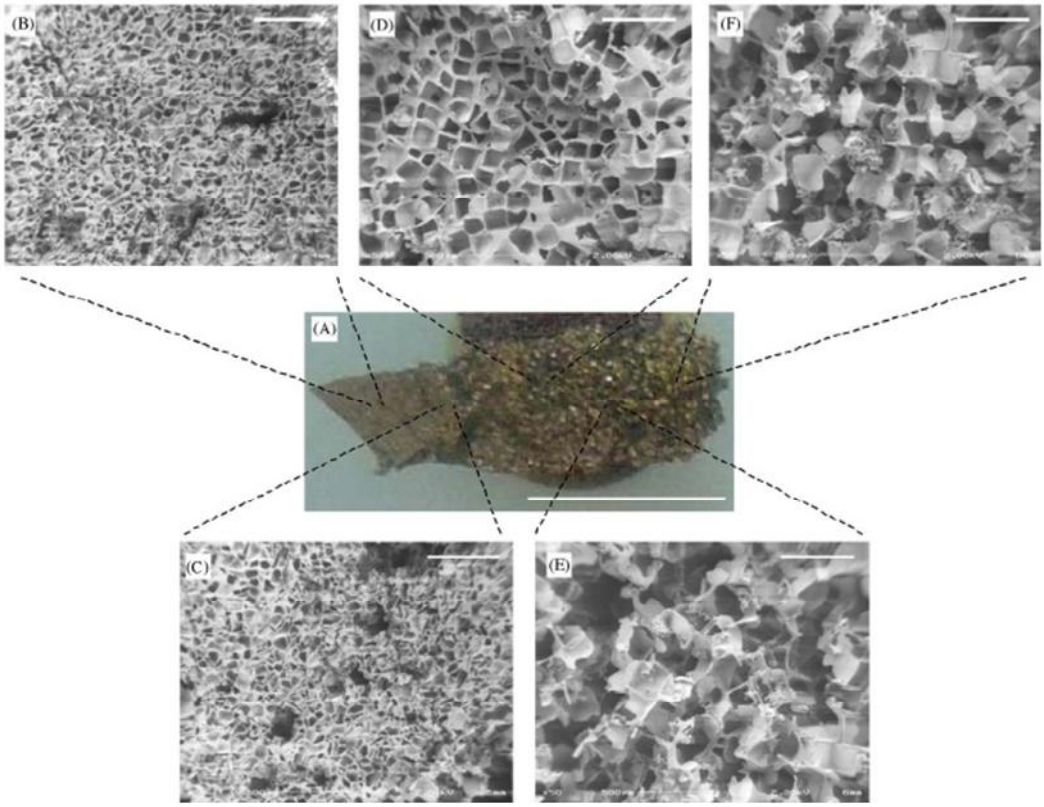

Figure 2.3 Pore size gradient across a sponge made of silk fibroin. Pore sizes are 76.3716.2mm (B), 100.7718.2mm (C), 182.0730.0mm (D), 221.3740.6mm (E), and260.3775.9mm (F). Bar lengths is 10mm (A) and500mm (B–F) [116].

2.4.5 Mechanical performance

Scaffolds should complement the biological and mechanical properties of tissues that they support. Adequate mechanical performance of a scaffold depends on specifying, characterizing and controlling the material mechanical properties including elasticity, compressibility, viscoelastic behaviour, tensile strength and failure strain [74]. Once the scaffold is produced and implanted, sufficient mechanical strength is important to manage any *in vivo* stresses and physiological loadings imposed on the engineered construct [118].

The formation of tissues with desirable properties depends on scaffold material mechanical properties at both the macroscopic and microscopic level.

Macroscopically, the scaffold must bear loads to provide stability to the tissues as it forms and fulfils adequate perfusion to take place as toxins are removed and nutrients are replenished. On a microscopic level, evidence suggests that cell attachment, proliferation, migration and ultimate tissue formation are dependent on mechanical input to the cells [74]. Hayashi suggested that hard tissue scaffolds should provide a mechanical modulus in the range of 10-1500 MPa whereas for soft tissue scaffolds, in the range of 0.4-350 MPa [119].

Table 2.2. Ultimate strength (MPa) and ultimate strain (%) of cortical bone from the human femur as a function of age [119].

	Age (years)						
Properties	10-20	20-30	30-40	40-50	50-60	60-70	70-80
Ultimate strength (MPa)							
Tension	114	123	120	112	93	86	86
Compression	-	167	167	161	155	145	-
Bending	151	173	173	162	154	139	139
Torsion	-	57	57	52	52	49	49
Ultimate strength (%)							
Tension	1.5	1.4	1.4	1.3	1.3	1.3	1.3
Compression	-	1.9	1.8	1.8	1.8	1.8	-
Tension	-	2.8	2.8	2.5	2.5	2.7	2.7

2.5 Microstereolithography

Researchers in tissue engineering fields are striving hard to design scaffolds that mimic the *in vivo* cellular microenvironment. It is essential to develop materials and be able to fabricate three dimensional scaffolds with various geometry shapes in order to achieve this goal. Rapid prototyping is possibly the best technique as it has the advantage of being able to build objects with predefined macrostructures as well as controlled multi-scale microstructures.

Rapid prototyping is also known either as solid free-form manufacturing, computer automated manufacturing, or layered manufacturing. Common and well-

established rapid prototyping technologies are stereolithography, selective laser sintering, 3D printing and fused deposition modelling. Of these techniques, stereolithography is the most versatile method with the highest accuracy and precision [120]. Most stereolithography systems (SL) and their micro-versions - MSL) predominantly work through an additive layer process, where each layer is cured into a photosensitive resin by a light source in a process called photopolymerization. In photopolymerization, a source of light such as UV laser or Near IR laser is used to trigger a chain reaction in the monomer, which induces the polymerization of liquid monomer into solid polymer [121].

The surface of photosensitive liquid (resin) is exposed to the light source creating a 2D image on the elevator platform. The first layer is cured, and adheres onto the plate surface. The elevator descends to a defined distance, and a fresh layer of resin is spread on top of the 2D object and the light induced solidification of the next layer is started. This process is repeated layer-by-layer by chemical crosslinking to construct a full 3D structure. The first commercially available layer additive process of rapid fabrication, directly from computer aided design databases was produced by 3D Systems in 1987 [98].

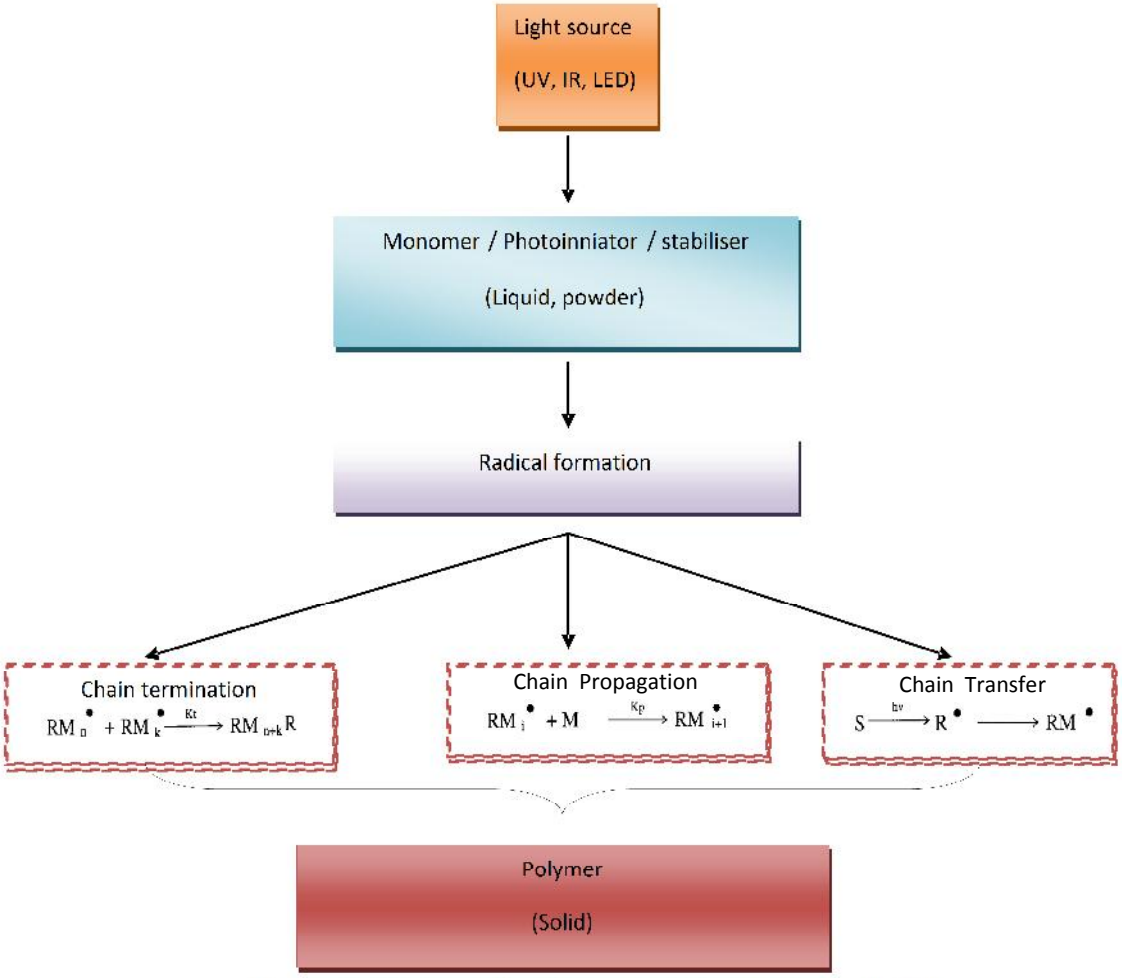

Figure 2.4 Schematic diagram of photopolymerization.

The principle of MSL is similar to that of stereo- lithography (SL) with the exception of a dramatic improvement in resolution |122|. There are 2 main categories of microstereolithography fabrication techniques |123|:

1) Vector-by-vector

2) Integral

2.5.1 Vector-by-vector microstereolithography

The basic principle of vector-by-vector microstereolithography is similar to stereolithography; where each layer is fabricated by focusing the light beam on the surface of the photopolymer resin. In the vector by vector scanning technique, the

laser beam focuses and cures the resin spot by spot. Although spot by spot curing is time consuming, it can produce a high resolution structure and reduce the spot size to a few micrometers in diameter, due to the fact that the UV light is focused optimally onto the resin surface. To obtain these, the position of the surface on which the beam is scanned has to be precisely and continuously measured, and the focus of the beam is determined by sufficient precision [124].

The first reported work on a micro 3D structure, using a vector-by-vector microstereolithography process, was made by N. Nakajima and T. Takagi in 1993. They demonstrated a constrained surface apparatus (Figure 2.5) that could produce a 3D structure at a resolution 0.8 μm [125]. In the same year, K. Ikuta and K. Hirowatari showed their apparatus which was able to achieve up to 0.25 μm in XY direction and 1 μm in the Z direction [126]. They focused the light beam and it remained fixed, through a transparent window, to trace every layer of the object vector-by-vector. The x-y translation stages are used to move the entire optical system to focus the light beam on the surface, or the photoreactor in which the object is made.

The use of a glass window to push on the liquid and obtain a layer of constant thickness avoids problems related to spreading the fresh resin on the already polymerised part of the object. However, polymerising through a transparent window has a major disadvantage: the formed polymer sticks to it, which can result in partial or total destruction of the part during the manufacturing process [124].

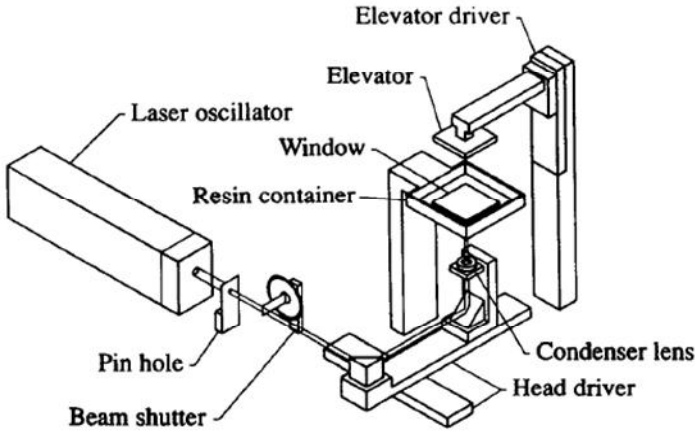

Figure 2.5 Stereolithography apparatus of Nakajima and Takagi [125].

The free-surface microstereolithography technique was developed to overcome the adhesion of the polymer to the transparent window; by displacing the reactor in a three dimensional space by an x-y-z stage [124]. The main disadvantage of this method is the difficulty in controlling the thickness of the deposited liquid layer once the liquid layer is spread on the surface. The time required to obtain a horizontal fresh layer of resin depends on the rheological properties of the resin. Low viscosity monomers have to be used as often as possible [127].

Photopolymerization is an essential process in MSL. The fabrication parameters such as exposure energy and layer thickness should be determined according to the photocurable resin because curing characteristics affect the resolution of the fabricated object. The intensity distribution of focused light on the resin surface has an effect on the precision, but the vector-by-vector method has a relatively high precision because a layer is built by scanning with a very fine beam spot. However, the integral method generally makes one layer at a time with the use of patterned light with a cross-sectional image. Therefore, uniform light intensity on the resin surface is an important factor in projection MSL [128].

2.5.2 Integral microstereolithography

The next generation of microstereolithography machine known as integral MSL uses a slightly different technique. In integral MSL, a pattern generator (dynamic mask/spatial light modulator) is used to shape light, and the modulated light is transferred through a reduction lens onto the resin surface a reduced feature size [129]. The layer is cured in one irradiation step by with a high resolution and a certain depth of focus. This method is significantly faster because a whole layer is cured in a single process, whereas the vector by vector technique requires every pixel to be cured one by one.

The first reported use of this technique is by Bertsch et al. in 1995, where they developed an integral MSL machine using 260 x260 pixel LCD as the UV light mask [130]. Every pixel of such LCD panels is a small cell that can set either to its transparent state or to its opaque state, by changing the orientation of the molecules contained. The insertion of LCD on the optical path of the light beam, makes the transmitted light modulated, and successfully manufactures complex shape objects in microstereolithography. The limitation with this technique was the incompatibility with UV light. In 1998 Laubere et. al has successfully developed an apparatus and a photosensitive resin reacting with visible light while Chatwin et al used polysilicon thin film twisted nematic LCD in an integral microstereolithography which operates in the UV light, transparent to wavelength above 350nm.

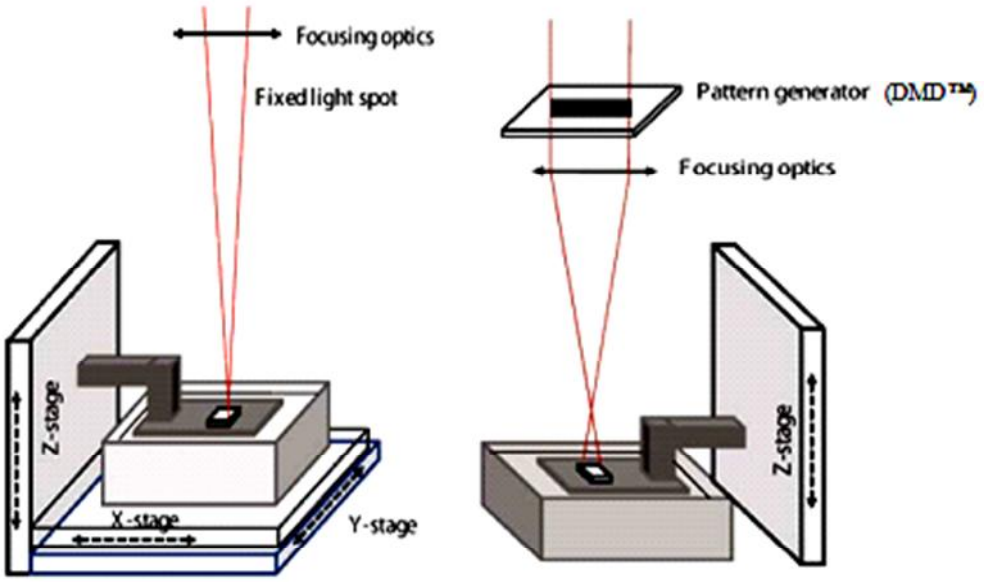

(a) (b)

Figure 2.6 Differential set-up of (a) vector by vector stereolithography and (b) integral method [127].

The next stage in the development of MSL machine is the use of digital micromirror device (DMD™) as pattern generator. Figure 2.6 shows the DMD™ developed by Texas Instrument. The pattern generator is an array of micromirrors actuated by electrostatic forces. The DMD™ is made of 16μm square aluminium mirrors that can reflect the light in one of two directions. The working principle is accomplished through electrostatic attraction of rotating mirrors. It is a microelecromechanical system working as a light switch [131]. In 1999, Bertch introduced an MSL machine to work with visible light, utilizing DMD technology as the pattern generator with VGA resolution at 640 x 480. The speed of this machine is about 200-300 layers per hour, depending on the shape of the layers, and the resolution is up to 3x3x3 μm^3.

Swiss Federal Institute of Technology in Lausanne has created a microstereolithography machine which operates in the UV, a DMD™ chip having an XGA resolution of 1024 x 768. An acrylate-based resin, which highly absorbs the irradiation wavelengths has been specially formulated for this machine. The mechanical properties of the resin are close to the conventional stereolithography resin.

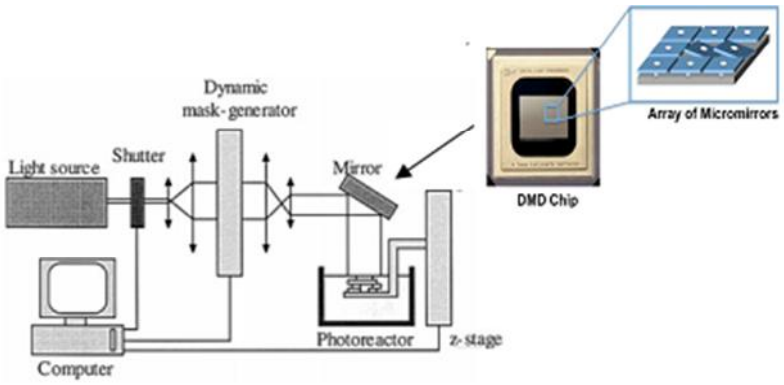

Figure 2.7 Schematic diagram of microstereolithography with digital micro mirror [127].

One of the major limitations of microstereolithography technology is only that there are a few choices of photopolymer materials that can be used in this technique. The polymers are generally acrylates and eventually epoxies. The materials should also have adequate mechanical, chemical or physical characteristics. The microstereolithography technique has offered new possibilities of not only as a prototyping technology, but as a manufacturing technique. The development of new materials, particular using composite materials made of ceramic particles embedded in polymer matrix as matrix has attracted lots of attention in the past few years. The ultimate aim is the production of micro-components in ceramic materials, which can be obtained by sintering the composite. In order to achieve this, there are a few

criteria have to be meet such as the load of particles embedded in the resin has to be sufficiently high. However, this will increases significantly the viscosity of the chemical media, which the researchers need to address.

2.6 Photopolymerisation

The use of light to initiate and propagate polymerization reaction on a liquid monomer or macromer has been used extensively in both commercial and clinical applications. It is a fast and controllable process under ambient or physiological condition. The sources of light suitable for tissue engineering application are from UV lamps (330-450 nm, I_o: 2-100 $mWcm^{-2}$) and halogen lamps (400-520 nm, I_o: 20-1200 $mWcm^{-2}$).

Photoinitiators are the main component in the photocurable resin to allow polymerization. They are responsible for initiating the reaction of polymerization by producing reactive species upon light absorption. Once the reactive species are excited, they will generate an induced free-radical polymerisation. Thus only a small percentage of volume is needed and it is crucial to find suitable photoinitiator with the accurate concentration.

The photoinniator should posses all the requirements suitable for tissue engineering applications [1], [132]. They should have:

1. high absorbing capacity for the light used to polymerise to maximize polymerizable-residue conversion;
2. high photosensitivity, to better match the wavelength of the light to polymerise or to find spectral window for opaque or pigments formulation,

3. fast inniation rates with high inniation efficiency,
4. solubility in aques media,
5. bio-compatibility with cells or molecules entrapped within the forming polymer, and cells and tissues in the eventuality of body implantation, and
6. non-toxicity both locally and systematically.

The monomers or macro-monomers in photopolymerizable resins usually have a photopolymerizable residue that is normally located at one or at both ends of the molecules.

Recently photopolymerised hydrogels have been investigated for a number of biomedical applications such as post-operative adhesion formation, drug delivery, and cell transplantation. Such monomers are poly(ethylene glycol) PEG, with its derivatives poly (ethelene oxide) (PEO), poly(vinyl alcohol) (PVA) and its derivatives, dimethacrylated poly(lactic acid) b-poly(ethelene glycol)-b-polylactic acid PLA-*b*-PEG-*b*-PLA, PLA-*g*-PVA, poly(D, L-lactide-co- ε-caprolactone), modified polysaccarides such as hyaluronic acid derivatives, poly(anhydrides) , urethanes , and, diethyl fumarate-poly(propylene fumarate).

Dimethacrylated anhydride monomers were successfully synthesized and photopolymerized by Anseth et al. in 1997 to produce highly cross-linked polymer networks. The mechanical properties of the networks were intermediate and comparable between that trabecular bones but significantly lower than cortical bone. The polymer networks also show excellent soft tissue compatibility and well tolerated by the surrounding tissue components [82].

A photopolymerizing hydrogel system provides an efficient method to encapsulate cells allowing increased efficiency and uniformity in cell seeding on the scaffold compared with solid scaffolds. A study done by Ellisseff et al. has encapsulated bovine and ovine chondrocytes in poly(ethylene oxide)-dimethacrylate and poly(ethylene glycol) semi-interpenetrating network by the means of photopolymerization process. Figure 2.8 shows the experimental protocol of cell photoencapsulate. The findings brings better prospect of photoencapsulation for tissue engineering and drug delivery purposes [81].

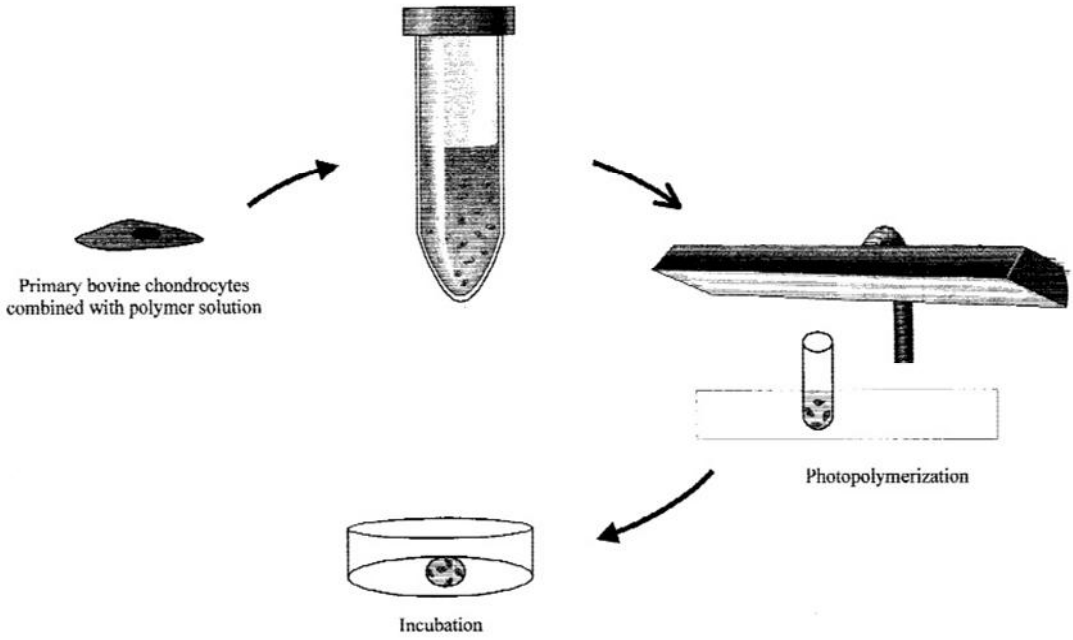

Figure 2.8 Schematic diagram of protocol for photoencapsulation chondrocytes in poly(ethylene oxide)-based semi-interpenetrating networks in Elisseeff et al. study. [81].

Lee et al. researchers has successfully optimised biodegradable photopolymer resin mixtures of poly(propylene fumarate) (PPF) and diethyl fumarate (DEF) for fabrication in stereolithography with defined pore sizes, pore shapes, and porosities as shown in Figure 2.9. In addition, the fabricated scaffold was found to be

biocompatible as the cells were able to attach to the scaffold surface and grow after the cells were fixed and freeze-dried after 4, 7, and 28 days of culture [135].

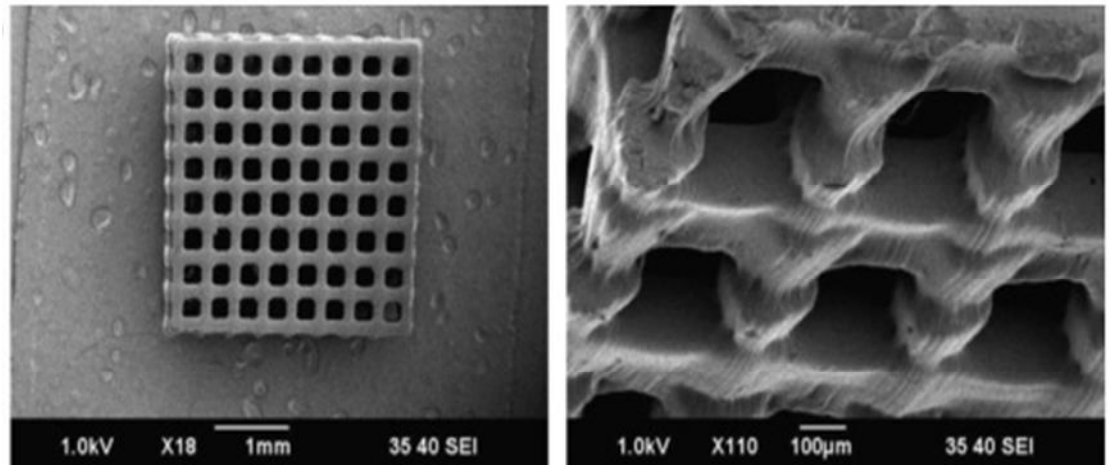

Figure 2.9 A 3D scaffold prepared from biodegradable photopolymer resin mixture of poly(propylene fumarate) (PPF) and diethyl fumarate (DEF) [135].

A development further conducted by Choi et al. on the microstereolithography technique with few modifications on the PPF/DEF formulation, has successfully fabricated a miniature 3D human kidney scaffold with interconnecting pores (Figure 2.10). Although there were some manufacturing limitations between the samples when compared to commercial resins, but the developed MSL system and the use of PPF shows promise for fabricating complex micro-scaffolds with prescribed microarchitectures [122].

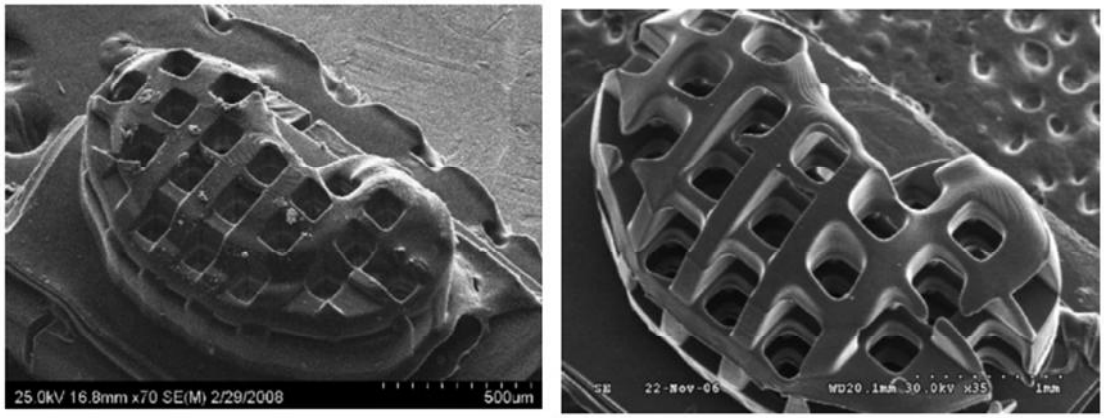

(a) (b)

Figure 2.10 SEM micrograph of the fabricated kidney scaffold using the (a) PPF/DEF and (b) commercial resin respectively [122].

Melchels et al. has successfully developed a resin based on poly(D,L-lactide) macromers and non-reactive diluents via stereolithography technique. The porous and non-porous hydrogels has narrow pore size distributions, excellent pore interconnectivity and possessed excellent mechanical properties, similar to those of linear high-molecular weight PDLLA. They also prepared hydrophobic scaffolds using a liquid resin based on a 2-armed PDLLA macromer and ethyl lactate. The clinical study shows mouse pre-osteoblasts showing good cell seeding characteristics, readily adhered and proliferated well on these networks. This anticipated the application of these hydrogel structures in tissue engineering, drug delivery, cell-transplantation and other biomedical applications [78], [136].

2.7 Polyethylene Glycol (PEG)

Polyethylene glycol is widely used in biological application owing to its biocompatibility, hydrophilicity, and the ability to be chemically tailored and passively excreted by the body [79]. Hydrogel structures prepared from polyethylene glycol (PEG)-based resins are suitable to be fabricated with stereolithography because the photo-reactive and crosslinkable groups like acrylates or methacrylates can be

easily attached. The photoreactive groups will crosslink the PEG into hydrogen in the presence of a photoinitiator and upon exposure to UV light. Figure 2.11 shows the structure of PEG. These hydrogels are permeable to oxygen, nutrients, and other water-soluble metabolites and have a soft consistency that makes them similar to soft tissues. PEG-based hydrogels are not bioactive, but the cell-specific bioactivity can be achieved by covalently attaching adhesion ligands, growth factors, and cytokines to the hydrogel or by simply trapping the bioactive agents within the hydrogel [137].

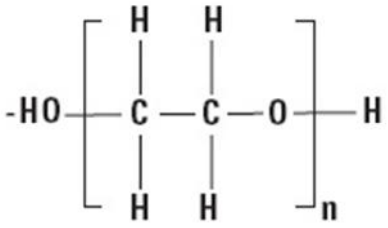

Figure 2.11 Structure of poly(ethylene glycol)

A complex three-dimensional (3D) structure was fabricated from photopolymerizable poly(ethylene glycol) diacrylate (PEGDA) using a commercially available stereolithography apparatus (SLA). Figure 2.12 shows the schematic illustration of the modified SLA and experimental protocol for cell photoencapsulation explored by Chan et al. in 2010. An angiogenic factors, RGDS peptide sequences were added to the resin which increased cell viability, proliferation, and spreading compared to pristine PEG hydrogels of the same molecular weight. The study shows the successful photo patterning of spatial 3D layer-by-layer and the feasibility of depositing multiple cell types and material compositions into distinct layers [138].

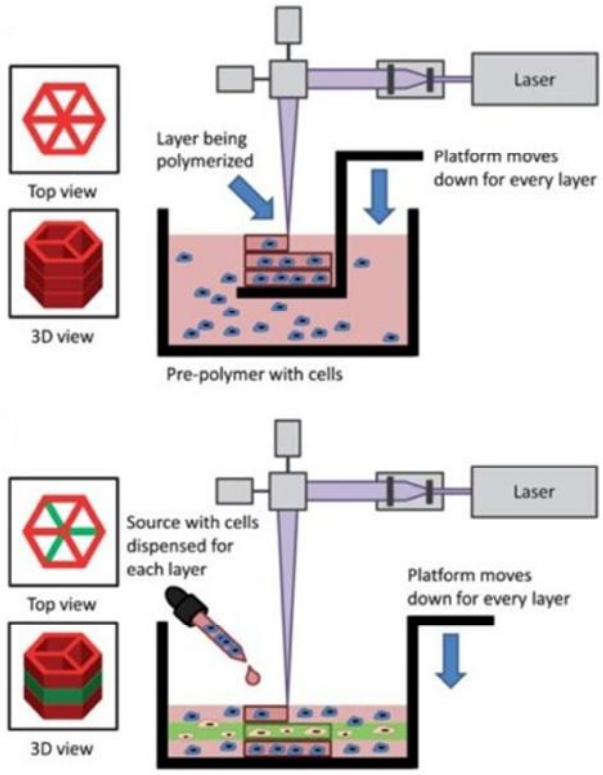

Figure 2.12 Schematic illustration of the modified SLA and experimental protocol for cell photoencapsulation [138].

As mentioned above, the biocompatibility of hydrogel based on PEG was excellent, even the encapsulation of living cells was made possible during the fabrication process. Nonetheless, it can be excreted by the kidneys at molecular weights up to 30 kg/mol [139]. However, the acrylates and methacrylates could create a non-degradable linear or crosslinked polymer network during photopolymerization, which are non-desirable in tissue engineering. The modification of backbone of the polymer by the introduction of degradable chemical bonds in the reactive site of the monomers such as ester, anhydrides or amide could improve the biodegradability of the polymer. These amide-based crosslinker may undergo hydrolytic or cleaved enzymatically *in vivo* and might be then excreted through glomerular filtration. The degradation rate also depends on the number and types of degradable chemical bonds introduced.

Molecular weight of the monomer and the hydrophilicity or hydrophobicity of the monomers could also influence the degradability of the tissue scaffolds. In the tight polymer network of low molecular weight of monomers, the degradation rate is slow because the degradable chains are hindered due to the density of the crosslinked network, whereas hydrophobicity will also decrease the degradation rate of the systems.

A recent study done by Seck et al. in 2010, prepared highly biocompatible hydrogels that degrade in the body by crosslinking macromers based on block copolymers of PEG and poly(D,L-lactide) (PDLLA) and built by stereolithography at high resolutions as shown in Figure 2.13. In contrast to PEG some researchers have crosslinked PEG with poly(D,L-lactide), a hydrophobic polyester with a glass transition temperature (Tg) of approximately 55 °C, and, can degrade by hydrolytic cleavage of the main chain ester bonds. The 3D structures were characterised with well-defined architectures and good mechanical properties. In addition the porous hydrogel structures with gyroid pore network architecture showed narrow pore size distributions, excellent pore interconnectivity and good mechanical properties. The structures showed good cell seeding characteristics, and human mesenchymal stem cells adhered and proliferated well on these materials [136].

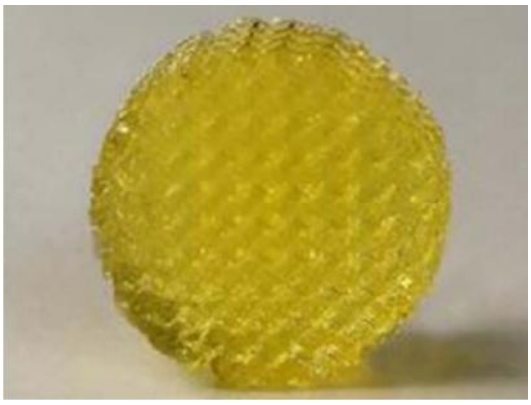

Figure 2.13 Hydrogel with gyroid pore network design built by stereolithography using PDLLA-PEG-PDLLA based resin [136].

2.8 Conclusion

To date, advances in scaffold fabrication methods have brought brighter and promising future in the field of tissue engineering. Amongst the majority of fabrication techniques, rapid prototyping or solid free from fabrication is possibly the most intriguing and interesting to explore as it offers high resolution of complex 3-D architectures of materials with tuneable physical properties. Furthermore, the scaffold is custom-made for patients to the shape of the defect or injury as the defect information could be obtained from clinical imaging data such as CT, MRI images. These fabrication techniques allow control over pore architectures, i.e. the pore shape and size, and perfect pore interconnectivity could be established. As a result, the formation has encouraged cell proliferation and tissue regeneration inside the scaffold.

Biodegradable scaffolds have played an important role in a number of tissue engineering attempts over the past decade especially in 3D tissue scaffolds. These scaffolds provide a template for cells to attach, proliferate, and form extracellular

matrix. The biomaterials must satisfy the following essential property requirement for scaffolds as listed by Agrawal and Ray [108]:

1. biocompatible,
2. biodegradable or capable of being remodelled,
3. biodegrade in tune with the repair or regeneration process,
4. adequate porosity,
5. highly permeable to allow for proper diffusion,
6. correct pore size for the candidate cells,
7. adequate mechanical properties to provide the correct microstress environment for cells,
8. provide a surface conducive for cell attachment,
9. encourage the formation of ECM by promoting cellular functions, and
10. able to carry biomolecular signals such as growth factors.

In the past few decades, researches have studied and investigated extensively on the first five properties listed above; however, for current and future research, a clear understanding of the latter five parameters is still fundamental and should be explored vigorously. With the abundance supply of knowledge on fabrication techniques and biomaterial, a vast opportunity for novel scientific findings and discovery in tissue engineering field is opened.

CHAPTER 3

Ceramic Composites

3.1 Introduction to Bones

Skeleton is formed of long bones (eg: femur), flat bones (eg: skull) and cuboids bones (vertebra and carpals). The primary functions of bones are to provide mechanical support system for muscular activity and physical protection on organ and soft tissue. Bone also acts as a storage facility for bone marrow, where red and white blood cells are harbours. Bone also has an important function of regulating the calcium and phosphate level in human body system [140], [141].

Bone is a porous material composed of cellular component (35%) and an extracellular matrix (65%). The cellular component is made of osteoblasts, bone-forming cells, osteoclasts, bone-destroying cells, and osteocytes, bone-maintaining cells which are inactive osteoblasts. The extracellular matrix is organic matter that consists mainly of calcium phosphate, significant amounts of citrate and carbonate ions and traces of fluoride, magnesium, sodium and collagen.

The unique combination of mineral and tissue in bone has provides excellent tensile and loading strength. The inorganic mineral phase is responsible for its stiffness whereas the organic phase (cell and tissue) responsible for maintenance, tensile strength and elasticity [141].The combination of mineral hydroxyapatite and collagen matrix gives bone great density and hardness [1], [142]. Figure 3.1 shows the internal structure of a cancellous bone.

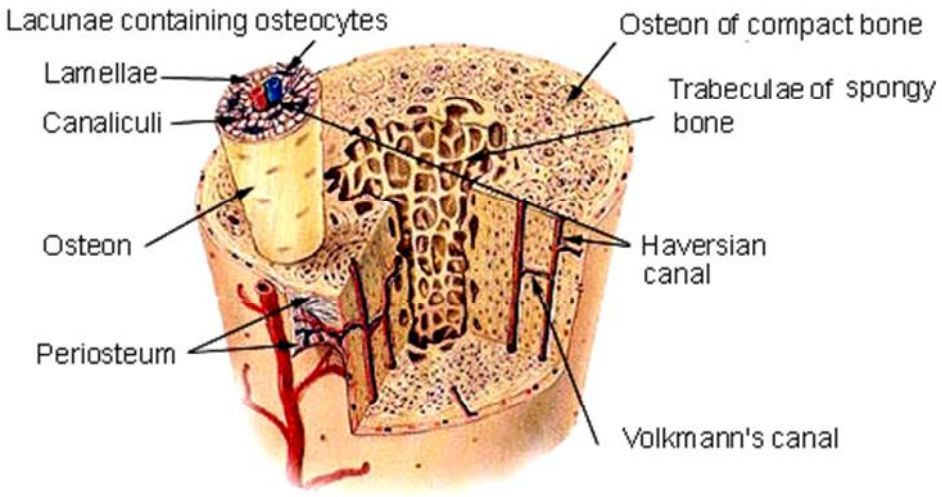

Figure 3.1 Structure of internal cancellous bone [143].

There are two types of bones tissues:

1) Cancellous bones
2) Compact /cortical bone

Cancellous bone is characterises with its spongy appearance with numerous large spaces and it is the most changing and active in growth. It makes up 20 percent of the human skeleton's weight and mainly located in large plates and rods known as trabecular. Cancellous bone also located in vertebral bodies and adjacent to articulating joint such as the knee joint [144].

Compact bone makes up 80 percent of the weight of a human's skeleton. They are stronger as the density is higher than cancellous bones. Compact bone forms a shell around cancellous bone and is the primary component of the long bones of the arm, leg and other bones, where its greater strength and rigidity are needed. Even though compact bones are dense, they are less porous, with a porosity level that ranges from 5 to 10 percent in comparison to cancellous bone's 50 to 90 percent

porosity range. Figure 3.2 shows the different structures of cancellous and cortical bones.

Despite these differences, compact and spongy bone tissue work together, as cortical tissue is the shell that covers the cancellous bone of the vertebrae and joint ends. In addition, the distribution of cortical and cancellous bones varies greatly between bones; depend on the function of the bone. For instance, the composition of cortical and cancellous bone in ulna is 92 and 8 percent respectively, whereas typical vertebra consists of 62 percent cortical and 38 percent cancellous bones [144].

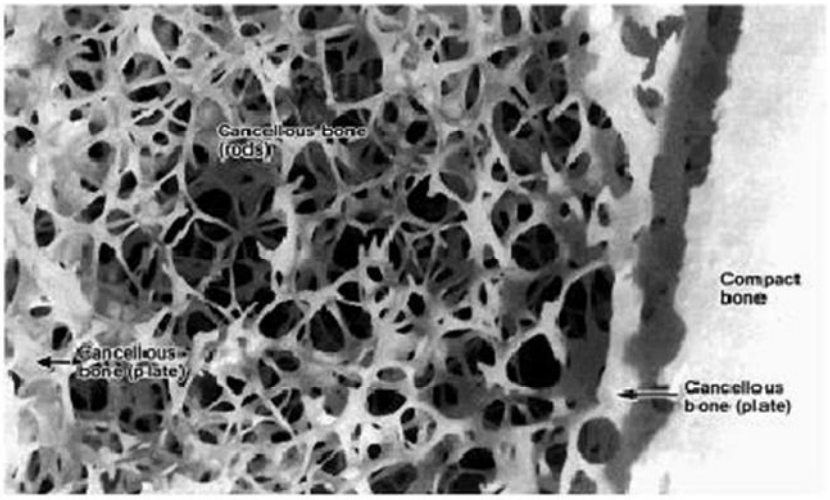

Figure 3.2 Micrograph of a thick ground section on part of the proximal tibia showing the cortical (compact) bone and the trabecular (cancellous) bone [144].

There are two types of cell that are responsible for bone renewal:

1. Osteoblast
2. Osteoclast

Osteoblasts are the cells that are responsible for new bone formation. They also come from the bone marrow and are related to structural cells. They secrete a collagen rich ground substance essential for later mineralization of hydroxyapatite and other crystals. The collagen actually strands to form osteoids: spiral fibres of bone matrix. They control calcium and mineral deposition and are found on the surface of new bone.

Osteoclasts are large, ruffled edge cells that come from the bone marrow mononuclear cell. They secrete bone-reabsorbing enzymes that dissolve the bone. They are found on the surface of the bone mineral next to the dissolving bone.

Osteocytes are cells inside the bone. They also come from osteoblasts that have been trapped in the osteoids. They are not isolated, however, because they send out long branches that connect to the other osteocytes. They play a role in controlling the extracellular concentration of calcium and phosphate, and are directly stimulated by calcitonin and inhibited by PTH (Parathyroid hormone). These cells can sense pressures or cracks in the bone and help to direct where osteoclasts will dissolve the bone [141], [145]. Figure 3.3 shows the schematic structure of osteoblast and osteoclast cells.

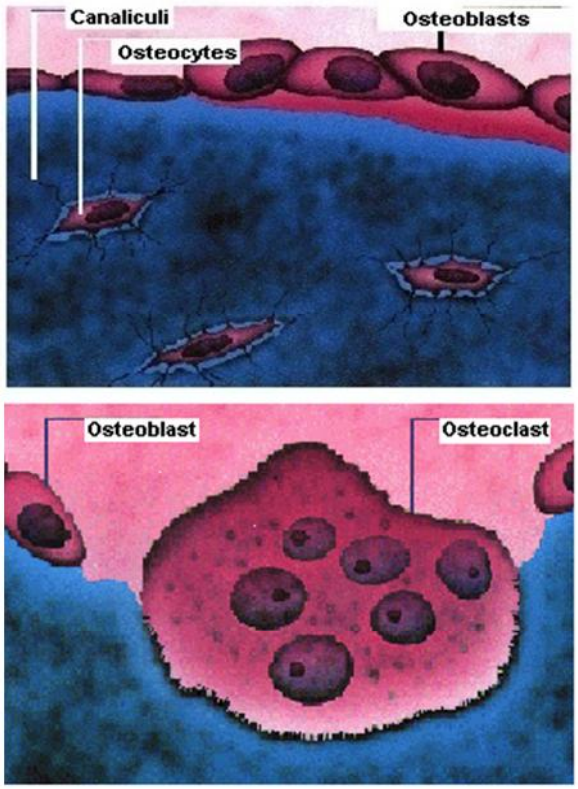

Figure 3.3 Schematic structure of osteoblast and osteoclast cells [145]

3.2 Mechanical Properties of Bone

The mechanical properties of bones are highly dependent on the structure of the bones as shown Table 3.1. There are also other factors that could give effect to the mechanical properties of the bone such as:

a) Age of the person
b) Sex of the person
c) Anatomical site
d) Mineral content
e) Amount of water present
f) Disease – e.g. osteoporosis

Table3.1Mean values for bone modulus of elasticity and ultimate strength [116].

	Tensile strength (MPa)	Compressive strength (MPa)	Young Modulus (GPa)	Fracture toughness (MPa ml/2)
Cancellous bone	7.4	4-12	0.02-0.5	N/A
Cortical bone	60-100	130-180	3-30	2-12
Cartilages	3.7-10.5	N/A	0.7-15.3	N/A
Ligaments	13.46	N/A	0.065-0.541	N/A
Tendon	24-112	N/A	0.143-2.31	N/A

Karageorgiou and Kaplan (2005) has reported that, the tensile strength and modulus of elasticity of femoral cortical bone decline by approximately 2 percent per decade after maturation [116].Table 3.2 shows the effect of age on the mechanical properties on bone.

Table 3.2: Ultimate strength (MPa) and ultimate strain (%) of cortical bone from the human femur as a function of age [144], [146].

Properties	Age (years)						
	10-20	20-30	30-40	40-50	50-60	60-70	70-80
Ultimate Strength (MPa)							
Tension	114	123					
Compression	-	167	120	112	93	86	86
Bending	151	173	167	161	155	145	-
Torsion	-	57	173	162	154	139	139
			57	52	152	49	49
Ultimate Strain (%)							
Tension	1.5						
Compression	-	1.4	1.4	1.3	1.3	1.3	1.3
Torsion	-	1.9	1.8	1.8	1.8	1.8	1.8
		2.8	2.8	2.8	2.5	2.7	2.7

Structurally, the mechanical properties of bones are determined by the external and internal architecture of the bone and by the tissue properties [147]. Cortical bone, for instance, is an anisotropic material; therefore its mechanical properties vary

according to the direction of load [145]. For cancellous bone, the mechanical properties is also determined by the arrangement of the bone material, in addition to its bone volume fraction [147]. Table 3.3 show how the direction and type of bone affect the modulus of elasticity and ultimate strength.

Table 3.3 Mean values for bone modulus of elasticity and ultimate strength as studied by previous researchers [140], [148].

Type of Bone	Direction and type of Bone	Apparent Density (g/cm^3)	Ultimate strength (MPa)	Modulus of Elasticity (GPa)
Cortical (midfemoral)	Longitudinal tension	1.85	133	17
	Longitudinal Compression	1.85	133	17
	Longitudinal shear	1.85	193	17
	Transverse tension	1.85	68	3
	Transverse compression	1.85	51	11.5
Trabecular (proximal tibia)			5.3	0.445
Trabecular (proximal femoral)	Axial		6.8	0.441

Although bone has its own ability to heal, as the body grows older, this ability decreases, sometimes due to disease and other factors, and the healing ability is only limited to small bone defects. Autograft is common for small bone defects. It is harvested from the patients' own body and has the advantages of biocompatibility and immunoresponse. It contains osteogenic cells and osteoinductive growth factors (such as bone morphogenetic proteins, BMPs), allowing rapid bone regeneration and reconstruction of bone loss, and is therefore still the "golden standard" and the most-used bone graft [105]. However, autograft is limited in amount, needs a secondary

operation, and causes pain and morbidity. Moreover it is not always successful in all cases.

On the other hand, for larger bone defects, such as excision of bone tumour, bone sarcoma or other bone diseases, in cases of bone loss in accidents, and in complicated fractured bones that cannot repair themselves; allograft is required. However, allografts, pose an increased risk for infection and disease transmission from the donor. It has osteogenic cells and osteoinductive growth factors as autograft does, but its osteogenic capacity may decrease due to its immunologic rejection. The recovery rate is lower because it takes long time to incorporate into the recipient's body. In addition, the infection rate is higher, and allograft bone is limited in supply [66], [149].

The shortcomings of autograft and allograft have encouraged scientists to develop artificial bone grafts. Biomaterials, such as metals, polymers, calcium phosphate biomaterials, bioglasses and combinations of thereof, has attracted much interest, with studies applied clinically for bone repair alone or with the combination of osteogenic cells or growth factors [116], [150], [151], [152], [153], [154], [155], [156], [157], [158], [159], [160].

3.3 Ceramics for Bone Tissue Scaffolds

Biomaterials are one of the keystones in tissue engineering research. There are three most common class of materials used in biomedical materials:

1. Synthetic: metal, polymer, ceramic, composite
2. Naturally derived: plants or animal- derived
3. Semi synthetic or hybrid

Ceramics are preferred materials as bone grafts because of their superior properties compare to other biomaterials. Their compositions are similar to natural bone, low density, high compressive strength, chemical and high wear resistance, and excellent adherence tissue. Ceramic such as calcium phosphate, silica, alumina, zirconia, titanium dioxide, and bioactive glass are amongst the extensively studied by researchers as they are considered biomimetic materials. They stimulate the formation, precipitation and deposition of calcium phosphate from solution and can results in enhanced bone tissue formation [38], [161].Calcium phosphate based scaffolds are used in a wide range of applications in tissue engineering, controlled drug delivery systems and in the treatment of bone disease [21], [162], [163], [164], [165].

Table 3.4 shows some of the currents application of other types of ceramics in medical field. In dentistry, blocks and granules of porous calcium phosphate with hydroxide-based materials has been used as endodontic filling materials and metal–ceramic alloys are applied for crowns. Intervertebral disc and joints made from calcium phosphate-based materials are well known in orthopaedic and ceramics are used for cranial defect in plastic surgery reconstruction. Characteristics of these ceramic materials are often high mechanical strength, good body-response and low or non-existing biodegradability [38], [166], [167].

Table 3.4 Currents application of other types of ceramics in medical field [38], [162], [166].

Types of ceramics	Current application
Calcium phosphate	Bone graft substitutes, surface coating on total joints replacement
Calcium sulphate	Bone graft substitutes
Zirconia	Hip implants
Aluminium oxide	Hip implants, dental implants, cochlear replacement
Glass	Bone graft substitutes, filler for dental materials
Carbon	Heart valve coatings, orthopedic implants

Ideally, the characteristics of a biomaterial candidate for bone tissue engineering should fulfil the following requirements [1], [38], [132], [168], [169] :

1. Biodegradability: resorbed completely by osteoclasts over time, while osteoblastic activity deposits new mineralised bone at the site
2. Osteoconductivity: ability to activate cellular response to attract osteoclasts and osteoblasts to the implant site; whilst enhancing the formation of new living bone
3. Osteoinductivity: ability to stimuli osteoprogenitor cells to differentiate into osteoblasts that then begin new bone formation.
4. Macroporosity that enables cell ingrowth into the composite
5. Mechanical stability/ease of handling
6. Carrier for growth factors/cells: The most widely studied type of osteoinductive cell mediators are bone morphogenetic proteins (BMPs).

Ceramic has slow degradability, which is a hindered property for tissue engineering purposes but, ceramic or ceramic-derivatives as a scaffold for bone tissues engineering has a lot of potential to study and explore. This is because of their osteoconductive properties especially for hydroxyapatite-based calcium phosphate compounds [40], [170] and bioactive glass [171].To overcome its slow degradability, whilst improves bone ingrowth, porosity with optimum pore size is introduced to the implants scaffolds [116].

3.4 Calcium Phosphate Ceramics

Calcium phosphate ceramics were introduced more than 30 years ago as bone substitutes. Most calcium phosphates are classified as resorbable biomaterials; meaning under physiological conditions or with placement within the human body; they will start to dissolve and slowly replaced by advancing tissue such as bone. The dissolution products are naturally metabolized and they do not induce abnormal calcium or phosphate levels in urine, serum, or organs [172].

In addition, calcium phosphate biomaterials are also known to be bioactive as they support bone in-growth and enhance bone tissue formation. Different phases of calcium phosphate ceramics are used in the modern health care industry depending upon whether a resorbable or bioactive material is desired.

Calcium phosphates exist in different phases depending on temperature, impurities and the presence of water [173]. The two phases that are stable at body temperature are dicalcium phosphate (DCP) and hydroxyapatite (HAP) [174]. HAP derived from coral or fabricated from synthetic apatite powders, partially decomposes to β-TCP in a low water environment when heated to about 1200–1300 °C depending

on the activity of the powder [175].Listed in the Table 3.5 below are some calcium phosphate compounds of biomaterials interest.

Table 3.5 List of calcium phosphate compounds of biomaterials interest.

Chemical Name	**Abbr**	**Chemical Formula**		**Ca/P**
Amorphous calcium phosphate	ACP	-	-	-
Dicalcium Phosphate	DCP	$CaHPO_4$	Monetite	1.00
Tricalcium Phosphate	α-TCP	$Ca_3(PO_4)_2$		1.50
Tricalcium Phosphate	β-TCP	$Ca_3(PO_4)_2$	Whitlockite	1.50
Pentacalcium Hydroxyl Apatite	HAP	$Ca_{10}(PO_4)_6(OH)_2$	Hydroxyapatite	1.67
Tetracalcium Phosphate Monoxide	TTCP	$Ca_4O(PO_4)_2$	Hilgenstockite	2.00

3.4.1 Hydroxyapatite

HAP has been one of the main and widely used as bioceramic materials for tissue engineering purposes.HAP is calcium orthophosphate containing water with a chemical composition of Ca_{10} $(PO_4)_6(OH)_2$. The chemical composition, structure and mechanical properties are similar to the mineral phase of human bone; the crystalline form of calcium phosphate ceramic[176]. The ceramics are commercially available in the form of dense, porous, as granules or blocks (with varying in pore sizes), porosities, and strengths [177]. Since 30 years ago, blocks and granules of porous HAP ceramics have been used in orthopaedic, dental or craniofacial surgery[178], [179].

HAP has been shown to have excellent biocompatibility, because it shows no sign of toxicity, inflammatory and progenetic response. It also has superior osteoconductivity, as it can bonds extremely well directly to the host bone and has good fibrous tissue formation implant between implant and bone[180].Tancred et al.

successfully made scaffolds from HAP, TCP, and HA/TCP in a ratio of 3:1 that substantially closer to cancellous bone. The scaffolds are biocompatible and have excellent osteoconductive properties [181]. Kitsugi et al. showed that the calcium phosphate ceramics ratio of calcium and phosphate (Ca:P) can be used as bone fillers for bone defects or bone cavities [182]. Besides HAP ceramics, other calcium phosphate ceramics including biphasic calcium phosphate ceramic (BCP) and tricalcium phosphate ceramic (TCP) have been demonstrated to be osteoconductive. For the past few years, many researchers has also investigates the possibility of HA and TCP in porous shape to act as tissue engineering scaffolds for cell and drug delivery [183].

Osteoconductivity is an important property for bone grafting materials, however, biomaterials may not positively stimulate bone formation as many researchers have had general thought. Past researchers reported that biomaterials can only be osteoconductive but not osteoinductive[176], [180], [182], [183]. They are five complex steps needed in order for the bone formation to occur by osteoinductive biomaterials [149]:

1) Attachment of mesenchymal cells on material surface,
2) Proliferation and differentiation of mesenchymal cells,
3) Bone matrix formation by induced osteogenic cells,
4) Mineralization of bone matrix and
5) Bone remodelling to form mature bone.

The time for different steps to happen varies with the osteoinductive potentials of calcium phosphate biomaterials. In 1998, Yuan and fellow colleagues has

investigated different type of calcium phosphate biomaterials and concluded that calcium phosphate biomaterials can be osteoinductive when they exhibit specific chemical and structural characteristics [184].

3.4.2 Calcium Pyrophosphate

Calcium pyrophosphate (CPP) is one of the types of calcium phosphate with a shortest linear polyphosphate. It is non-toxic and osteoconductive that can form good bonding with bone [182]. The ratio of calcium to phosphorus ratio (Ca/P = 1.0) is lower than that of tricalcium phosphate (Ca/P = 1.5) and therefore they are more soluble[185]. These properties have made it favourable to be evaluated as a possible bone replacement material.

The mineral phase of CPP is one of the intermediate products in the bio-mineralisation process and it regulates the onset of calcification in bone [186]. A small proportion of the total phosphate in normal bone salt occurs in the form of pyrophosphate ion[187]. Pyrophosphate ions are strong inhibitors of the crystallization of calcium phosphate. Polyphosphate ions are present in many tissues throughout the entire body, but they are most highly concentrated in osteoblasts. The high content of exopolyphosphatases, which split the orthophosphate ions off polyphosphate compounds, in osteoblast cells indicates that polyphosphate ions have a large effect on the formation and growth of bone mineral[188].The regulation process of feedback between alkaline phosphate and membrane plasmatic glycoproteis is considered to be very important for mineralization of bone[189].

3.4.2.1 Preparation of calcium pyrophosphate (CPP)

CPP is prepared through the dehydration and decomposition of brushite by heating treatment at 800 °C with the release of structural water according to the following equations[190]:

$$2CaHPO_4 \cdot 2H_2O \rightarrow 2CaHPO_4 + 4H_2O\uparrow \quad (3.1)$$

$$2CaHPO_4 \rightarrow Ca_2P_2O_7 + H_2O\uparrow \quad (3.2)$$

The transformation of brushite CPP on heating in air can be simplified as below [188]:

Transformation	Temperature (°C)
$CaHPO_4 . 2H_2O \rightarrow CaHPO_4$	60–100(in solution or with prolonged storage in air)
$CaHPO_4 \rightarrow \alpha\text{-}Ca_2P_2O_7$	270–500
$\alpha\text{-}Ca_2P_2O_7 \rightarrow \beta\text{-}Ca_2P_2O_7$	500–750
β-Ca2P2O7→α- $Ca_2P_2O_7$	1165

CPP has the same structure as potassium dichromate. There are three modifications of CPP, of which $\beta\text{-}Ca_2P_2O_7$is tetragonal and $\alpha\text{-}Ca_2P_2O_7$ is monoclinic. Their crystal structure is shown in Figure 3.4.In the temperature range 700 – 800°C CPP transforms into the $\beta\text{-}Ca_2P_2O_7$ modification, this is stable up to at least 1000°C. Table 3.6 present density value of monoclinic CPP is and tetragonal modification [188]. According to some data, on cooling, this high-temperature phase of CPP can remain in the structure of materials containing HAP as a second phase[37].

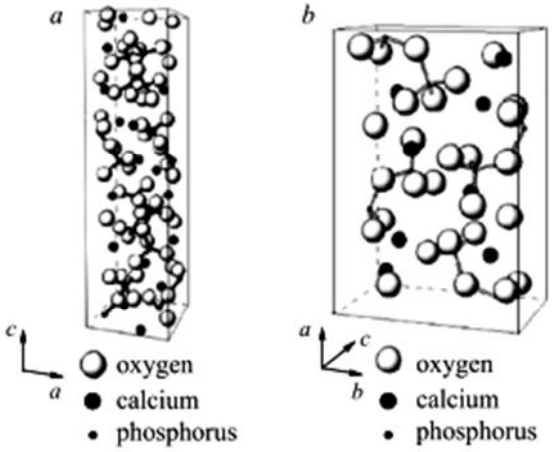

Figure 3.4 Crystal structure of β- $Ca_2P_2O_7$ (a) and α-$Ca_2P_2O_7$[188].

Table 3.6 Density value of monoclinic CPP is and tetragonal modification[188].

Card No.	CPP	
	Modification	Density (g/cm^3)
73-440	Monoclinic	2.936
9-345	Orthorhombic	2.950
33-229	Tetragonal	3.128
71-212	Tetragonal	3.129
81-2257	Tetragonal	3.127
9-346	Tetragonal	3.120

3.4.3 Solubility of calcium phosphate compounds

Solubility is one of the most important properties of calcium phosphate. Solubility is the property of materials to dissolve amount of solid into a unit volume of homogenous solution. Solubility determines dissolution, precipitation, and hydrolysis and phase transformation of calcium phosphate. It plays a major role in formation and resorption of hard tissue and pathological classification. For calcium phosphate, the solubility is depends on pH changes, temperature and concentration of acids and bases, such as HCl and NaOH[191].

While the forming method and exact stoichiometry will have an effect on solubility, the generally accepted order of solubility is:

$$ACP > DCP > TTCP > \alpha\text{-}TCP > \beta\text{-}TCP >> HAP$$

Table 3.7 Data on solubility of calcium phosphate [192].

Calcium phosphate	Ca: P ratio	pH interval	SP* at 37°C
Monocalcium phosphate (calcium dihydrophosphate), $Ca(H_2PO_4)_2$	0.50	< 1	soluble
Dicalcium phosphate dihydrate $CaHPO_4.2H_2O$	1.00	2-4	$10^{-6.63}$
Dicalcium phosphate (calcium hydrophosphate) $CaHPO_4$	1.00	2-4	$10^{-7.02}$
Octacalcium phosphate $Ca_8(HPO_4)_2(PO_4)_4.5H_2O$	1.33	6-7	$10^{-95.9}$
Hydroxyapatite $Ca_{10}(PO_4)_6(OH)_2$	1.50-1.67	>5	$10^{-117.2}$
Amorphous calcium phosphate	1.33	-	Not determined
Calcium pyrophosphate $Ca_2P_2O_7$	1.00	-	-
Tricalcium phosphate (calcium orthophosphate) $Ca_3(PO_4)_2$	1.50	-	-
Tertracalcium phosphate $Ca_4P_2O_9$	2.00	-	-

*the solubility product (SP) is the product of the concentrations (in respective degrees) of ions in the solution above precipitate. Thus, for hydroxyapatite $Ca_{10}(PO_4)_6(OH)_2$ $SP= [Ca^{2+}]_{10}[PO_4^{3-}]^6[OH^-]_2=10^{-117.2}$

Hydroxyapatite (HAP) is relative insolubility when compared to the other calcium phosphate phases as it is the only the calcium phosphate compound that is stable at pH's above 4.2. Below this, dicalcium phosphate dihydrate ($CaHPO_4.2H_2O$)

is the stable compound. It is not uncommon for unstable calcium phosphates to dissolve and reprecipitate as the stable compound at a given pH. Under normal physiological conditions of pH 7.2, hydroxyapatite is the stable calcium phosphate compound. This may drop to as low as pH 5.5 in the region of tissue damage, although this would eventually return to pH 7.2 over a period of time. Even under these conditions hydroxyapatite is still the stable phase [192]. Table 3.7 shows the data on the solubility of calcium phosphate.

Recent studies have shown the good osteoconductivity properties of CPP and improvement in bone mineral content during clinical observation. Kitsugi et al. [182] produced and implanted bulk dicalcium pyrophosphate ceramic into mature male rabbits and found the ceramic to be non-toxic and osteoconductive. It was reported that no fibrous tissue layer was formed at the bone and ceramic interface [182].]The mechanical strength of sintered $Ca_2P_2O_7$ ceramic was found to improve when a liquid additive, sodium pyrophosphate ($Na_4P_2O_7.10H_2O$) up to 5 wt%, was implanted in a New Zealand white rabbit. The bone tissue ingrowth into the macropores of the ceramic and gradually dissolved over time to be replaced by a bony structure [185], [193].

Sintered dicalcium phosphate (SDCPP) has been shown to be effective artificial bone filler for repairing bone defects. Sun et. al (1999) has evaluated the effect of SDCPP particle size on Newborn Wistar Rat osteoblasts. The addition of smaller sized SDCP particles (0.5–3.0 and 37–63 μm) into osteoblast culture has significant affect on the cell counts of osteoblasts and inhibit proliferation of the osteoblast [189].

CPP has also been explored as a possible treatment for osteoporosis, a common disorder which affects mostly affects elderly women and is characterised by increase bone resorption relative to bone formation. This occurs generally with an increase bone turnover. In 2002, Sun et al. has treated ovariectomized rats, a condition of increased bone turnover and higher bone porosity with sintered dicalcium pyrophosphate. They found increases in bone mineral content in long bones was higher and porosity of the trabecular bone was decreased in rats that ingested CPP than those which ingested alendronate [194]. Successive applications of these materials depend on the degree of bio-resorption, mechanical strength and bio-compatibility.

3.5 Ceramic Composite

Another possibility is the use of other materials, like polymers, that are physically or chemically mixed with a ceramic compound. The fabrication could include polymer/ceramic blends, precipitating ceramic onto polymer templates, and coating polymers onto ceramics[117]. Examples of polymers that are commonly used in combination with ceramics are the polylactic acid-based polymers [195] and biopolymers like chitosan[196] and collagen[197]. By combining polymer and ceramic into one composite material, minimize the drawbacks but maintain the advantages-increase the bioactivity and bio-mimicking of the matrices formed.

Advantages of polymer.

i) Vast array of polymers available with varying mechanical properties, degradation times and physical structure. Also the inherent strength and biomimetic nature of ceramic

ii) Reduce the overall brittleness.

Advantages of ceramic

i) Increase bioactivity and its capacity to take up and deliver factors and therapeutic substances.

Calcium phosphate cement (CPC) has been extensively studies as bone replacement for the past decades. To make a CPC, Chen et al. [198] has developed a calcium phosphate cement (CPC) of tetracalcium phosphate/dicalcium phosphate anhydrous (TTCP/DCPA)-polyacrylic acid based. The polymer phase is important in dentistry as luting materials in the composite, as polyacrylic acid is proved to adhere to tooth mineral or bone and thus could also be applied as biomaterials. The polymer could also acts as processing aids especially in high shear mixing of, for example, polypropylene (PP) and TCP. PP could improve the plasticity and processibility of the composite, as studied by Kalita et al. [173]. The study shows the promising application of the controlled porosity polymer-ceramic composite scaffolds.

Rhee and Tanaka has synthesized ceramic nanocomposite compromised of hydroxyapatite/type II collagen/chondroitin sulfate nanocomposite through a novel precipitation method [199]. Type II Col has been known to provide specific binding sites to chondrocyte via integrin and ligand interactions whilst ChS proteoglycan stimulates chondrocytes adhesion. The nanocomposite may be applicable for use as a

bone substitute, as it is expected to provide specific binding sites to chondrocyte, which is vital in bone remodelling.

A novel biodegradable nanocomposite porous scaffold, comprising of β-TCP and HAP nanofibers were integrated with monomers (acrylamide, methylenebisacrylamde), was developed by Ramay and Zhang in 2004 [21]. The inclusion of HAP nanofibers as a second phase in β-TCP porous ceramic has better mechanical properties than the scaffolds of single-phase calcium phosphate prepared previously.

A.M. El Kady et al has prepared composites containing CPP powder into the copolymer matrix containing the grafted chitosan or grafted chitosan–gelatine [200]. They found that the CPP powder had induced a bone-like apatite layer onto the surface particles. As a result, the compressive strength of the CPP/polymeric composites was comparable to those of cancellous bone. *In vitro* test results showed that CPP/chitosan and/chitosan–gelatine polymeric composites successfully promoted the formation of apatite onto their surfaces, especially the CPP composites containing chitosan–gelatine matrices. [200].

3.6 Polymer Ceramic in Microstereolithography

3.6.1 Principle and theory

In ceramic MSL, the photo-curable resin is a combination of monomers, photoiniatiators and ceramic powders, and is normally called a ceramic suspension. The green body of polymer ceramic is build when the ceramic particles in the suspension are bonded by the polymer through UV polymerization. MSL of ceramic suspension is much more complicated than the MSL of pure polymer. A conventional

resin is absorbing medium and the attenuation of the light energy with depth can be accurately modelled with Beer's Law:

$$E = E_o \exp(-\gamma L) \qquad (3.3)$$

where:

E= energy density

L= depth

Υ = extinction coefficient

In the ceramic MSL, the light scattering becomes significant when the light propagates through the highly concentrated ceramics suspension. When a photon travels through the ceramic suspension, it is scattered by ceramic particles and its direction of propagation will be changed. Consequently, the photon is absorbed either by the photo-curable solution or the ceramic particles. The portion of the initial photons absorbed by the photo-curable solution will initiate the polymerization reactions. [201].

Curing depth and curing radius are the two critical parameters in MSL. A dose of light/UV of energy *E* will cause polymerization to a depth C_d as described by the Jacob's equation;

$$C_d = D_p \ln[\frac{E}{E_c}] \qquad (3.4)$$

Where C_d is cure depth, E is energy density, D_p is depth penetration and, E_c is critical exposure. Depth penetration, (D_p) for the ceramic suspension is controlled by the particle size (*d*) an inversely proportioned to the volume fraction (φ) of ceramic

and strongly dependent on refractive index diffraction between ceramic and the photo-curable solution (Δn). β is the interparticle spacing and the UV wavelength. The complexity of the process is shown as the below [202];

$$D_p \approx \beta \frac{d}{\varphi} \frac{1}{\Delta n^2} \qquad (3.5)$$

Based on the equation above, particle size and the refractive indexes of the ceramic powder and the solution are additional factors that influence the line width and the curing depth in ceramic stereolithography. A minimal curing depth and curing radius are essential to ensure strong bonding within the whole microstructure and to achieve high spatial resolution [203]. To identify the spatial resolutions of MSL, the mechanism of light scattering due to the particles suspended in monomer solution is the most important to determinant.

3.6.2 The influences of the particle size and its distribution on microstereolithography of ceramic composite

According to the light scattering theory, both particle mean size and distribution affect light scattering. In a typical ceramic MSL process, the mean size of the ceramic particles varies from 0.3 to 1 μm. Strong light scattering will occur when the particle size is close to the wavelength of UV light (0.364 μm) [204]. As the scattering effect becomes stronger, the incident photons will more likely be scattered into the surrounding area and consequently, fewer photons can penetrate deeper. The result suggests that a particle size larger than 0.5 μm is preferred to eliminate the scattering effect in the ceramic MSL. The scattering effect in ceramic MSL can be greatly minimized by choosing the ceramic particles that have the refractive index close to that of the solution [204].

3.7 Sintering of A Polymer Ceramic

Sintering is an important step in the fabrication process of ceramic bodies, which involves consolidation of ceramic powder particles by heating the green body to a high temperature below the melting point. Sintering process may be conducted in different atmospheres, for example air or an inert atmosphere. The process occurs in three stages: an initial, intermediate, and final stage. These stages significantly affect the microstructure and properties of materials. Figure 3.5 shows the illustration of the sintering stages.

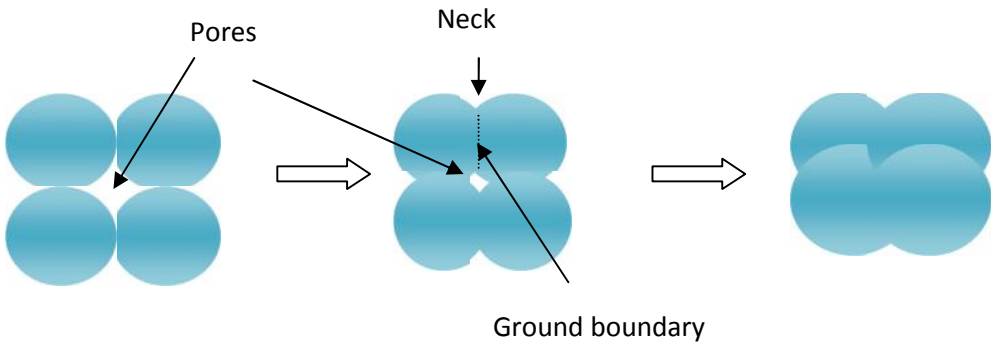

Figure 3.5 Schematic illustrations of stages in sintering process; (i) initial, (ii) intermediate and (iii) final stage [205].

In the initial stage, the green body of calcium phosphate has a low-density and is generally lacking in physical integrity. There is a small degree of adhesion between adjacent particles. Then, the necks begin to form as their vapour-solid interfaces decreasing at the contact points between the particles. This neck occurs due to the reduction of surface energy between the particles, in this intermediate stage, hence the porosity reduced. In the final stage, diffusing happens where the separate particles start to diffuse to the neghbouring's powder particles and diminish or even close up the pores and promote densification of the materials[205]. The degree of porosity

after sintering is determined by the level of the initial porosity of the green body, sintering temperature and time. In addition, pore size, porosity and pore size distribution at the sub-micron level can be controlled by sintering at different temperatures. Calcium polyphosphate for instance is sensitive to the sintering temperature; its crystalline phases may be transformed even in a narrow temperature zone[206]. Past studies has shown that throughout the sintering process, the amorphous calcium polyphosphate is firstly transformed to γ-CPP, then to β-CPP and finally is transferred α-CPP. The chronology transformation of the calcium polyphosphate is shown as following:

$Ca(PO_3)_2$	25 – 580°C	amorphous $\gamma-Ca(PO_3)_2$ [207]
	585– 600°C	$\gamma-Ca(PO_3)_2$[208]
	600– 700°C	$\beta-Ca(PO_3)_2$[208]
	900– 960°C	$\alpha-Ca(PO_3)_2$[209]

During sintering process, linear shrinkage of the ceramic composite is inevitable. It is distributes by:

i) Loss of polymer in the early stages

ii) Loss of porosity at the sintering temperature

In order to avoid deformation and cracking during polymer removal, to reduce shrinkage during sintering and to obtain homogenous and dense ceramic pieces after sintering, the organic concentration in the suspension should be minimized [210]. After sintering, due to the changes on the morphology, the microstructure, phase composition and phase purity has resulting no improvement of its mechanical properties [211]. Wang et al. has investigated the effect of sintering time on the

microstructure, degradability and mechanical property of CPP bioceramics synthesized by gravity sintering. They have discovered that the that CPP has different microstructures and properties with relative density, grain size and mechanical property of CPP increased and the degradation rate decreased as the sintering time increased [205], [206].

3.8 Conclusion

The extensive research has been performed in developing better materials for tissue/bone/organ replacement, which has been the driving force in the tissue engineering field. The ultimate goal is to find biomaterials that have the mechanical and physiologic bio-mimicryto fulfil the demands of the host tissue .Calcium phosphate ceramics are the most common and interesting bioactive materials, due to their similarity between their surface composition and structure with the mineral phase of bone.

The major drawback of bioactive ceramics is their low fracture toughness; brittleness and being non-osteoinductive and non-osteoconductive in nature .Bioceramics are often used in combination with a biodegradable polymer in order to find the optimum mechanical and biological performances. Nevertheless, with the current activity in materials selection and 3D fabrication, the search for a3D scaffold with an interconnected pore network of tailored structure, morphology and mechanical properties suitable for a given application, is looking bright and promising. It is thus anticipated that the further knowledge gained from this research will help bring the required technology to the field of tissue engineering.

CHAPTER 4

The Development of Three Dimensional (3D) Fabrication Apparatus

4.1. Introduction

A material that can be used as a tissue engineered scaffold must satisfy a number of requirements. These include biocompatibility, biodegradation to non-toxic products (within the time frame required for the application), and process ability into complicated shapes (with desired porosity). Furthermore, the ability to support cell growth and proliferation and appropriate mechanical properties, including maintaining mechanical strength during most of the tissue regeneration process.

In this project, microstereolithography has been chosen as a means for the creation of 3D tissue scaffolds. It offers a unique way to precisely control matrix architecture including size, shape, interconnectivity, branching, geometry and orientation, which will yield biomimetic structures varying in design and material composition. Currently, biopolymers that are in use are based on polyesters such as polycaprolactone (PCL) or polyhydroacids (PHA), copolymer of lactic and glycolic acid. These materials are not suitable for the fabrication of scaffolds, by direct or indirect methods using stereolithography, as they can only be processed by melting or in solution. On the other hands, polyethylene glycol (PEG) with an acrylate group is a suitable candidate for this kind of rapid prototyping technique. PEG has useful characteristic properties, such as high hydrophilic, good tissue biocompatibility, lack

of toxicity and availability of reactive sites for chemical modification, whereas acrylate monomers are known for their high reactivity and polymerise rapidly in the presence of photogenerated free radicals. It produces strong crosslinked bonds between acrylate groups and has showed promising biocompatibility from cellular tests [111], [195], [212].

This chapter focuses on the stereolithography apparatus, both commercial and-in house systems, used in this project. Before deploying a commercial system, some initial material development was undertaken using existing hardware with the School of Engineering. This allowed some understanding of the process to be achieved, with small volumes of test material, before moving to a commercialise setup. The equipment that was developed in this project were:

1. Light projector and;
2. UV light engine;

This development involved transferring and modification of a non-functional Envisiontec system and a high power ultra-bright light emitting diode (LED) device, which emits light at wavelengths similar to the Envisiontec Desktop projector (365 nm).

To benchmark the in-house equipment to the commercial system, a standard commercial resin (envisionTec's R11) was used. This would allow characterisation of layer-by-layer formation and curing process this equipment produced before moving to new materials. Mechanical characterization of the polymerized samples was also performed in this study to aid characterisation of the cured resin. Due to the small dimension of the built area on the instruments, a Deben Microtensile tester (Deben,

United Kingdom) was chosen as a means to measure the tensile strength of the samples. Soares et al (2008) studies show that dumbbell-shape sample is a suitable shape for microtensile test, as it improves stress distribution compared to rectangular and hourglass-shape samples [213]. In these study, different dimension of dumbbell-shape were prepared in order to find the right dimension with homogeneous stress distribution tailor-made to the Deben Microtensile tester.

4.2. Development of Light Projector

4.2.1 Materials and methods

A decommissioned Envisiontec Perfactory® Mini was acquired from the Microsensor and Bioelectronic Laboratory, University of Warwick. The current and well functional Envisiontec Perfactory® Mini consists of a projector (containing: dynamic mask modulator (with a DMD chip), visible light source, focusing optics with shutter), a build platform (photoreactor), a Z-stage for moving the base (build platform) and an embedded PC, which allows the system to work independently from the pre-processing workstation [214]. Out of the non-functional system, the projector was recovered, which was operational, and deployed in developing new materials. In addition, the light projector could be fitted into a fume hood cupboard to remove any issues of exposure to any fumes from the materials.

To ensure that the projector was directly equivalent to the present machine, the wavelengths of light from both the recovered projector and the present Envisiontec system were measured with a spectrophotometer (USB 2000+, Ocean Optic, UK) and compared. As shown in Figure 4.1, the wavelength of the projector was almost

identical to the present system, though the amplitude was reduced probably due to the age of the light source within the projector.

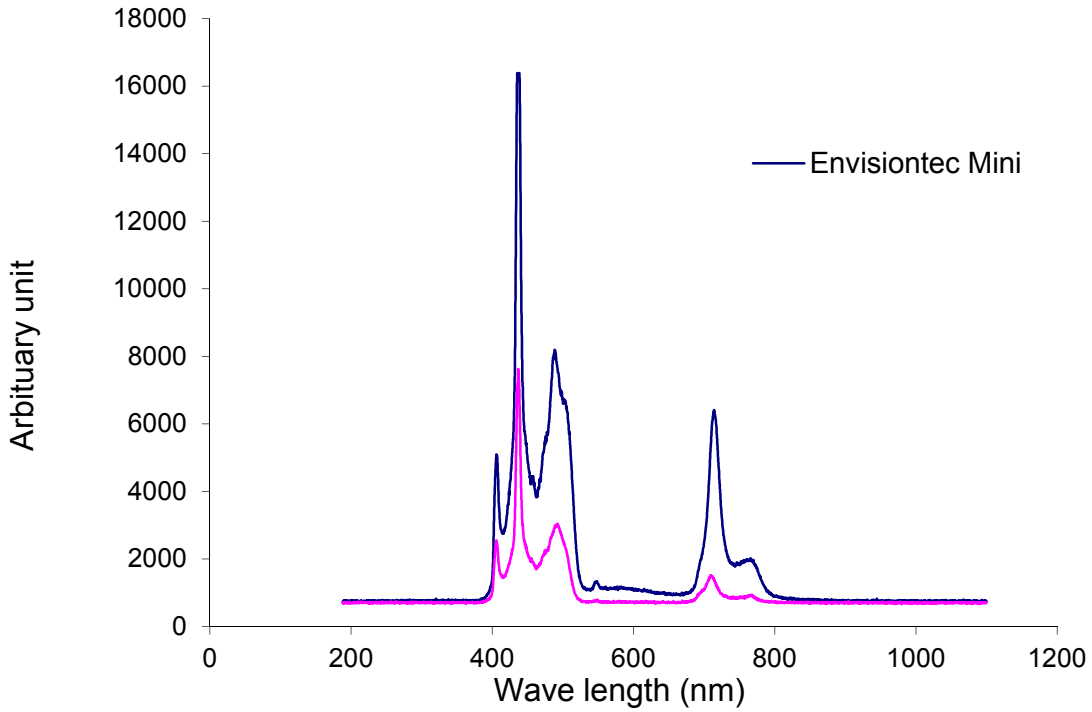

Figure 4.1 Spectrum of wavelength between the Envisiontec and recovered projector.

In order to replicate the working principle of the SLA, some modification had to be made on the projector. Firstly, the focus point of the light projector was determined and a steel framework was built. A 60 × 60 mm glass plate was fitted on top of the steel frame to act as the basement for the machine. This plate was cut from an old build platform from the Envisiontec Perfactory Mini System. To determine the focal length of the lens, a piece of paper was placed on the glass plate and the light focussed through it until a focal point (a dot of focussed bright light) was spotted by adjusting the height of the steel framework. The focal length was determined at 35 ± 0.1 cm. Finally, stainless steel mould, with a dimension of 30 × 40 × 30 mm and with

5 holes of 5 mm in diameter, was fabricated. The mould was used to polymerize the acrylate in small volumes. Figure 4.2 shows the modified light projector.

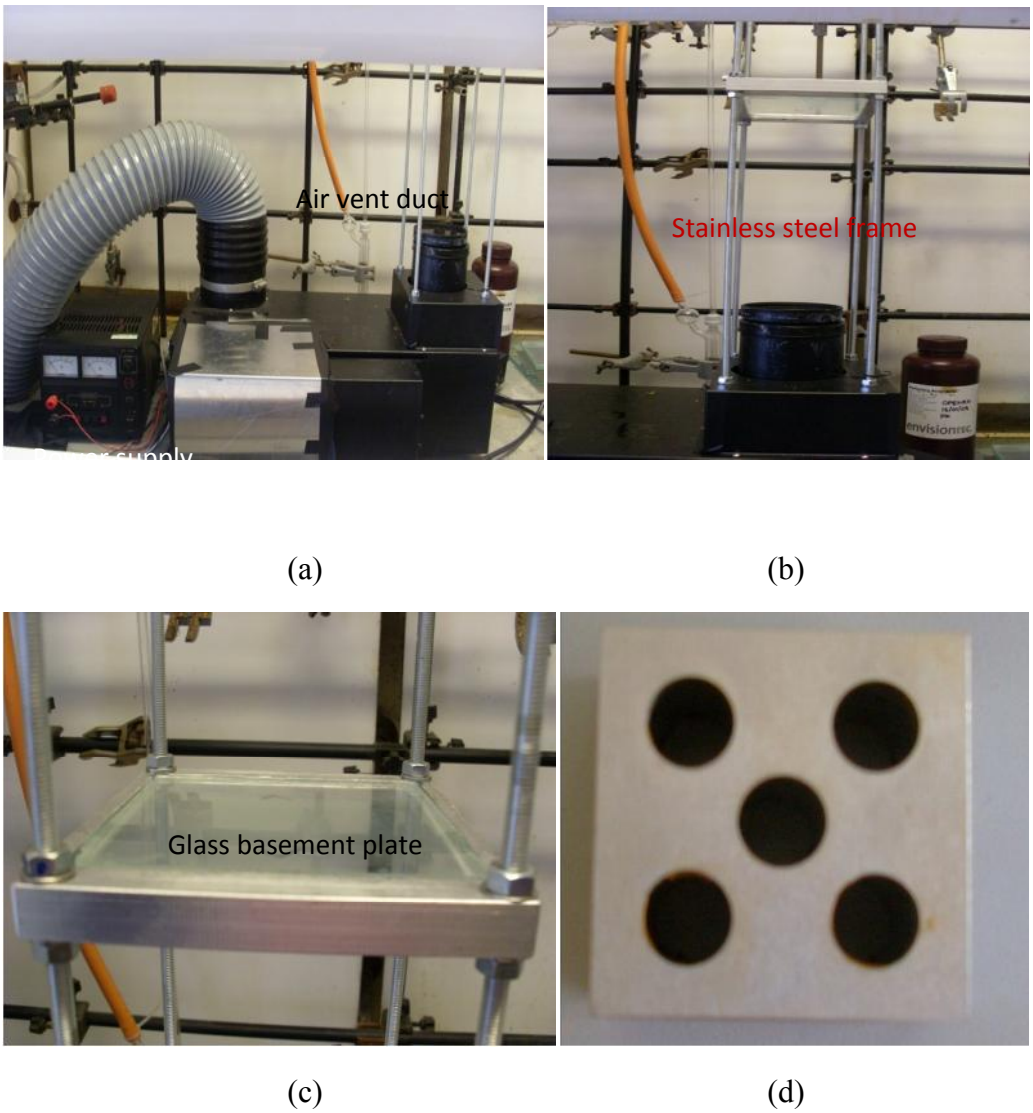

Figure 4.2 (a) Modification of recovered Envisiontec Perfactory, (b) designed stainless steel frame, (c) glass basement plate and (d) stainless steel mould for layer curing determination.

R11 is a photo-reactive acrylate that was chosen as a control material. It is the standard commercial resin that is used within the Envisiontec systems. It is a liquid, orange, poly-methyl-methyl-acrylate resin that only requires a high-pressure mercury vapour lamp to stimulate photopolymerisation. Table 4.1shows the composition and properties of R11, as supplied by manufacturer [215].

Table 4.1 Properties of photo-reactive acrylate resin, R11 [215].

Composition (%)	
Acrylic oligomers	40-70
Dipentaerythritol pentaacrylate	0-20
Propoxylated trimethylol propane triacrylate	< 5
Photoinitiator	0.1-0.5
Stabiliser	0.1-0.5
Properties	
Tensile strength	54.0 MPa
Elongation at break	3.70 %
Elongation at yield	7.94 %
Flexural Strength	87.9 MPa
Flexural Modulus	2250 MPa
Density	1.219 g/cm³
Glass Transmission Temperature	151 °C - 192 °C

About 1 ml of R11 was put into each of 3 holes of the mould and exposed to the light for 10, 20, 30, 40, 60 and 120 s. After each curing time, the cured resins were removed and cleaned with isoproponal in a beaker to remove any uncured resin on its surfaces. To study the layer controlled of the light projector, Form Talysurf (Taylor Hobson, UK) was used to measure the thickness of the sample Figure 4.3 shows the results of sample thickness of R11. An increase in thickness as a function of increased exposure time was measured. This is expected as the resin, R11, is a highly reactive photopolymer. In addition, Figure 4.4 shows the colour intensity, as the time of exposure increased, which is in line with the sample thickness increment.

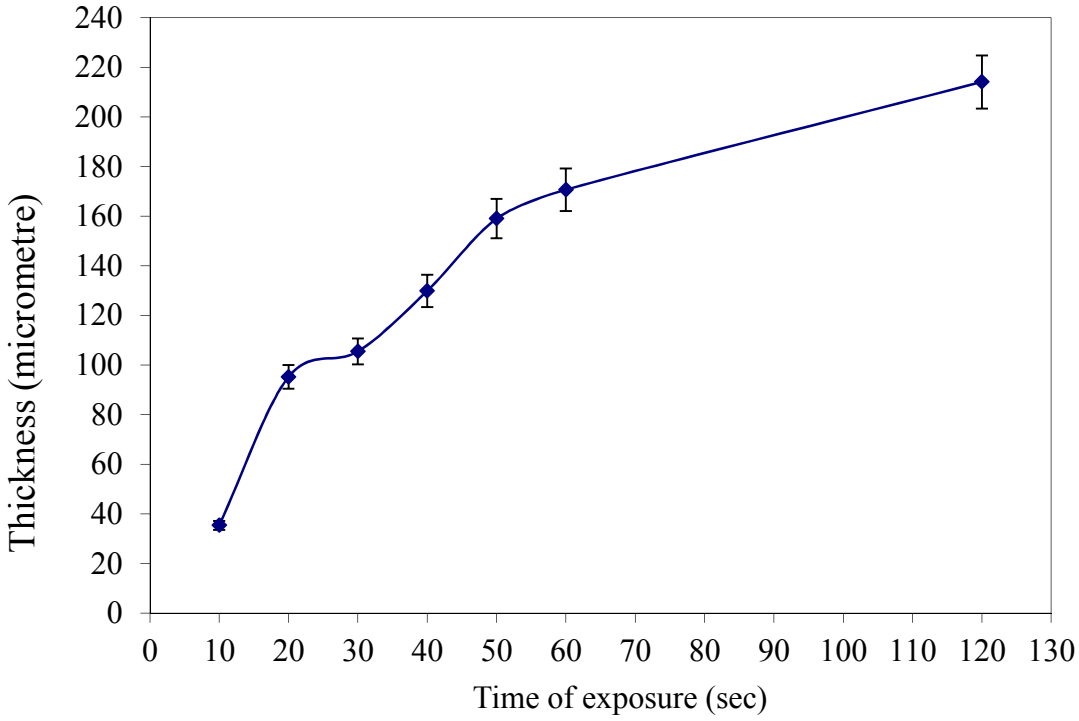

Figure 4.3 Sample thickness of Rll versus the time of exposure (average of there samples).

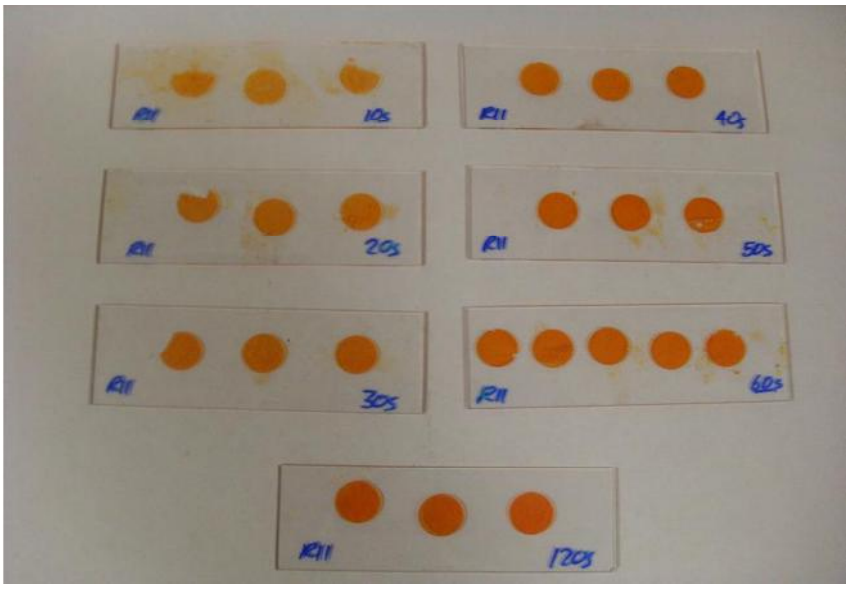

Figure 4.4The fully cured of R11 resin.

R11 resin was successfully cured and layer thickness for each time of exposure was determined. As expected, the thickness of cured resin was increased as the time of light exposure increased. However, the presence of a photoinhibitor in R11 limits the total maximum thickness of each layer. Unfortunately, the equipment has no vertical moving parts, thus cannot be used to form multi-layer structures. The commercial system contains these moving components. Figure 4.5 show a moving stage in envisionTec Perfactory Mini.

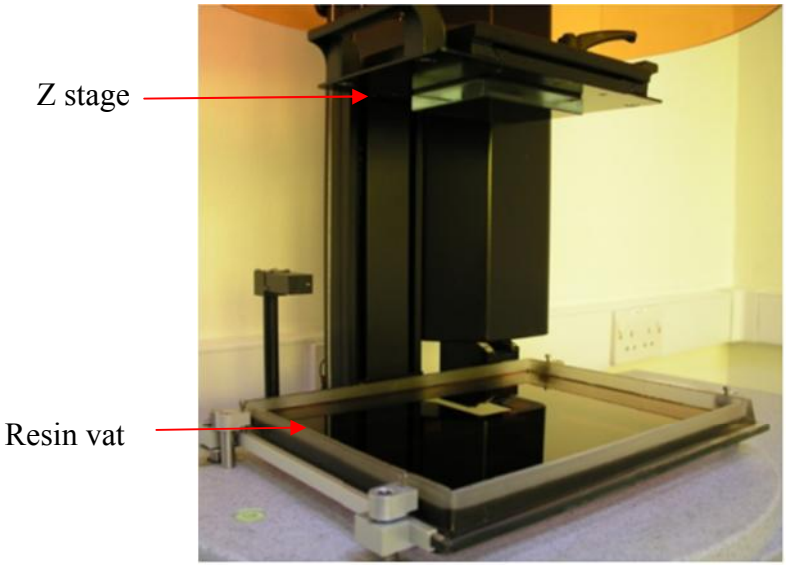

Figure 4.5 envisiontec Perfactory Mini

Development on formulation of new photopolymer resin is not favourable with this modified equipment unless a Z-stage or elevator is to be introduced to the modified machine. Due to time constraint, and lack of knowledge in the mechanical/electronic field by the author, it was decided to purchase a smaller version of Envisiontec Perfactory® SXGA^{+} W/ERM Mini Multi Lens; a Desktop Digital Shell Printer (Desktop) for materials development purposes. The desktop only

requires a small volume of photopolymer resin; less than 400 cm^3 and with some modification on the resin tray the volume could be reduce to 40 cm^3.

Desktop Digital Shell Printer (Desktop) is a rapid manufacturing system manufactured by envisionTec GmbH, Germany especially for hearing aid applications. It was purchased to further develop materials for photopolymer formulation as the modified light projector did not satisfy the project's objective. The Desktop is a relatively low cost (sub £30k), easy maintenance and user friendly machine, using state of the art Digital Light Processing (DLP®) technology from Texas Instruments®. Figure 4.6 and Table 4.2 show the Desktop available in the Microelectronic and Biosensor lab, and specification of the machine respectively. Like most of 3D fabrication, the Desktop has a built in Ethernet interface and can be connected directly to a PC workstation, and integrated into a network.

Figure 4.6 envisionTec Desktop Digital Shell Printer (Desktop).

Table 4.2 Specification of the machine extracted from the envisionTec homepage [218].

Machine properties	
Lens system	Fixed focal UV lens
Build envelope XYZ (±2mm)	100 x 75 x 100 mm
Native voxel size XY	71 µm
Dynamic voxel thickness Z	25 µm to 150 µm
Resolution SXGA	1400 x 1050 pixel

The Desktop was used as a microstereolithography apparatus for the fabrication of the formulated photopolymer resin both for soft and hard tissue applications described in this thesis.

4.3 Optimisation of Test Piece Shape for Mechanical Characterisation on 600N tensile stage Deben Microtester

4.3.1 Strength of materials

When designing or formulating new materials for any application, the properties and mechanical characteristics of the materials are very important to investigate. Strength, hardness, toughness, elasticity, brittleness, and ductility are amongst the mechanical properties used as measurements of how materials behave under a load. The new materials are subjected to a wide variety of mechanical tests to measure their strength, elastic constants, and other material properties as well as their performance under a variety of actual use conditions and environments. Mechanical tests often involve the deformation or breakage of samples of material.

Tensile strength is the stress needed for a sample to develop necking and finally break at the fracture point before it fails. Figure 4.7 shows the engineering stress-strain curve and illustration of tensile characterisation. Strength is highly dependent on microstructure because it is proportional to the difficulty of moving

dislocations through (and between) the grains boundary. The way tensile strength is measured is dependent upon the type of material. For ductile materials, tensile strength is measured by their ability to return to its original state in an elastic manner. The measurement could also apply for permanent deformation after the load has been removed from the material or until the materials become weakened and brittle after cyclic loading. For brittle materials, such as ceramic and concrete, the starting point for a crack or a break in materials is the indication of the tensile strength of the materials. If one applies a large enough load to a ductile material (of uniform cross-section) plastic deformation will result in the following (typical) behaviour.

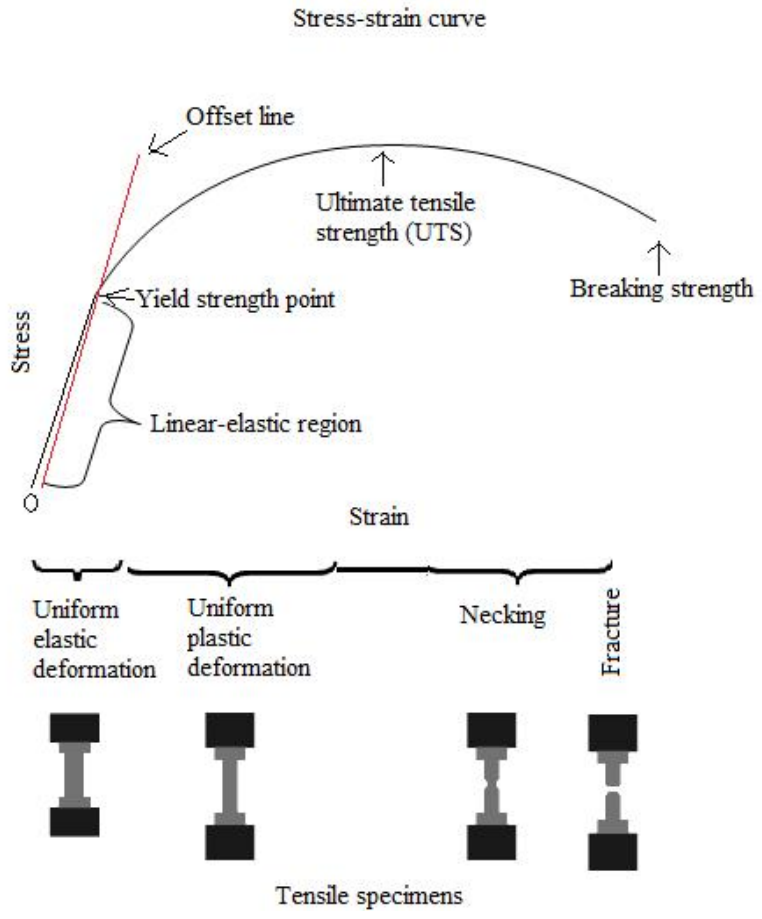

Figure 4.7 A typical stress-strain cure of a material (www.ndt-ed.org)

The stress-strain behaviour of a material is dependant predominantly on the strain rate, temperature, and environmental conditions. The tensile stress (σ) on a material is defined as the force (F) per unit area (A) as the cross-sectional area may change if the material deforms when subjected to force.

$$\sigma = \frac{F}{A} \qquad (4.1)$$

Whilst strain measures the change in shape of a material when a force is applied.

$$\varepsilon = \frac{\Delta L}{L_o} \qquad (4.2)$$

ΔL = change in length and L_o= original length.

Since strain is always a ratio of lengths then it is unit-less. Young's modulus is the slope of stress to strain. It is shown at the initial part of the stress-strain curve (Figure 4.7) and represents the linear-elastic region. At this region, there is no permanent deformation if the load is removed. It also is called the modulus of elasticity or the tensile modulus.

Compressive strength measures the capacity of a material to withstand axially directed crushing forces and the deformation at various loads. The compressive strength is calculated from the failure load divided by the cross-sectional area resisting the load and reported in Megapascal (MPa). Typically, the compression strength for polymer is higher than in tension while for ceramics it is much larger than the tensile strength. The test indicates the maximum compressive stress that a material is capable of developing.

4.3.2 Mechanical characterisation on Deben Microtester

Microtest modules have been specifically designed to allow real time observation of the high stress region of a sample with an SEM, optical microscope, AFM or XRD system. The 600N tensile stage uses standard miniature load cells in the range 2N to 600N was purchased for this project (Figure 4.8). Samples are mounted horizontally, clamped to a pair of jaws and supported on stainless steel slide bearings. A dual threaded lead-screw drives the jaws symmetrically in opposite directions, keeping the sample centred in the field of view.

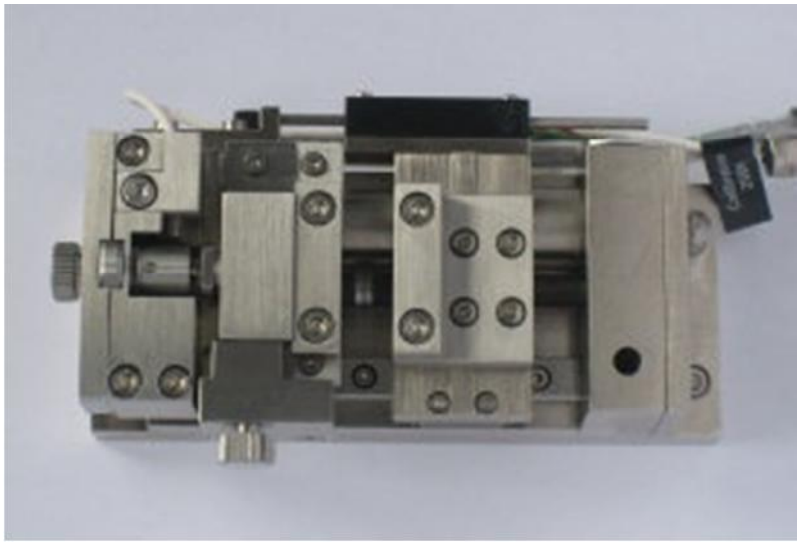

Figure 4.8 Deben Microtest machine

Mechanical characterization of the polymerized samples was performed to study the properties of materials after curing. Due to the small dimensions of the built area on the Desktop, a 600N microtensile stage from Deben, United Kingdom was purchased for this project as a means to measure the tensile strength of samples. Microtensile test permit a more homogeneous stress distribution on the mechanical loading device and the stress distribution is influenced by the test piece shape. Soares et. al [213] has investigated the effect of stress distribution inside 3 types of testing

specimen; rectangular, hourglass-shaped, and dumbbell-shaped, all with a 1 mm^2 cross-sectional testing region (Figure 4.9). The study shows that dumbbell-shape sample is a suitable shape for microtensile test as it improves stress distribution compare to rectangular and hourglass-shape samples [213].

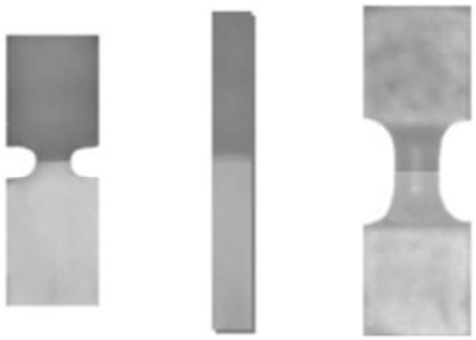

Figure 4.9 Microtensile specimen shape as investigated by Soares et. al. [213]; (a) rectangular, (b) stick and (c) dumbbell shape.

In these studies, different dimensions of dumbbell-shape were prepared in order to find the right dimension, with homogeneous stress distribution, tailor-made to the Deben Microtensile tester.R11 was chosen as the control sample. To find the optimum size and dimension of the dumbbell shape, ten sets of test pieces with varies gauge length of 4-6 mm, thickness of 1.5 mm, width 3 mm and length 26 mm were fabricated and then subjected to tensile test. The optimum design is determine by 2 characterisations:

1.) A good breaking point anywhere along the gauge length as shown in Figure 4.10 and;
2.) Tensile strength is comparable to the properties given by manufacturer; 54 MPa.

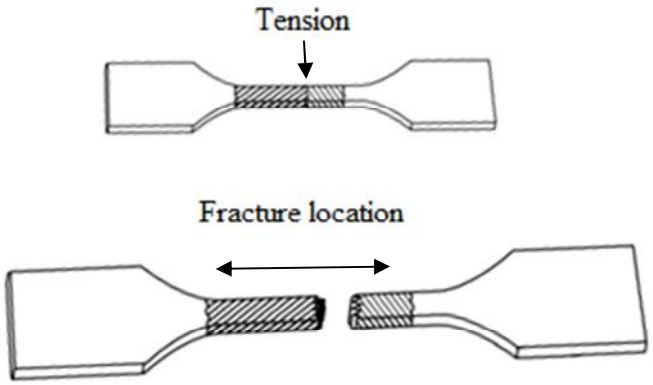

Figure 4.10 Schematic illustration of acceptable breaking point (marked as dark area).

Stereolithography technique offers free-mould 3D fabrication. The different gauge length of dumbbell shape was designed with Solidworks 2006, a 3D mechanical CAD program and saved as 'STL' (stereolithography) file. The 'STL' files were then transferred to the Desktop. The 3D object is then sliced to 2D layers using the Desktop application software and manufactured on the Envisiontec machine. In this system, the DMD has an array of mirrors 1400 x1050with each mirror measuring 13 μm to define the each shape of specimen. The wave length and curing time were set to 490nm and 6 sec respectively.

4.3.3 Results and Discussion

Table 4.3 Data collection on microtensile measurement with different gauge length.

Specimen	Gauge length (mm)	Number of test pieces with acceptable fracture location	Tensile strength (MPa)
A	4	3	-
B	5	5	27
C	6	7	38
D	7	4	-

*Number of test piece before tensile measurement was 10 pieces.

Based on Table 4.3, only specimen B and C, were acceptable for tensile strength measurement as both of these test pieces produced more than 5 specimens with acceptable fracture locations, compared to the other specimens. Sample C, showed the highest tensile strength compared to sample B, thus specimens with a 6 mm gauge length appeared to be the optimum length for tensile strength measurement. Figure 4.10 shows the optimum design of dumb-bell shape for Sample C.

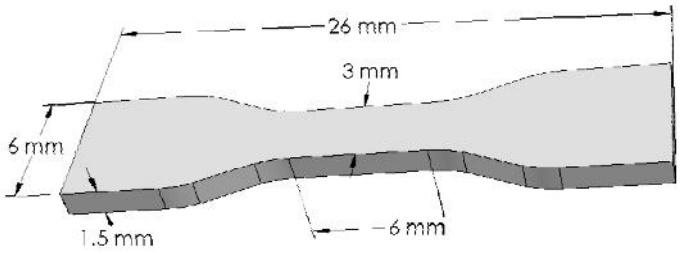

Figure 4.11 The optimum dumbbell-shape for microtensile characterization.

On the other hand, sample C only satisfied one requirement as an optimum design for tensile strength measurement i.e. acceptable fracture location. Nonetheless, the value of tensile strength is still 63% less than the manufacturer's technical data. In order to satisfy the second requirement of being the optimum design of dumb-bell specimen, the curing time during fabrication was prolonged to 9 sec. It is believed that the longer curing time will strengthen the bonding between each layer. Figure 4.12 represent the stress-strain curve of the dumb-bell shape after exposed to a blue light pattern for 6, 9 sec for 5 repeatable samples.

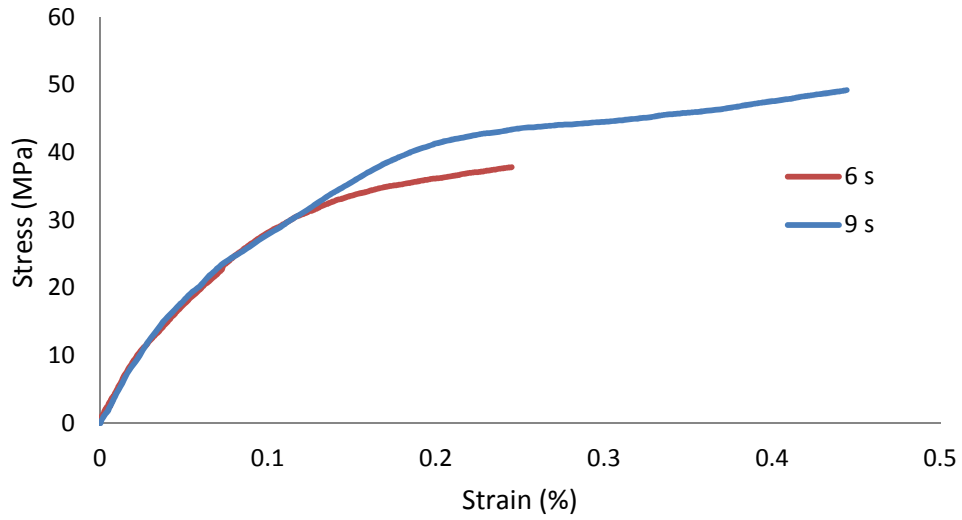

Figure 4.12 Stress-strain curve of R11 for difference time of photocross-linked exposure tme (5 repeatable samples).

The tensile strength, for the selected design of dumb-bell shape, after 6 sec and 9 sec of exposure was 38 and 49 MPa respectively. This shows that 9 sec of exposure time is favourable as it yields a value only 9% off the manufacturer's value (54 MPa, this is for a bulk material – not based on a layered process) compared to 6 sec with 30% off manufacturer's value. These results indicate that 6 sec is insufficient to fully cure each layer, consequently reducing the amount of polymer branching during crosslinking between each layer, thus the sample could only attain 0.25% strain before its failure. Even though, the Young's moduli for both samples are similar at 576 MPa, but after 0.15% strain only the samples with 9s of exposure had higher yield strength.

The evidence is in the increased value of stress for 9 sec samples. The increment of stress occurs because of strain hardening, when the cross-sectional area decreases, becoming greater than the increase in load carrying. Further imposed stress has resulted in strain concentration at the 'necked' portion of the sample, indicating

the failure of the sample. This shows that further curing time, during fabrication, results in drastic improvement in strength as it corresponds to the fully crosslinking of the polymer branches.

4.4 Fabrication of Three Dimensional Structures (3D) of Bioceramic on Enfis UNO AIR LE (Light Engine)

Currently, bioceramics have drawn worldwide interest as a substitute for bone grafts materials as they have similar composition to natural bone, osteoinductive and osteoconductive properties, low density, and chemical inertness. Rapid prototyping techniques such as microstereolithography have an excellent advantage for fabricating 3D tissue engineered structures, i.e. their ability to manufacture predefined macrostructures or microstructures of complex shapes in shorter time. As discussed in the previous chapter, they are limited by the number of different photosensitive resins. This section discussed the design and development of a new MSL apparatus, employing the Enfis UNO AIR LE also known as “Light Engine”. Here, polymer ceramic formulation was developed by mixing hydroxyapatite with polymer acrylate. The designed Light Engine allows development of new resin formulation without the restrictions of light level, exposure time, photoinhibitor etc. produced by the Desktop. In addition, it also allows exploring of materials with a lower cross-linking frequency.

Enfis Light Engine (Figure 4.13) is a high power ultra-bright LED device, which compromise density array up to 100 LEDs within 0.5cm^2 apertures. It emits light wavelength similar to the envisiontec Desktop projector, 365 nm. Table 4.4explained the electro-optical characteristic of the Light Engine

Figure 4.13 Enfis UNO AIR LE from Enfis, UK or known as Light Engine.

Table 4.4 Electro-optical characteristic of Light Engine as supplied by manufacturer [219].

Colour	Peak wavelength (nm)	Typical light output (mW)	Total electrical power (W)
SUVA	365	600	18
UVA	375	1150	18
Violet	405	4900	38
Blue	465	5750	38
Green	520	1850	38
Amber	595	1150	30
Red	630	3890	30
NIR	870	1750	16
Neutral white	3900-4600K	-	38

4.4.1 Designed of Enfis Light Engine

The basic requirement for a microstereolithography system is:

1. Light source
2. Focusing lens
3. Resin tray
4. Elevator/Z-stage

Figure 4.14 demonstrates the designed light-engine based microstereolithography apparatus used in this project. The basic frame was built similarly to the designed and development in the light projector (section 4.2).

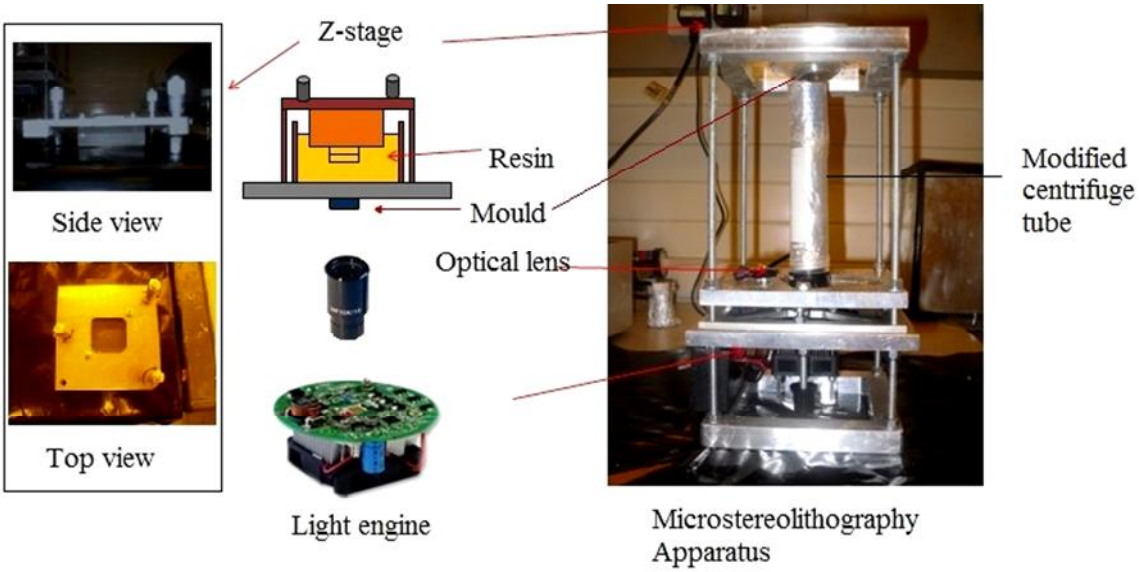

Figure 4.14 Microstereolithography system developed from Enfis Light Engine.

Different to the Light Projector, the Enfis Light engine requires a focusing lens to control and focus the ultra bright LED, thus the typical microscope lens was used and stationed on top of the Enfis Light engine, as shown in Figure 4.15. The length of focal point was determined similarly to the Light Projector method in section 4.2.

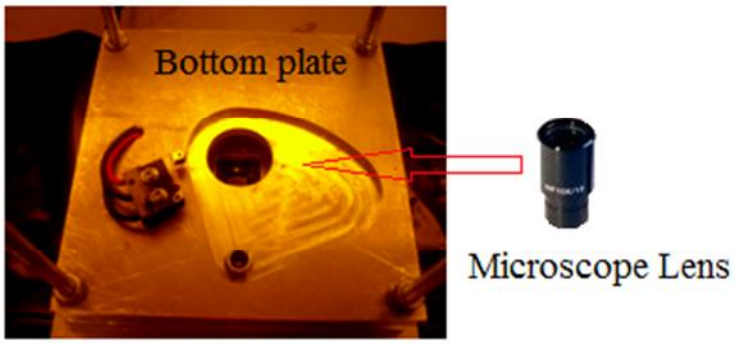

Figure 4.15 Bottom plate of Enfis Engine light system.

The Z-stage was designed based on a manual elevating system, where 3 pieces of 10mm ratchet stop micrometer heads were mounted on a stainless steel plate (Figure 4.16).

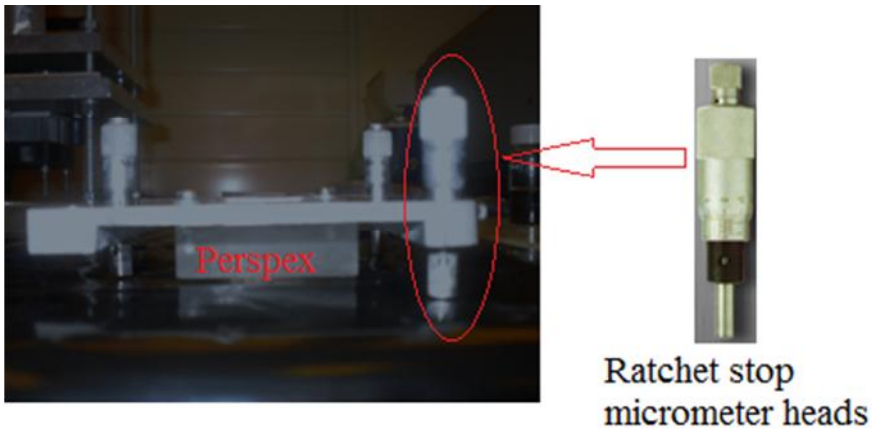

Figure 4.16 Close-up on the designed Z-stage

For preliminary study of ceramic polymer resin formulation, only a small volume resin vat was used. A 100 × 70 mm ×5 mm rectangular tank was made out of Blue Tack and built on top of a glass plate as shown in Figure 4.17. The ceramic suspension was then poured in the self-made resin vat.

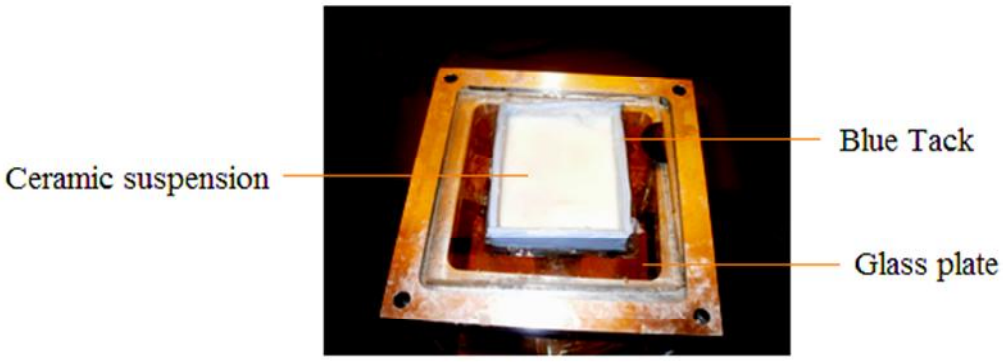

Figure 4.17 Ceramic suspension resin vat

A centrifuge tube was cut and its inner wall was covered with aluminium foil to control and direct the projected light to the glass plate for fabrication (Figure 4.14). To build a cylinder structure, a circle shape of Al plate (5mm thick with 15mm in diameter) was fabricated, and strategically stick onto the bottom part of the glass plate with double-sided tape, right on the path of the projection light.

4.4.2 Polymer Ceramic Test Part

All materials were purchased from Sigma-Aldrich, UK. For this preliminary study, hydroxyapatite for was chosen as a precursor and mixed with 1, 6 hexanediol diacrylate, HDDA and 3 wt% 2-benzyl-2-(dimethylamino)-4'-morpholino-butyrophenone as photoinitiator as shown in Table 4.5.

Table 4.5 Recipe of the ceramic suspension.

		Abbreviation	Ratio
Monomer	1, 6 hexanediol diacrylate	HDDA	10 gram
Ceramic	Hydroxyapatite	HAP	*70 wt %
Photoinnitiator	2-benzyl-2-(dimethylamino)-4'-morpholino-butyrophenone	PI	*3 wt%

*Weight % was based on the mass of the monomer

Every 10 wt% of ceramic powders was added to the HDDA and stirred on a magnetic stirrer for 15 minutes. This step was repeated until 70 wt% of HAP was homogenously mixed. The ceramic suspension was kept stirring for 24 hour. Photoinitiator was added into the ceramic suspension and stirred 1 hour prior fabrication.

To study the layer control of polymer ceramic during fabrication, the exposing time was vary from 10 to 60 sec and the methodology of fabrication on Enfis Light engine has been established as followed:

1. Ceramic suspension was poured in the resin vat.
2. The switch was turned on for each curing time.
3. After each exposing time, the switch was turned off.
4. After each curing time, the cured resins were removed and cleaned with isoproponal in a beaker to remove any uncured resin on its surfaces. 3 samples were repeated for each curing time.
5. The thickness of each cured samples were measured with electronic digital calliper (± 0.01 mm).

Table 4.6 Thickness of each cured polymer ceramic (taken from 3 test piece each time).

Time of exposure time (sec)	Thickness (mm)
5	0.06
10	0.17
15	0.25
30	0.34
60	0.41

As expected, the thickness increased as the time of curing increased. Figure 4.18 shows the disc manufactured by this instrument, showing that the system worked correctly and 10 sec curing time was suffice to fabricate a layer of sample as 5 sec exposure time was too short and the cured layer was too fragile. For the next step, a 3D structure in the shape of cylinder with certain height was expected to be successfully fabricated with Enfis light engine.

Figure 4.18 Cured layer of 70 wt% HAP fabricated on Enfis Light engine.

Based on the layer controlled determination, the selected curing time and layer thickness were 10 sec and 0.20 mm respectively. The methodology for 3D fabrication was similar to the methodology for controlled layer determination, but with the introduction of designed Z-stage (Figure 4.16) which plays a major role in fabricating a 3D structure on Enfis Light engine. Before fabrication, thickness of each layer was pre-determined by turning the thimble to desired height. The light engine was switched on for 10 sec and switched off after each layer was cured. The first layer of polymer ceramic resin was cured and attached onto the Perspex surface, and for the next layer, the thimble was turned to determined height, the switch was on and the process was continued until a 3D structure was fabricated. Figure 4.18 shows the successfully fabricated 15mm height and 15 mm diameter of 70wt% HAP polymer ceramic.

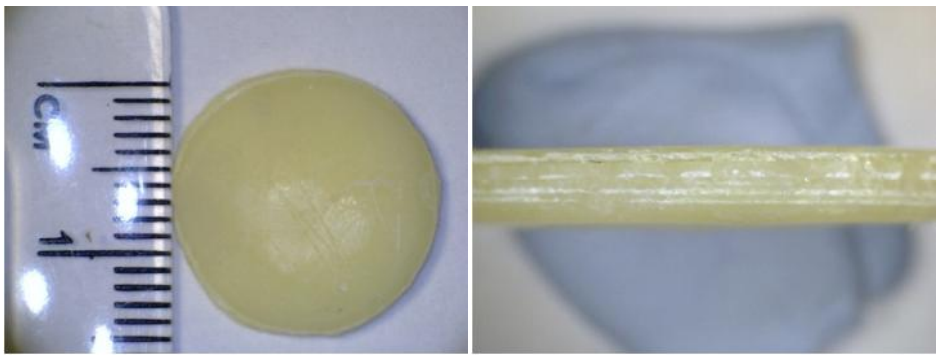

Figure 4.19 Surface microscopy of 50wt% HAP captured with Veho VMS 001, USB Digital Microscope, UK.

By adding a smaller size Al plate (5mm in diameter), a 3D cylinder with 2 different diameters was also successfully fabricated with Enfis Light engine, as shown in Figure 4.20.

Figure 4.20 A 3D cylinder with different size of diameter.

This opens the opportunity for other researchers to further manipulate and improve Enfis light engine as a microstereolithography system to fabricate a 3D scaffolds polymer ceramic composite for hard tissue application. To make the Enfis Light engine a proper microstereolithography system, the Z-stage need to be automates; to ease the layer by layer fabrication; and Ethernet interface can be connected directly to a PC workstation, and integrated in a network to fabricate custom-made shape and sizes. Currently, the manually adjustable thimbles were tedious to control and affected the shape and size of the 3D structure.

4.5 CONCLUSION

In this chapter, the optimisation of sample size and dimension for materials characterisation on the new Microtensile machine has been presented. Based on this investigation, the optimum dimension dumb-bell will be standardised for all measurement in this project, in order to obtain reliable and precise measurements.

Initial work using a decommissioned light projector gave an indication of possible layer thickness and exposure times, but due to absent an elevator or Z-stage, a 3D structure with layer by layer fabrication for any shape and sizes could not be produced. As a result, an envisionTec Desktop machine was chosen as the main microstereolithography machine for further development of biomaterials in this study. A second 'in-house' instrument was produced based on an Enfis light engine. r. It was specifically designed to fabricate a 3D structure from formulated photo-curable ceramic suspensions. The Enfis Light engine has shown the feasibility to fabricate a 3D structure but with further upgrade on the Z-stage and linked with a network, it could be a good microstereolithography system for photo-curable resin formulation. Nevertheless, the decommissioned Light projector and Light engine have given abundance of knowledge and clear understanding on the principle of microstereolithography techniques.

CHAPTER 5

The Development of a Biodegradable Polymer for Soft Tissue Scaffolds

5.1 Introduction

Rapid manufacture is the process of creating a product or part directly from a CAD (Computer Aided Design) file. This method has developed from the considerable technical steps achieved in rapid prototyping. One technique of rapid manufacture (employed here) is the additive layer process. Here a 3D object is sliced into a series of 2D (cross-sectional) layers, with each of these layers manufactured one after another, until the 3D part is formed. There are a number of technologies that can achieve this, these include stereolithography, selective laser sintering, 3-Dimensional printing, and fused deposition modelling. In this project, microstereolithography (MSL) was chosen as a means of fabricating 3D tissue scaffolds because of its ability to produce complex 3D microstructures with geometries and inner structure, like the cellular structures, as they appear in natural bone and cartilage. It offers a unique method to precisely control the matrix architecture such as size, shape, interconnectivity, branching, geometry and orientation, which will allow the production of biomimetic structures that vary in design and material composition.

Currently biopolymers are based on polyester such as polycaprolactone (PCL) or polyhydroacids (PHA), a copolymer of lactic and glycolic acid. These materials are not suitable for the fabrication of scaffolds by direct or indirect methods using

stereolithography, because they can only be processed by melting or solution techniques [220]. Generally, only a few special acrylic and epoxy-based monomers have the appropriate photoabsorption characteristics to allow affective stereolithography photopolymerization to take place. These polymers were not developed for medical applications and were created for the rapid prototyping market. The use of stereolithography in tissue engineering has not been significantly explored, possibly due to the lack of commercially available implantable or biocompatible materials from the SL industry.

On the other hand, polyethylene glycol (PEG), with an acrylate group, is a suitable candidate for this type of rapid prototyping technique. PEG has characteristic properties such as high hydrophilicity, good tissue biocompatibility, lack of toxicity and availability of reactive sites for chemical modification, whereas acrylate monomers are known for their high reactivity, polymerise rapidly in the present of photogenerated free radicals. It produces strong crosslinked bonds between acrylate groups and showed promising biocompatibility from cellular test.

The aim of this project is to develop a range of new bio-compatible/degradable materials that are compatible with a commercial 3D direct manufacture system (Envisiontec Desktop). It is hoped that we can develop formulations that will support biological cell growth and have a spectrum of mechanical properties. In order to achieve this, optimization of the formulation of the photocurable resin was investigated. This optimisation comprised of:

1. Monomer selection
2. Ratio of photo initiator and inhibitor
3. Mechanical characterisation

5.2 Formulation of Photopolymer Resin

The basic formulation of photocurable polymers are:

1. Oligomers/monomer/polymer
2. Photoinhibitor
3. Photoinitiator

It is necessary to find a suitable highly reactive monofunctional base monomer that has lower shrinkage during polymerisation, little swelling of the polymer in the monomer and offers good mechanical properties. Reactive diluents, either monofunctional or multifunctional, are needed to aid the processing properties of the formulation and tuning the network density of the polymer [221]. The network density of the polymer is dependent on the number of functional groups and on hydrogen bond formation by hydroxygroups. For instance, by tailoring the chain length of PEG chains of PEG-diacrylates, the hydrophilicity of the hydrogel could be tailored [222] and small crosslinkers and monomers with H bonding capacity give significantly better performance in term of stiffness and strength [220].

Photoinitiators are responsible to initiate the reaction of polymerization by producing reactive species upon light absorption. Once the reactive species are excited, they will generate an induced free-radical polymerisation. Photoinniators operate in the opposite ways; they reduce the excitation during photopolymerisation to certain curing depths in order to build layer by layer fabrication a success.

5.2.1 Materials and Methods

Commercially available multifunctional polymers were chosen as precursor in this study as to show the simplicity of the photopolymer resin preparation. Table 5.1 lists all the multifunctional polymers, photoinitiator and photoinhibitor used in the study. All chemicals were purchased from Sigma Aldrich, UK unless mentioned otherwise.

Table 5.1 List of monomer/polymers for the development of photopolymer resin.

Multifunctional polymer	Molecular weight (M_n)	Abbreviation
Polyethylene glycol diacrylate	575	PEGDA
Diethylene glycol diacrylate	214	DEGDA
Trietyleneglycol diacrylate	286	TEGDA
1, 6- hexanediolpropoxylatediacrylate	350	HDPA
Dipentaerythritol penta-/hexa-acrylate	524	DPA
Trimethylolpropane triacrylate	428	TMPTA
n-methylpyrrolidone	99	MP
1,6 Hexanediol ethoxylate diacrylate	314	HDeDA
Photoiniatiator		
2-benzyl-2-dimethylamino-4'-morpholino-butyrophenone		PI
Photoinhibitor		
Orasol orange (Kremer Pigmente GmbH & Co. KG, Germany.)		Dye

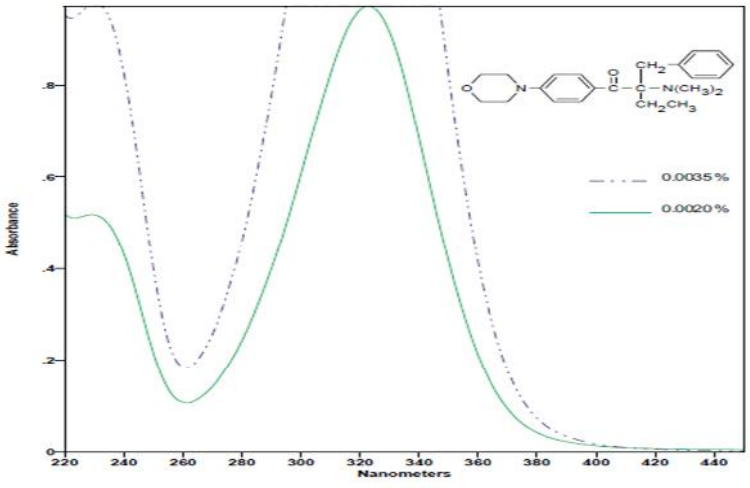

Figure 5.1 UV Absorption Spectra of 2-benzyl-2-dimethylamino 4'morpholino-butyrophenone (provided by the manufacturer) [223].

Based on the spectra provided by Perkin –Elmer UV/Vis Lambda 2 (Figure 5.1), 2-benzyl-2-dimethylamino-4'-morpholino-butyrophenone was chosen as a photoinitiator due to its broad range of absorption and its overlapping with the wavelength or frequency of the light source of the Light projector (Figure 4.1) [223]. On the other hand, orange Orasol is the inhibitor used in R11, the commercial photopolymer resin dedicated for envisionTec Perfactory machine.

For the formulation of photocurable resin development, the Light Projector; a modification, decommissioned EnvisionTec Perfactory® SXGA$^+$ W/ERM Mini Multi Lens Figure 5.2, (discussed in Chapter 4) is utilised in order to find the suitable acrylate as a candidate in a formulation with correct amounts of photoiniatiators and photoinhibitors.

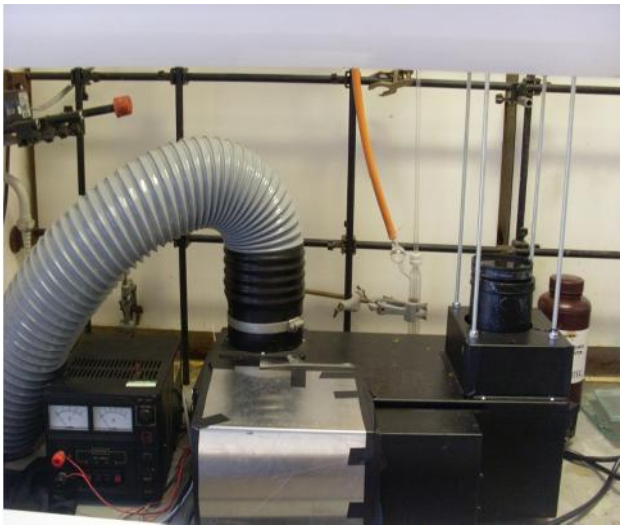

Figure 5.2 Modified envionTec Perfactory® SXGA$^+$ W/ERM Mini Multi Lens.

First, a formulation of 100% diethylene glycol diacrylate, DEGDA was investigated. The photoinitiator was varied by weight percent (wt %) of polymer from 1.0 – 5% and the dye concentration was kept constants at 0.5 wt% for varying levels of photoinitiator. The mixture of DEGDA, photoinitiator and dye was measured and

magnetically stirred for 1 hour to ensure homogeneity of the solution. The beaker where the solution was prepared was kept covered with aluminium foil to avoid any unnecessary photopolymeration from the outside environment.

A few drops of the mixture were then dropped into the cavity of the mould and exposed for photopolymerisation by the light projector from 5 to 20s (Figure 5.3). There were 5 samples for each exposing time.

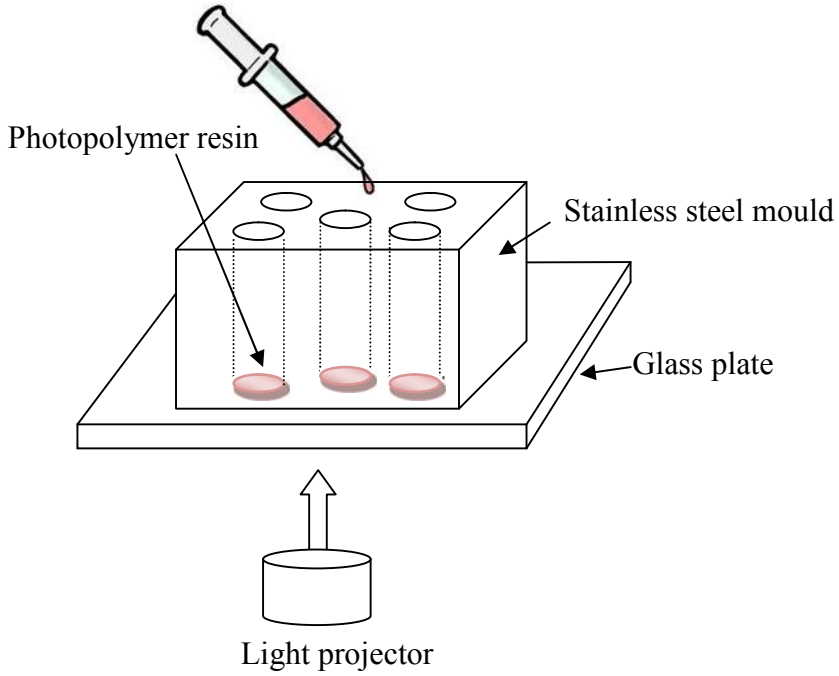

Figure 5.3 Illustration of photopolymerisation of photocurable resin.

Figure 5.4 envisionTec Otoflash Post Curing System..

After each exposure, the cured samples were then picked from the glass plate, and cleaned with isopropanol to remove uncured polymer. The cleaned polymers were post-cured with an EnvisionTec Otoflash Post Curing System for 50 flashes (Figure 5.4). To study the effect of photoinitiator on the layer control of the photopolymerised formulation, the thickness of each sample was determine with Form Talysurf (Taylor Hobson, UK).

To study the degradation behaviour of the hydrogel, swelling ratio for cured polymers were monitored. Past studies has shown that the molecular weight of the PEG repeating unit in the macromer affected the hydrogel swelling ratio and as a result affect the mechanical properties of the hydrogel [224]. The swelling occurs when a polymer network is in contact with an aqueous solution or biological fluid and reach thermodynamic compatibility between the polymer chains and water [225]. The swelling ratios of the gels were determined by measuring the weight of the swollen gels after 24 hours in pH 7.4 buffer solutions at 37 °C and the weight of the dried gels (5 samples each formulation). Hydrogel composites were transferred to PBS and cultured statically at 37 °C for 4 weeks. At day 1, 7, 14, 21, and 28, the swelling ratio

and sol fraction of DEGDA hydrogel composites were then determined by the following equations [3, 4]:

$$Swelling\,Ratio = \frac{W_s' - W_d'}{W_d'} \qquad (5.1)$$

$$Sol fraction = \frac{W_i' - W_d'}{W_i'} \qquad (5.2)$$

where W_i'= Weight of dried hydrogel composites after cross-linking;

W_s'= weight of hydrogel composites after swelling in PBS, and;

W_d'= weight of dried hydrogel composites after swelling.

The swelling ratio is defined as the fractional increase in the weight of the hydrogel due to water absorption. The sol fraction represents the fraction of the polymer following a cross- linking reaction that is not part of a cross-linked network. A decrease in sol fraction over time reflects polymer loss and characterizes the extent of hydrogel degradation.

10 pieces of dumbbell shape for each formulation were fabricated on the desktop and were then subjected to micro-tensile measurement. The measurement was done with Deben Microtest machine with motor-speed of 0.05 mm/min. The elastic modulus (E) of the sample was calculated using the slope of the stress (σ) vs. strain (λ) curve from the strain limit to the first 10% [138].

5.2.2 Results and Discussion

5.2.2.1 Layer control determination

During polymerization of 100% DEGDA, it was difficult to get a good sample for thickness measurement. Most of the samples were either partly crosslinked or with a sol-gel state, furthermore if the samples were in a solid form there were not stiff enough for thickness measurement. There were not concrete conclusions on which variables effect the curing of 100% DEG-DA.

Figure 5.5 100%DEG-DA after cured.

Table 5.2 Thickness measurement for 100 DEGDA, 50:50 DEG-DA: DPA-DHA and 80:20 DEG-DA: DPA-DHA.

Photoinitiator Concentration (wt %)	Time of Exposure (s)	Thickness (µm) 100:0 DEGDA	50:50 DEGDA:DPA	80:20 DEGDA:DPA
1.0 2.0 3.0 4.0 5.0	10	No cured samples/ partly crosslinked		
1.0 2.0 3.0 4.0 5.0	15	No cured samples/ partly crosslinked		
1.0 2.0 3.0 4.0 5.0	20	No cured samples/ partly crosslinked	No cured samples/ partly crosslinked 125.07 133.34 158.61	 145.69 148.66 180.54

Due to the inconsistency of the variables and unacceptable sample for thickness measurement, new compositions of photopolymers were investigated; 50% DEG-DA : 50% DPA-DHA and 80% DEG-DA : 20% DPA-DHA. Dipentaerythritol penta/ Hexa-acrylate, DPA was added in the prepolymer of DEG-DA to give increased rigidity and so allow for better layer formation.

Figure 5.6 shows the cured polymer resin after increasing the exposure time. The thickness for both compositions was still higher and not as expected because the objective of the study was to get a control layer of 50µm less than 10 seconds of exposure time (Table 5.2). This requirement is necessary in order to fabricate new photopolymer resin on envisionTec Perfactory equipment available in the Engineering as the Z-build thickness of the machine is only 50 µm. Even though the initial studies were unsuccessful, but the knowledge and the experience in formulating new photopolymer resin on modified equipment has given author some understanding on the principles and process involved in the microstereolithography technique.

(a) (b)

Figure 5.6 The polymerized composition of (a) 50:50 DEG-DA: DPA-DPA and (b) 80:20 DEG-DA-DPA.

5.3 Development of Photopolymer Resin on Desktop Digital Shell Printer (Desktop).

Development on formulation of new photopolymer with the decommissioned EnvisionTec Perfactory® SXGA^{+} W/ERM Mini Multi was not possible due to the unsatisfactory results above. In order to formulate a new photopolymer, the experiments were continued on the envisionTec Desktop Digital Shell Printer (Desktop), which is a smaller version of Envisiontec Perfactory® SXGA^{+} W/ERM Mini Multi Lens (Figure 5.7).

Figure 5.7 envisionTec Desktop Digital Shell Printer (Desktop).

Table 5.3 shows the recipe for new photopolymer resin for materials development on the desktop and the sample preparation was described previously. 3.75 wt% photoinitiator and 0.15 wt% dye for each formulation were added to each formulation.

Table 5.3 Formulation of multifunctional acrylate for photopolymer resin.

Sample	Monomer/polymer	Ratio (%)
A	DEDGA	90
	HDPA	10
B	DEDGA	80
	HDPA	20
C	TEGDA	90
	HDPA	10
D	PEGDA	80
	HDPA	20

For swelling ratios determination, 5 disks (6 mm diameter, 1 mm thick) of each formulation were fabricated in the Desktop machine. The swelling ratios (Q) were measured from these gel disks and the swelling ratio is shown in Table 5.4. Elastic modulus for sample B was omitted, due to failure during micro-tensile measurement.

5.3.1 Results and Discussion

During measurement, the samples were broken outside the breaking gauge as discussed in Chapter 4.

Table 5.4 Swelling ratios measurement for each cured polymer. (5 test pieces for each cured polymer; ± standard deviation).

Sample	Swelling ratio, Q	Elastic Modulus, E (kPa)
A	6.5 ± 0.2	10.39 ± 0.2
B	7.1 ± 0.3	-
C	8.4 ± 0.2	3.70 ± 0.3
D	10.8 ± 0.4	1.61 ± 0.2

As expected, the swelling ratios (Q) increased and elastic modulus (E) decreased as the acrylate functional group increased. During photopolymerisation, the free radicals recombine caused by the chains of polymers cross-linking together and as a result, increasing the molecular mass of the polymer. Past studies have shown

that molecular weight and concentration of macromer, and cross-linker and initiator can influence the swelling ratio of a cross-linked composite. Theoretically, as the molecular weight of the cured polymer increases, the spacing between the cross-links becomes larger and therefore the resulting hydrogel will have a larger mesh size, exhibited by a higher swelling ratio [224].

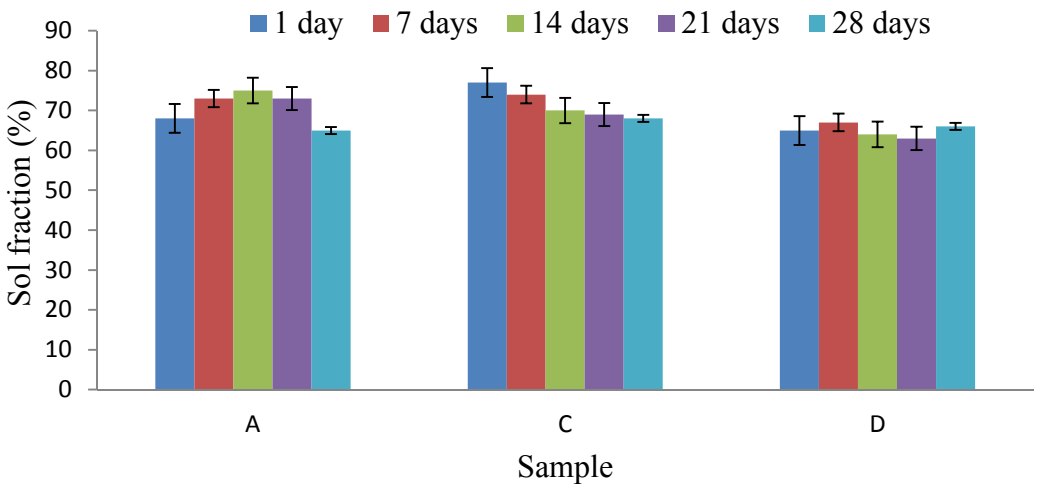

Figure 5.8 Sol fraction of cured polymer after immersion in PBS for up to 28 days. The data was taken from 5 samples for each formulation. Error bars represent the standard deviation for each measurement.

The sol fraction of the samples over times is shown in Figure 5.8. For each formulation, there was little decreased percentage in sol fraction. These results show that the polymerised formulation exhibit degradation properties, which is a vital requirement for a biomaterial. Nevertheless, these results promise potential for the use of this resin for soft tissue scaffold applications.

Furthermore, it is interesting to note that the different multifunctional acrylates and the ratio of photopolymer resins have not affected the tensile strength of the cured polymer, as shown in Table 5.5.

Table 5.5 Tensile strength of polymer fabricated from different type of multifunctional acrylate resin. The standard deviation obtained from five data for each formulation.

Samples	Tensile strength (kPa)
A	13 ± 0.1
C	14 ± 0.1
D	12 ± 0.1

These results were attributed by the inconsistent of the fabricated dumb-bell. They had reproducibility problem because their successfully fabricated yield was low, shape-defect (distortion and warping) and delamination. Figure 5.9 shows a fabricated dumb-bell test piece for micro-tensile measurement. Here, the delamination of the sample can be seen clearly seen.

Figure 5.9 Delamination occurred on the dumb-bell test piece fabricated on the envisionTEC Desktop.

5.4 Development of Glycopolymer Resin on Desktop Digital Shell Printer (Desktop).

Even though the mechanical properties of the cured polymer were not promising, they were sufficient to allow the exploration/functionalization of these resins by investigating the addition of a carbohydrate groups to the polymer system for biomedical application of hydrogels.

Hydrogels are hydrophilic, which explains their swelling properties and their capability of maintaining encapsulated cell viability. Unfortunately, they are also a poor environment for cell attachment and proliferation, which is unfavourable in *en vivo* applications. Currently, glycopolymers have attracted a lot of attention from the materials science community due to their biocompatibility and their bioactivity for applications in tissue engineering and targeted drug delivery systems.

Glycopolymers are synthetic polymers with pendant carbohydrates, which if the carbohydrate displays on the cell surface, it can play critical a role in cell-cell recognition, adhesion and signalling between cells [226]. For instance; saccharide units in glycopolymers can be capable of molecular recognition and interact with specific carbohydrate receptors. The participation of saccharides in biological recognition has led to the development of glycosylated drug and gene delivery carriers in which the carbohydrate receptors are used to direct the drugs to specific organ or cell targets and of carbohydrate-sensitive biosensors to monitor saccharide molecular recognition processes. Due to their excellent biocompatibility, glycopolymers have been proposed for use as scaffold materials in tissue engineering, while sugar-based hydrogels, are attractive as biocompatible water-absorbent materials [227]. In addition they also play an important role in cell growth regulation, differentiation, adhesion, cancer cell

metastasis, cellular trafficking, inflammation by bacteria and viruses, and immune responses [228].

There are two ways of synthesising glycopolymers; protected and unprotected carbohydrates. There are two major linkages by which carbohydrate chains can be attached to proteins: either N-linked through an asparagines residue or O-linked through a threonine or serine. A given glycoprotein may contain only N-linked, only O-linked, or both types of oligosaccharide chains [229]. The choice of employing protected or unprotected sugars is dependent on the ease of stereospecific functionalization of the sugar, the solubility of the monomer and polymer, the potential incompleteness of the removal of the protective group, and the ease of purification [228]. In this study, the synthesis of glycopolymers synthesis with unprotected carbohydrate and was done in collaboration with a researcher from Department of Chemistry, Warwick University. The synthesis was done according to Ohno et. al. method (1990) and explained as following section.

5.4.1 Preparation of PEGDA/HDPA-GlcAc

5.4.1.1 Synthesis of 1,2,3,4,6-Penta-O-acetyl-beta-D-glucopyranose; Acetyl 2,3,4,6-tetra-o-acetyl-beta-D-glucopyranoside (GlcAc)

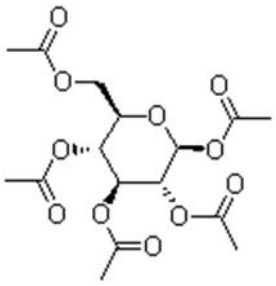

Figure 5.10 Molecular structure of 1, 2, 3, 4, 6-Penta-O-acetyl-beta-D- glucopyranose; Acetyl 2, 3, 4, 6-tetra-o-acetyl-beta-D-glucopyranoside (GlcAc) (http://www.chemblink.com/products/604-69-3.htm).

The synthesis was made by a slight modification of the method proposed by Ouchi et al. [230]. Dry acetone, triethylamine, and acryloyl chloride was added drop wise at 0 °C to cold solution of 1,2,3,4,6-Penta-O-acetyl-beta-D-glucopyranose. The mixture was magnetically stirred for 1 hour at 0 °C and then for another 2 hours at room temperature. The system was diluted with cold water and extracted three times with chloroform. The combined extracts were dried over anhydrous sodium sulfate. After the solvent was evacuated, the crude product was purified by flash silica gel chromatography with a 2:3 (v/v) hexane/ ethyl acetate mixture as an eluent to yield pale yellow syrup. Crystallization of the syrup was induced in cold hexane to give a slightly yellow powder.

5.4.1.2 Deprotection of GlcAc

The protected polymer was dissolved in 80% formic acid and stirred for 48 hours at room temperature, to which water was added and stirred for another 3 hours. The solution was dialyzed against distilled water for 2 days, concentrated *in vacuo*, and finally lyophilized to give GlcAc as a white powder in quantitative yield. Table 5.6 shows the final formulation of the glycopolymers as a photopolymer resin.

Table 5.6 Formulation of glycopolymers photopolymer resin

Sample	Ratio (%)		
	PEGDA	HDPA	GlcAc
Control	70.0	30.0	-
2.5Glc	72.5	25.0	2.5
5.0Glc	70.0	25.0	5.0

To study the effect of introducing carbohydrate onto the acrylate branches, the glycopolymers were subjected to swelling ratio and microtensile measurements. The

methodologies for both measurements were described in section 5.2.1 and 4.3.2 respectively.

5.4.2 Results and Discussion

Table 5.7 Swelling ratios measurement for each glycopolymers. ± is the standard deviation of three five data obtained at each formulation.

Sample	Swelling ratio, *Q*	Elastic Modulus, *E* (kPa)
Control	9.9 ± 0.1	9.84 ± 0.5
2.5Glc	11.8 ± 0.2	8.70 ± 0.3
5.0Glc	13.2 ± 0.2	5.62 ± 0.2

Table 5.7 represents the swelling ratios measurement for each formulation. Swelling studies indicated that the addition of the glycopolymer has a significant effect on the swelling ratio after 24 hours. As a comparison, the swelling ratio has increased 20 and 33% after 2.5 and 5.0 % of GlcAc was added to the PEGDA/HDPA. The modification and increases of GlcAc has increased the molecular weight of the polymer mixture and as a result increases the swelling ratio of the cured polymer. The ability to absorb water and coupled with optimum rate of degradation are amongst the main characteristics required in a drug delivery system. Sol fraction of the material explained the degradation rate of the cured glycopolymers. Figure 5.11 represents the degradation behaviour of glycopolymers after immersion in PBS for 1, 7, 14, 21 and 28 days.

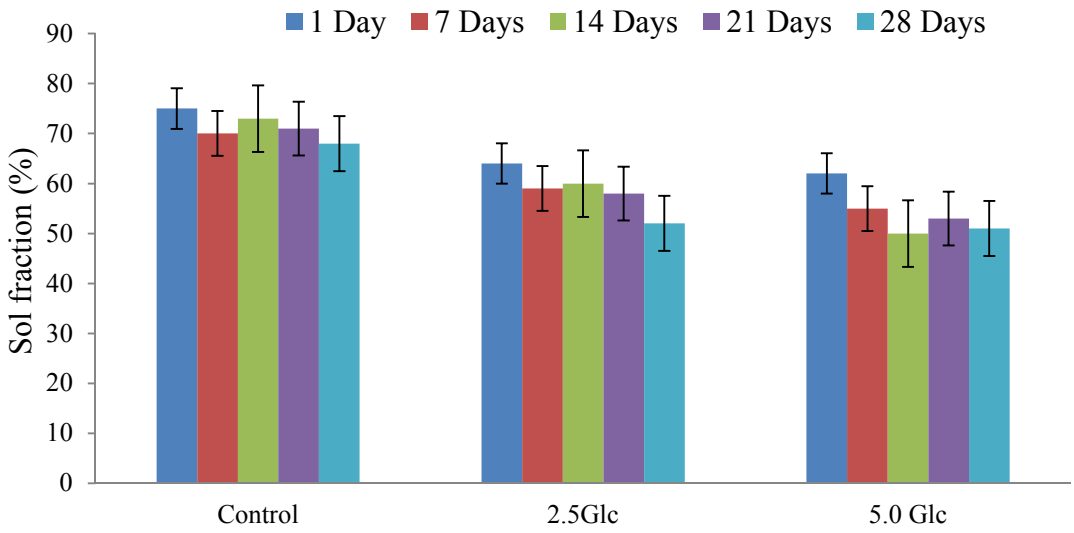

Figure 5.11 Sol fractions of glycopolymers after immersion in PBS for up to 28 days. The error bars is the standard deviation of five data obtained at each soaking time.

The engineered carbohydrate based materials has significant effect on the degradation rate of the cured glycopolymers. As a comparison, the rate of degradation has decreased 33% after 5.0% of GlcAc was branched onto the acrylate backbone and immersed for 28 days in the SBF solution. This results show the role of polysaccharide in promoting the hydrolytic scissioning of the polymer backbone hence increased the degradation rate.

However, sugar-based glycopolymers has no significant effect on the tensile strength of the cured polymers as shown in Figure 5.12. These results were related to the shape of fabricated dumb-bell from the gycopolymers resin; which was still not optimal. The sample showed delamination and warping, a sign of stress after post-curing.

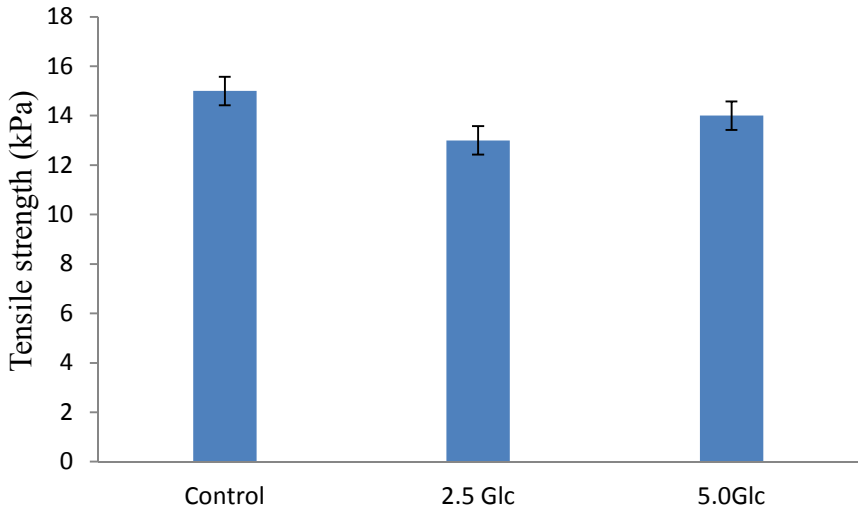

Figure 5.12 Tensile strength of glycopolymers with different ratio of GlcAc. The error bars is the standard deviation of five data obtained at each soaking time.

Figure 5.13 shows the surface morphology analysis on sample 5.0 Glc and the control sample after fabrication. The morphology clearly shows the differences between the two specimens. The control sample has a smooth and less contaminated surface (Figure 5.13 (a)) whereas the sample with 5.0% GlcAc has induced more stress post-curing, which promotes delamination and uneven surface (Figure 5.13(b)).

Further magnification on the SEM (Figure 5.13 (c)), shows the gap of delamination was about 50µm and the surface roughness shows brittleness of the sample which explained the low tensile strength. Bartolo et. al indicated that as the differences between the temperature within the irradiation volume and the surrounding resin that can produce stress gradients [231]. These suggest that the fabrication needs to be in a controlled environment, which is very interesting to explore in the future

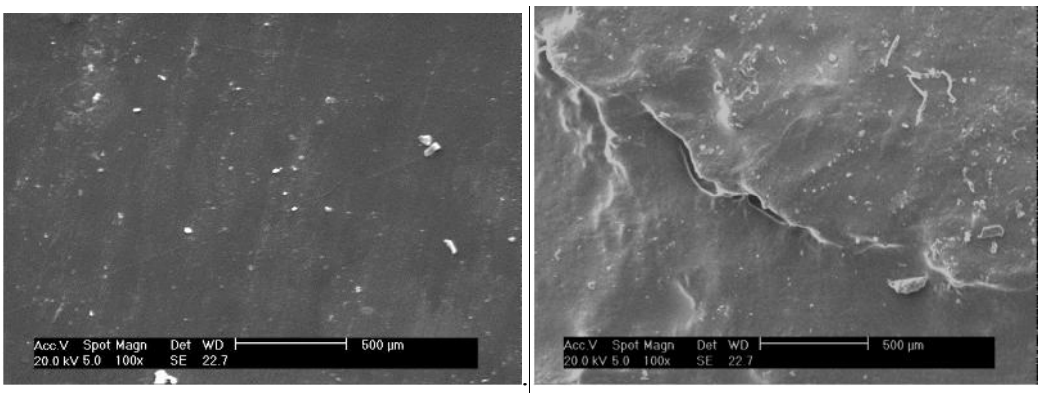

(a) (b)

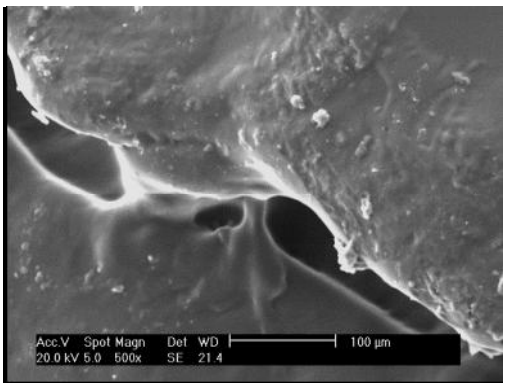

(c)

Figure 5.13 Surface morphology of (a) control sample, (b) 5.0% Glc with 100x magnification and (c) 5.0 Glc with 500 x magnifications.

5.5 Conclusion

In this study it was shown that it was possible to synthesize a new photopolymer resin with different type of multifunctional acrylate polymer that compatible with a microstereolithography technique. However, the hydrogels suffered with stress post-curing, which promote delamination and warping of the sample.

For further material development, carbohydrate-based polymers were also synthesized, in order to explore their feasibility with microstereolithography technique to further enhance the diversity of the technique. The glycopolymers was

successfully fabricated on the Desktop machine but further development during fabrication is needed in order to tackle the stress problem of the cured sample.

In summary, the highly hydrophilicity of PEG and an active site of PEG chain for easily modification through a variety of synthetic reactions has make PEG an interesting and robust biomaterials for hydrogel. With more knowledge and understanding in the tailoring the polymer properties, structure and mechanism during polymerisation, the development of novel materials that are able to fabricate on the microstereolithography technique will be very exciting. This will open up more possibility of new application of hydrogel in tissue engineering field and offer an alternative option to patients.

CHAPTER 6

Preparation and Fabrication of Ceramic Tissue Scaffolds via Envisiontec Desktop

6.1 Introduction

This chapter describes the development of photo-curable polymer ceramic resins employing different calcium phosphates for 3D manufacture. Three types of calcium phosphate have been used; synthesised calcium pyrophosphate (CPP-A), as-received calcium phosphate (CPP-B) and hydroxyapatite (HAP). The influence of particle size, composition, and viscosity of calcium phosphate within the photopolymer resin has been studied. Thermal degradation of the green body parts was carried out using thermogravimetrical analyser (TGA) to determine the sintering temperature of the composite. The fabricated biocomposites were also characterized by X-ray diffraction (XRD), and scanning electron microscope with X-ray elemental analysis (SEM-EDAX). The mechanical properties of the different biocomposites were studied and the formations of apatite layer onto the surface of the materials were determined in bioactivity test.

6.2 Materials and Methods

In this chapter, three types of calcium phosphate were studied and characterised:

1. Synthesised calcium pyrophosphate, $Ca_2P_2O_7$ (CPP-A);
2. As-received calcium pyrophosphate from Sigma-Aldrich, Dorset, UK (CPP-B);
3. Hydroxyapatite from Plasma Biotal Limited, UK (CAPS).

Properties and method of preparations for each calcium phosphate is discussed in the next sections.

6.2.1 Preparation of Ceramic Suspension

6.2.1.1 Synthesise of calcium pyrophosphate (CPP-A)

Calcium pyrophosphate (CPP-A) was synthesised at the School of Chemical Engineering, University of Birmingham [232]. The brushite cement was synthesized by combining β tricalcium phosphate (β-TCP) with 3.5 M phosphoric acid (H_3PO_4) (Fisher Scientific, Dorset, UK) containing citric acid at a concentration of 50 mM (Fluka, Dorset, UK) (equation 6.1). The β-TCP was mixed with H_3PO_4 solution in powder form, to a liquid ratio (P:L) of 1.25 g/mL. The resulting paste was cast into a polytetrafluroethylene (PTFE) split mould to form cylindrical samples of diameter 6 mm and height 12 mm.

The cylinders were allowed to harden at 37°C for 24 h prior to testing or further heat treatment. The hardened cement cylinders were subsequently sintered at temperatures between 400 and 1200°C for 5 h using a muffle furnace (CWF 1300; Carbolite, UK), the heating and cooling rate of the furnace was set at 10°C/min converting the brushite cement into monetite and then calcium pyrophosphate ceramic ($Ca_2P_2O_7$) in accordance with equation 6.2 and 6.3:

$$\beta - Ca_3(PO_4)_2 + H_3PO_4 + 6H_2O \rightarrow 3CaHPO_4.2H_2O \quad (6.1)$$

$$2CaHPO_4.2H_2O \rightarrow 2CaHPO_4 + 4H_2O \quad (6.2)$$

$$2CaHPO_4 \rightarrow Ca_2P_2O_7 + H_2O \quad (6.3)$$

The hardened cylinders CPP were then crushed with a pestle and mortar into a powdery form. Upon crushing, the CPP's powder was then ball milled with Luckham, Multimix Major, [TM] for 24, 48 and 72 hours in order to get superfine particle size of less than 10 μm. Calcium pyrophosphate from Sigma-Aldrich, Dorset, UK (CPP-B) and hydroxyapatite with the commercial name of CAPTAL ®S from Plasma Biotal Limited (CAPS), UK, were obtained and ball milled as well for comparison purposes. To study the effect of ball milling to the particle size of the calcium phosphate, the distribution of calcium phosphate powder was characterised with a Mastersizer 3000 (Malvern, UK).

6.2.1.2 Ceramic suspension

The photopolymer resin consists of precursor monomers; dipentaeryolacrylate and hexanediol ethoxylate diacrylate and Bisphenol A as reactive diluents. The polymer component of the suspension was prepared prior to mixing with the ceramic. The formulation in table 6.1 was chosen as the optimum formulation based on previous study in Chapter 5. The polymer, monomer and photoinitiator were purchased from Sigma Aldrich, UK whilst the dye was from Kremer Pigmente, Germany.

Table 6.1 Optimum formulation of photo-curable polymer resin.

		Abbreviation	Ratio (%)
Monomer	Dipentaeryolacrylate	DPA	60*
Reactive diluents	Hexanediol ethoxylate diacrylate	HDeDA	30*
	Bisphenol A	BPA	10*
Photoinitiator	2-benzyl-2-(dimethylamino)-4'-morpholino-butyrophenone	PI	3*
Dye	Orasol ® Orange G		0.5**

*: base on the weight of the polymer/monomer
**: base on the weight of the ceramic

The liquid components were mixed and stirred on a magnetic stirrer for 15 minutes. The percentage of the ceramics powder was varied from 50-150 wt% of polymer weight, where every 10 wt% of ceramic powders was added to the suspension every 15 minutes. Dye with 0.5 wt% of ceramic filler was added before leaving the suspension stirring for 24 hours. The photoinitiator was added and stirred for 1 hour prior to testing or used in the manufacturing process.

6.2.2 Viscosity measurement

Measurements were carried out in a Size 25 capillary viscometer of from Cannon Instrument, Cole Palmer, UK (Figure 6.1). By using the equations printed in the ASTM D 446 standard, the viscometer constants of Cannon-Fenske can be calculated at temperatures other than those at which the viscometers were calibrated. The following equation permits the calculation of the viscometer constant C at any temperature from a viscometer constant determined experimentally at another temperature.

$$C = C_0(1 - B\,[T_T - T_F]) \qquad (6.4)$$

C_0 = the viscometer constant when filled and tested at the same temperature

T = temperature, °C

B = the temperature dependence factor

t, = values at the test temperature

f = fill temperature

The following procedure was used when measuring the viscosity (this is in accordance to ASTM D445, D446 and ISO 3104, 3105 standards [2-3]):

1. The viscometer was cleaned using suitable solvents, and by passing clean, dry, filtered air through the instrument to remove the final traces of solvents. Periodically, any traces of organic deposits were removed with chromic acid or non-chromium cleaning solution.
2. To charge the sample into the viscometer, the instrument was inverted and suction was applied to tube L, immersed tube N in the liquid sample, and drew liquid to mark F. After cleaning the arm N, the instrument was turned to its normal vertical position.
3. The viscometer was placed into the holder, inserted and aligned vertically into the constant temperature bath.
4. Approximately 10 min was given to allow the sample to come to the bath temperature at 40 °C and 15 min at 100°C.
5. The liquid was drawn slightly above mark E, suction was applied to tube N.
6. To measure the efflux time, the liquid sample was allowed to flow freely down past mark F, measured the time for the meniscus to pass from mark E to mark F.
7. To ensure consistent and persistent reading, step 5 and 6 were repeated.
8. The kinematic viscosity in mm2/s (cSt) of the sample was calculated by multiplying the efflux time in seconds by the viscometer constant.

$$\eta' = At \qquad (6.5)$$

where η' is the kinematic viscosity, A is the viscometer constant (cSt/sec), and t is the efflux time in seconds. The viscometer constants, A at 40 °C and 100 °C are 2.540 and 2.528 mm^2/s^2, (cSt/s) respectively. The S.I. unit of viscosity

is 1 pascal second (ps), and is equal to 10 poises. One centistokes is equal to one millimetre squared per second (mm^2/s).

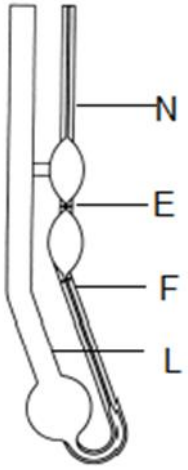

Figure 6.1 Schematic diagrams of Cannon-Fenske Routine Viscometer for Transparent Liquids [234].

6.2.3 Determination of decomposition Temperature

To determine the decomposition temperature of the calcium pyrophosphate suspension, 90 wt% of CPP-B was mixed in the polymer matrix and acted as a controlled sample for the measurements. The formulation is shown in Table 6.2.

Table 6.2 Composition of ceramic suspension for sintering temperature determination.

Calcium Phosphate	Weight % (wt%) [i]	Photopolymer Resin	Ratio (%)[ii]
CPP-B	90	*HDeDA	70
		*DPA	20
		*BPA	10
		PI	3[a]
		Dye	0.15[b]

[i] : weight percent of total weight of prepolymer (*)
[ii]: ratio based on total weight of prepolymer (*)
[a] : weight percent of PI based on the total weight of prepolymer (*)
[b]: weight percent based on the weight of ceramic added to the total weight of prepolymer (*)

A 3 mm thickness, dumbbell shaped test piece was fabricated using the Envisiontec Desktop machine. The dumbbell shaped was then cut into small chunks and about 15 mg of the chunks were used in the Simultaneously Thermal Analysis (STA), Polymer Labs STA1500 for thermogravimetrical analysis (TGA). TGA is used to characterise the decomposition temperature of polymer and ceramic phase respectively. Three different heating rates; 2°C/min, 10°C/min and 20°C/min were chosen to investigate effect of different heating rates on the decomposition temperature. The heating was tested between 25–1000°C in air and at a flow rate of 50 mL/min.

The crystalline composition of the sintered ceramics, from TGA analysis, was verified by X-ray diffraction (XRD) using a Philips 1820 diffractometer fitted with a quartz Johansson monochromator operating in subtractive transmission mode at 50 kV and 40 mA. The ceramic was ground and placed on the sample holder. X-radiation was pure monochromatic Cu Kc (λ= 1.54056 Ab) over a 2θ range of 10 – 70° at room temperature, using a step size of 0.020° and a step time of 0.9 s. From the X-ray diffraction (XRD) patterns the relative proportions of CPP and HAP were determined using relative peak intensity. The crystalline phases were deduced from a comparison of the registered patterns according to the Joint Committee on Powder Diffraction Standard (JCPDS) (JCPDS 9-432 for hydroxyapatite, JCPDS 9-169 for β-tricalcium phosphate, and JCPDS 9-346 for calcium).

SEM micro- graphs and analysis by EDAX of the composites were also studied using an SEM (Model Carl Zeiss Sigma), with an EDX unit with an accelerating voltage of 20 kV and magnification 500 x up to 2000x. For SEM-EDAX analysis, if the Ca/P ratio of the material is lower than 1.67, it decomposes into β-

tricalcium phosphate and hydroxyapatite, and if the Ca/P ratio is higher than 1.667 it decomposes into calcium oxide and hydroxyapatite. If the Ca/P ratio is lower than 1.5, it decomposes into β -tricalcium phosphate and calcium pyrophosphate.

6.3 Characterisation of Ceramic Composite

6.3.1 Determination of sintering temperature and time

It is important to determine the sintering temperature and time as they affect the microstructure and composition of the resulting ceramic, which contributes to the properties of the material. Ceramic discs of calcium phosphate (5 mm height x 4 mm diameter) were designed and fabricated via the Envision Desktop®. In order to determine the sintering temperature of the ceramic composite, different heating profiles were designed based on the analysis from TGA and XRD. The sintering time was varied over 5-20 hours and sintering temperature from 600 – 1300°C.

The mass, height and diameter changes before and after sintered of the ceramic discs were measured to provide linear shrinkage. The mass loss and volume shrinkage are given as follows:

$$M_S\,(\%) = \frac{M_i - M_0}{M_0} \times 100 \qquad (6.6)$$

Where M_S is the mass loss from the ceramic upon sintering, M_0 is the mass of green body and M_i the mass of the sintered ceramic.

$$V_S\,(\%) = \frac{V_i - V_0}{V_0} \times 100 \qquad (6.7)$$

Where V_S is the volumetric shrinkage, V_0 is the volume of greenbody and V_i is the volume of the sintered ceramic.

The density of the samples was measured using a Micromeritics 1330 AccuPyc Pycnometer. The machine uses helium as a medium because helium atoms are small, ergo are able to penetrate very small pores within the ceramic to a limit of 0.1 nm [4-5]. This gives an accurate measurement of the volume of the ceramic, which in turn gives the true density of the material.

6.3.2 Porosity measurement

The porosity of the sintered ceramic was determined by using the gravimetric method (GM) and Micromeritics 1330 AccuPyc Pycnometer. The calculation consists of the evaluation of the structural porosity by measuring the effective density. This is achieved by measuring the size parameters and the weight of the scaffold as follows:

$$Effectivedensity = \frac{Massof\,the\,porousstructure,g}{Volumeof\,the\,porousstructure,cm^3} \quad (6.8)$$

$$Relativedensity = \frac{Effectivedensity}{Truedensity} \quad (6.9)$$

The true density is measured from the Pycnometer. Then, the porosity, P, was evaluated by subtracting the relative density from 1.

$$Porosity = 1 - Relativedensity \quad (6.10)$$

6.3.3 Mechanical Characterisation

6.3.3.1 Compressive Test

Bones play a major function in the mechanical support of the body weight and endure lots of stress during motion. Any biomaterial development as a bone replacement must have optimal mechanical properties, as they are exposed to compression and shear stresses. A simple compromise on the stability of a bone replacement could lead

to the collapse of a reconstruction trauma, recurrence of the deformity and even increased implant morbidity [237]. It is important to investigate the mechanical behaviour of a newly fabricated biomaterial, especially for biomaterials produced by a sintering process. Thermal processes, such as sintering, could exhibit numerous surface and internal flaws, which act as stress concentrators and lead to compression failure [238].

Compressive test samples, for each formulation of ceramic compound, were prepared similar to the sintering study. The compressive strength was measured with a universal testing machine (Instron 5569, Instron Corp., Canton, MA) with a crosshead speed of 0.1 mm/min.

The compressive stress of the sintered ceramic (σc) can be calculated in accordance with the equation:

$$\sigma_C = \frac{4F}{\mu d^2} \qquad (6.11)$$

where F is the load at failure (N) and d is the diameter of the ceramic sample (mm).

6.3.3.2 Bioactivity Test

In order to study the bioactivity, samples were soaked in simulated body fluid (SBF) [239] at body temperature (37 °C) and pH=7.4 for several periods. The SBF has a composition similar to human blood plasma and has been extensively used for *in vitro* bioactivity tests [239]. Table 6.3 presents the ratio of ion concentrations of the simulated body fluid and human blood plasma.

Table 6.3 Ion concentrations of the simulated body fluid and human blood plasma [239].

Ion	Concentration (mmol/dm^3)	
	Simulated body fluid (SBF)	Human blood plasma
Na^+	142.0	142.0
K^+	5.0	5.0
Mg^{2+}	1.5	1.5
Ca^{2+}	2.5	2.5
Cl^-	147.8	103.0
HCO_3^-	4.2	27.0
HPO_4^{2-}	1.0	1.0
SO_4^{2-}	0.5	0.5

For each period, the pH value of the sample was measured with an Automatic Potential Titrator (China). Three samples were prepared for every scaffold and the reported pH was the average of the three samples. After soaking, specimens were taken from the fluid, rinsed with deionised water, and dried at 37 □ for SEM connected with energy dispersive spectroscopy (SEM-EDAX), Model Zeiss Sigma, UK.

Planimetric procedure (also known as the Jeffries' Method,) was used. This is a grain counting method employed to determine the grain size of a composite by following Section 9 of ASTM E112-10 [240]:

a) Inscribe any shape of known area, *A*, on an image magnification, *M.*

b) Count the number of grains that are *completely* within the area.

c) Count the number of grains that are *partially* within the area.

d) Divide the results from (*c*) by 2.

e) Add the result from (*d*) to the result from (*b*).

f) Divide the result from (*e*) to the grains/in^2 at 100 x magnification.

g) Use the definition of ASTM grain size number to determine the grain size, *n*.

From definition, grain size can be express as follow;

$$n = 1 + log_2 N = 1 + 3.32 \log N \qquad (6.12)$$

6.4 Results and Discussion

6.4.1 Particle size and distribution

Table 6.4 summarises the results obtained from the measurements of particle size (from an average of three repeat measurements). As expected, milling time has a significant effect on the distribution and particle sizes of the calcium phosphate. After 24 hours, the size has been reduced due to particle fracture, which was caused by the high energy impacts of the ceramic balls during milling. However, after 48 and 72 hours, the ceramic powders started to agglomerate and stick on the vial wall and the ball surface, consequently reducing the powder volume, as collection was difficult. Author decided to exclude the 48 and 72 hours powder for particle size and distribution measurement.

Table 6.4 Properties of calcium phosphate used in the study.

Sample		Particle Size (μm)	
	Abbreviation	0 h	24 hours
Calcium pyrophosphate (Synthesized)	CPP-A	14	4
Calcium pyrophosphate (Sigma-Aldrich)	CPP-B	119	35
Hydroxyapatite	CAPS	7	5

Table 6.4 show the effect of milling time on the distribution of the particle size for each calcium phosphate. It shows that the optimum milling time for the production of the smallest calcium phosphate powder was 24 hours. Further milling time for 48 hours has induced agglomeration and unfavourable in preparing of a ceramic

suspension. For CPP-A, 24 hours of milling time exhibited 3 broad peaks covering the size range 1.2 to 60.00 μm, with the largest peak believed to arise mainly from particle agglomeration.

Figure 6.2(b) shows the broad peak of particle size distribution of calcium pyrophosphate from Sigma-Aldrich. The broad peak only shifts to the left after 24 hours, indicating that milling time only gives a significant effect to the distribution of the particle size from 119 to 35 μm, but not the percentage of a particle's volume. This is believed to be attributed to the bigger structure of the calcium pyrophosphate, as shown in Figure 6.2 (b), and presumably due to the synthesization of CPP in a well-established and controlled environment.

CAPS hydroxyapatite, received from Biotal Plasma, also had the same distribution of particles size. The as-received CAPS was synthesized and manufactured to a size of 5μm, and milling time does not produce any significant effect on the size of the hydroxyapatite particles, as the particles size distribution only differs by 1 μm. Surface morphology of each calcium phosphate showed a clear difference in particle size after 24 hours of milling. This has demonstrated that 24 hours of milling time is sufficient to reduce the particle size and was used throughout the whole project.

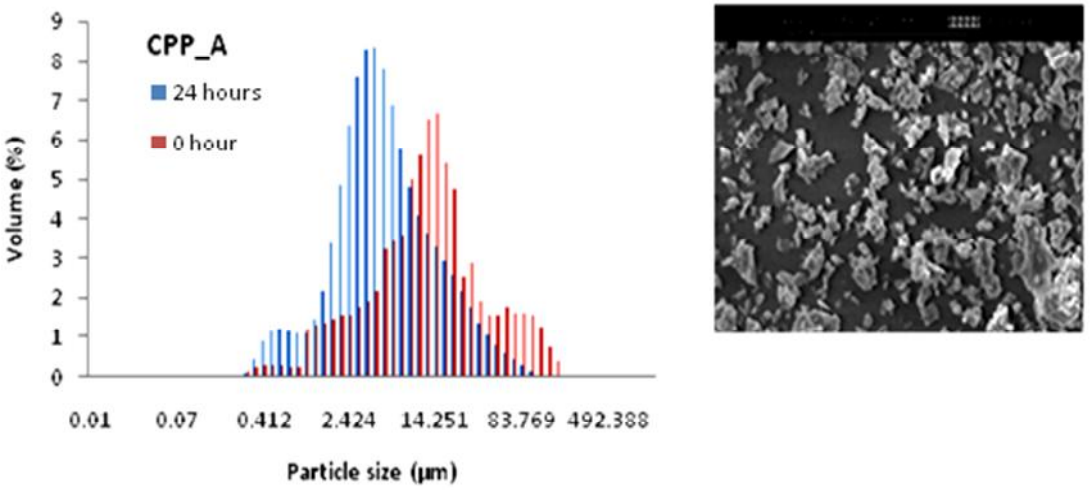

(a)

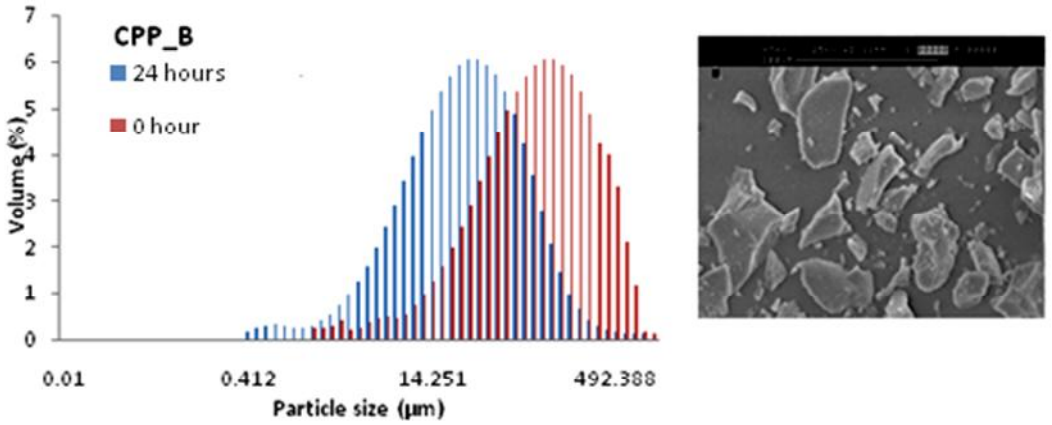

(b)

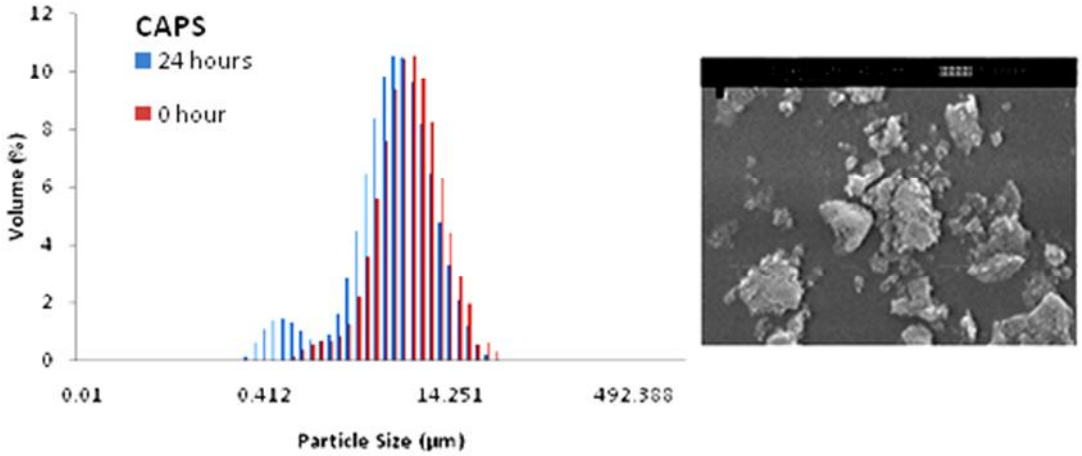

(c)

Figure 6.2 Particles size distribution and surface morphology (magnification of 500x) of (a) CPP-A, (b) CPP-B and (c) CAPS before and 24 hours milling time.

6.4.2 Determination of decomposition temperature

The decomposition thermal cycle was optimised based on the TGA studies of the cured green bodies. Based on Figure 6.3 (a), there are two steps of pyrolysis. The first decomposition temperature is HDeDA; around 410 °C and the second onset temperature is DPA at about 500 °C (Figure 6.3 (b)). The increase in heat flow within the ceramic is associated with the decomposition of HDeDA, DPA, photoinitiator and the dye.

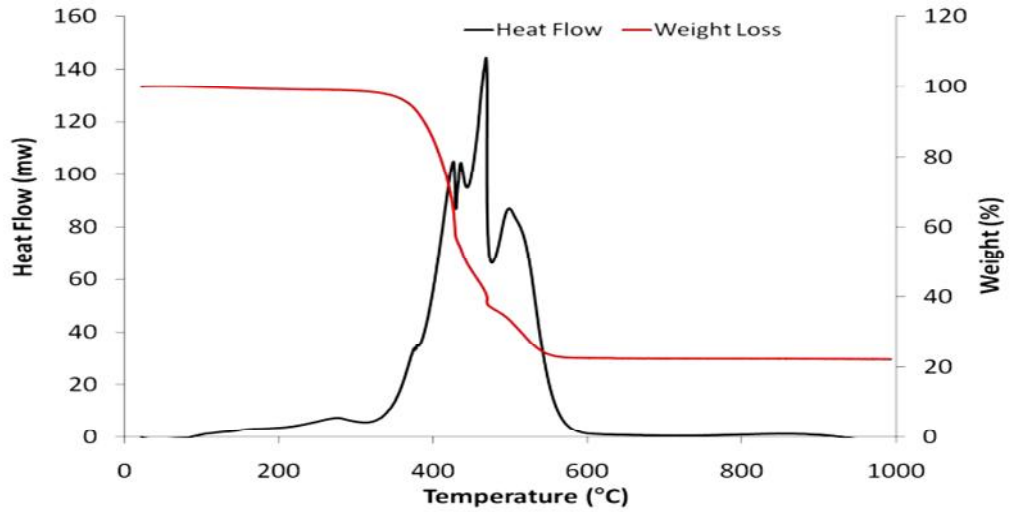

(a)

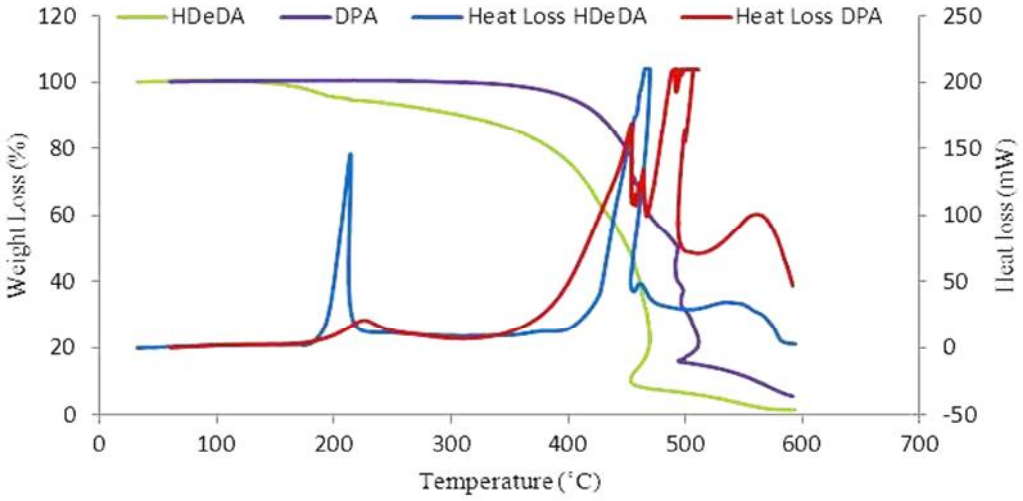

(b)

Figure 6.3 TGA/DTG analysis of (a) 90CPP-B ceramic composite and; (b) HDeDA and DPA.

With different heating rates, the decomposition temperature will change significantly. Figure 6.4 illustrates the TGA/DTG for 2, 10 and 20 °C/min. As the heating rate is increased, the onset of decomposition is moved from 380 °C to 370 °C., whereas for the slower heating rate, the thermal degradation occurs at 310 °C. At 2 °C/min, the peak for heat flow is broad and prominent, due to the slow decomposition rate of polymer chain.

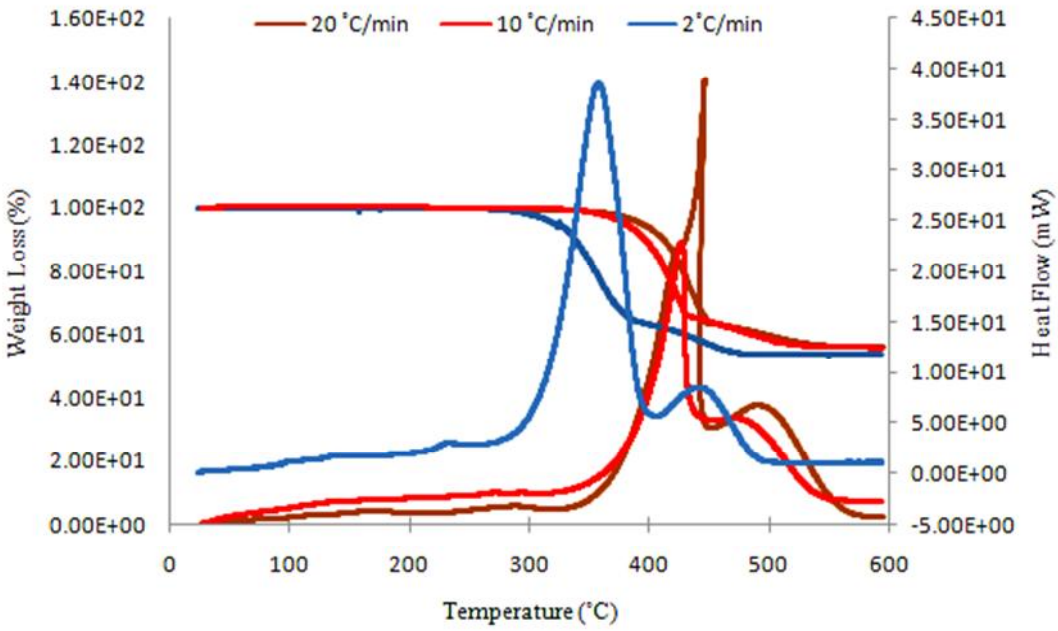

Figure 6.4 TGA and DTG for 90CPP-B at different heating rate.

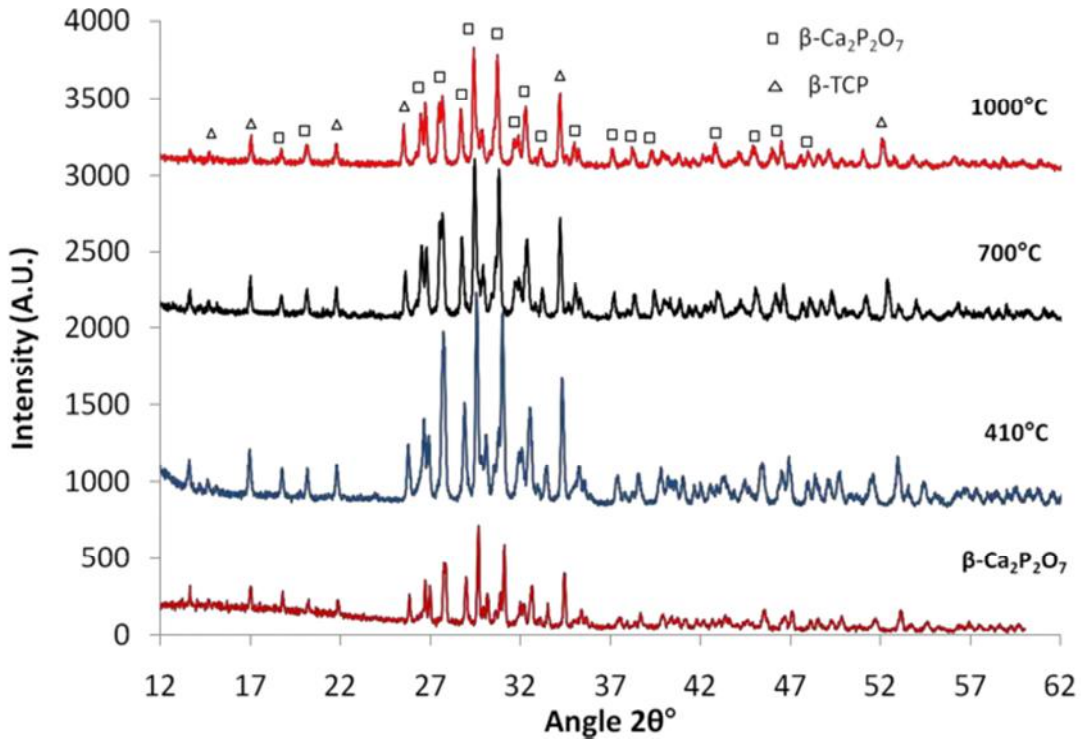

Figure 6.5 XRD analysis of 90CPP-B composite at difference temperature.

XRD analysis was done at the different decomposed temperatures to confirm the crystalline composition of the sintered CPP-B. Figure 6.5 shows that the amorphous CPP-B has changed into crystalline phase at peak 26.6°, 27.7° and 29.5° (2θ). The XRD analysis of CPP-B at different temperatures was found to contain β-TCP as well as β-$Ca_2P_2O_7$. This shows the complete removal of the polymer phase and the existence of CPP-B in the sintered composite.

6.4.3 Heating profile

The heating profile, as defined by the TGA/DTG analysis, was used throughout this study. Apart of complete removal of the polymers phase, this cycle also avoids deformation and the appearance of air bubbles or cracking in the sintered sample. The sintering temperature was varied at 600, 800, 1200 and 1300°C and holding time for each temperature was varied to 3 hours (Figure 6.6).

Heating profile:

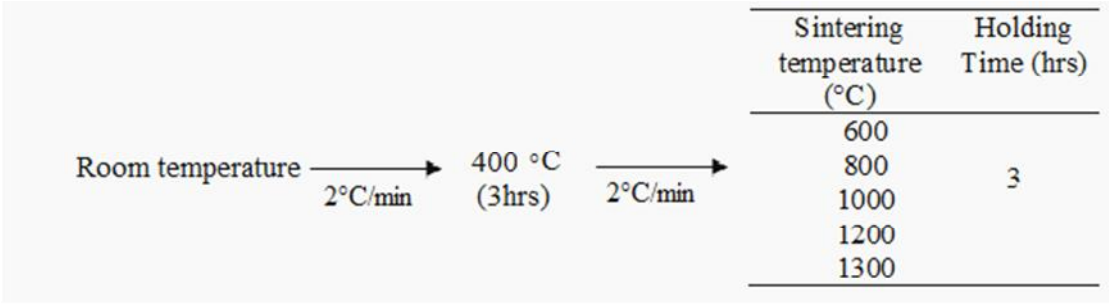

Figure 6.6 Heating profile designed to determine the sintering temperature and holding sintering time

Table 6.5 Shrinkage of polymer composite after sintering at different temperatures for 3 hours.

Sintering Temperature (°C)	Shrinkage (%)			
	Mass	Height	Diameter	Density
600	Brittle and crumble			
800				
1000	75	28	22	140
1200	75	28	23	140
1300	Melted			

After sintering at different temperatures, the shrinkage of each composite was measured, as shown in Table 6.5. Figure 6.7(b) shows the final 3D structures after sintering at 600 and 800°C.Here the composites had difficulty in holding their integrity, as they were brittle and crumbling. As expected, the low temperatures were insufficient to reduce the surface free energy, for these grain sizes, to diffuse to the neighbouring powder particles and increase the density of the composites.

On the other hand, when the temperature was increased from 1000°C to 1200°C, the integrity of the composites improved, as clearly shown in Figure 6.7 (d) and (e). In order to further improve the density of the composite, the composites were held for 12 hours and at 1200 °C, and then increased to 1300 °C and held for 3 hours. This resulted in total glassy phase change of the composites, as shown in Figure 6.6

(g) and (h) respectively, due to the formation of a glass phase from TCP and calcium pyrophosphate above 1280 °C.

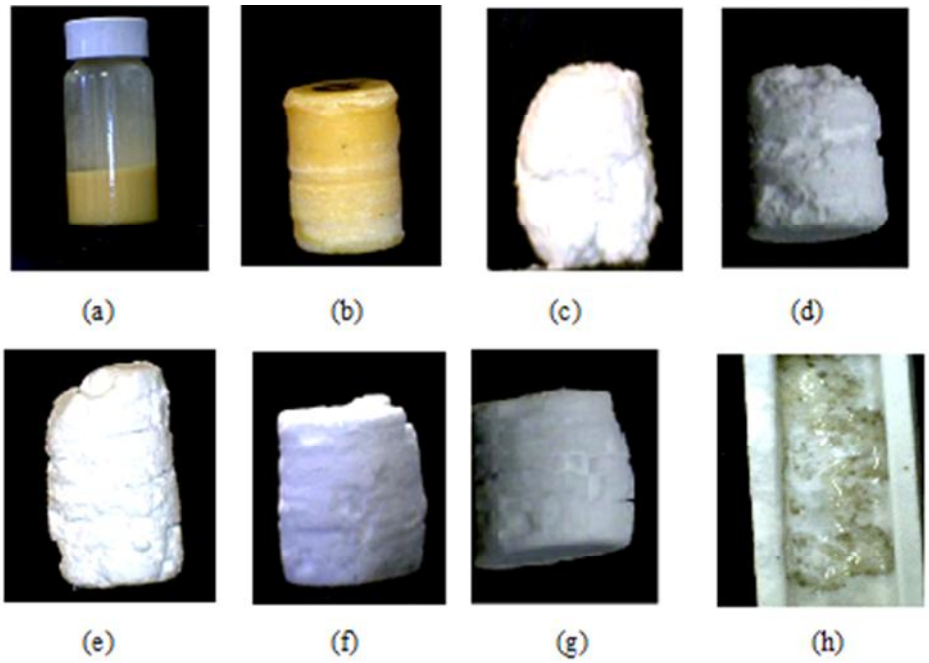

Figure 6.7 Effect of temperature and holding time on the polymer composite before and after sintering; (a) resin, (b) green body, (c) 600°C for 3 hours, (d) 800°C for 3 hours, (e) 1000°C for 3 hours, (f) 1200°C for 3 hours, (g) 1200°C for 12 hours, (h) 1300°C for 3 hours.

Figure 6.8 shows the effect of sintering temperature on the morphology of the composites. At 1000°C, very little sintering has taken place. The phosphate particles appeared not to be adhered or adsorbed to each other. There was a significant difference in the surface of the ceramic held at 1200 °C for 3 hours (Figure 6.8 b); the surface was smooth and completely sealed with a small pore size. When the holding time was increased to 8 hours, as shown in Figure 6.8 (c), the pore size increased, the particles looked rounder and necking appeared. This micrograph shows the starting point of phase changing; from ceramic phase to glassy state, as discussed previously.

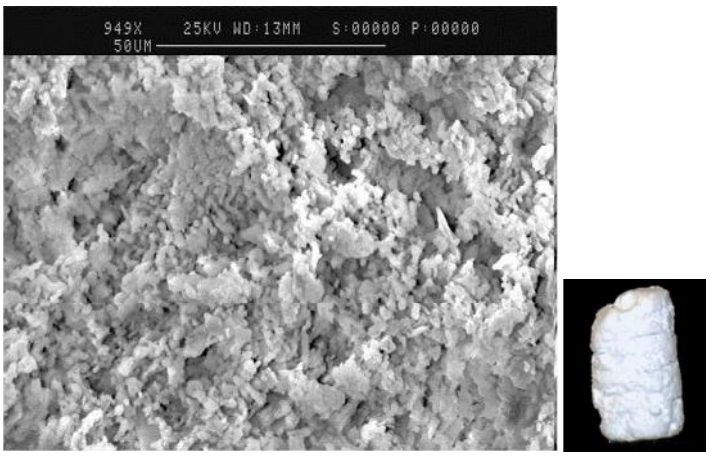

(a)

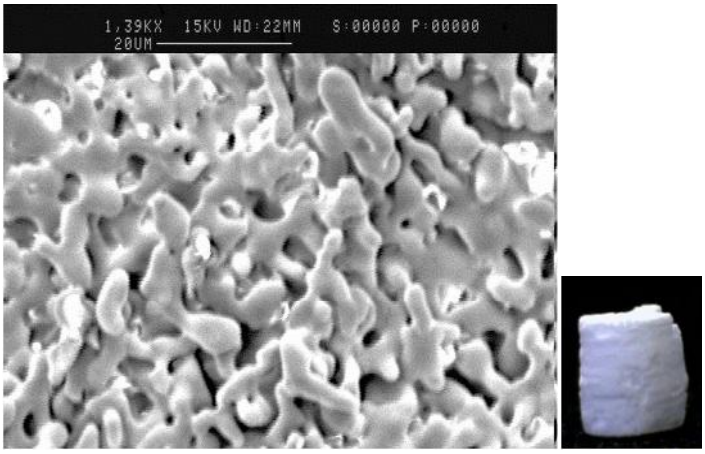

(b)

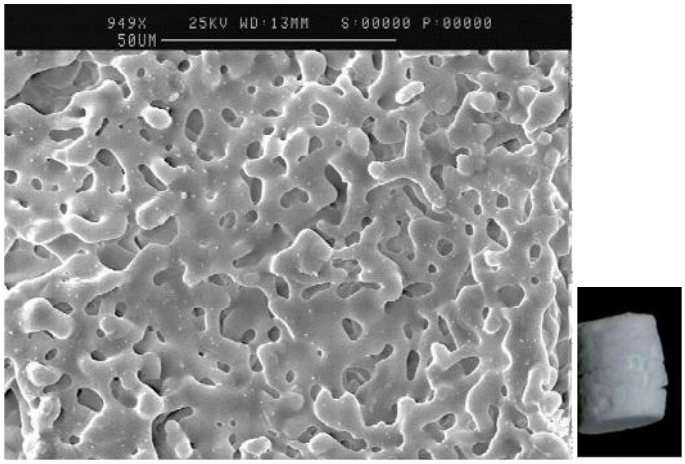

(c)

Figure 6.8 SEM micrograph for: (a) 1000°C for 3hours, (b) 1200°C for 3 hours and (c) 1200°C for 8hours with a 1000x magnification.

For the further development of the ceramic composite study, CPP-A, CPP-B and HAP with different ceramic loadings were prepared in order to find the new biomaterial with optimal properties required as a tissue scaffold. Based upon the finding from the sintering temperatures and time determinations, a new heating profile, to improve the microstructure and properties of the ceramic scaffold, was designed. The sintering temperature was maintained at 1250°C, but varied in sintering time from 5-20 hours. Table 6.6 shows the recipe for the ceramic suspension.

Table 6.6 Composition of ceramic suspension.

Calcium Phosphate	Weight % (wt%) [i]	Abbreviation	Photopolymer Resin	Ratio (%)[ii]
CPP-A	50	50A		
	70	70A		
	100	100A	*HDeDA	70
CPP-B	50	50A	*DPA	20
	70	70A	*BPA	10
	100	100A	PI	3[a]
HAP	50	HAP50	Dye	0.15[b]
	70	HAP70		
	100	HAP100		

[i] : weight percent of total weight of prepolymer (*)
[ii]: ratio based on total volume of prepolymer (*)
[a] : weight percent of PI based on the total weight of prepolymer (*)
[b]: weight percent based on the weight of ceramic added to the total weight of prepolymer (*)

Heating profile

Room temperature $\xrightarrow[10°C/min]{}$ 300°C (1 hr) $\xrightarrow[2°C/min]{}$ 500°C (1hr) $\xrightarrow[2°C/min]{}$ 1250°C RT1, RT2, RT3, RT4 RT5

where RT1, RT2, RT3, RT4 and RT5 was 5, 7, 10, 12, and 20 hours respectively.

The design of heating profile was based on the DTA/ TGA analysis for 90wt% CPP ceramic composite in Figure 6.3. From the TGA graph, the polymer phase started to decompose 315°C and continues to around 600°C. From the TGA graph, the polymer phase started to decompose 315°C and continues to about 600°C. The slower heating rate of 2°C/min and 1 hour holding time, at the decomposition temperature of the phase, caused massive volume reduction of the green bodies via a chemical reaction, as shown on the DTA graph. Therefore the mass loss from the ceramic phase is expected to be unchanged with increasing sintering temperature.

6.4.3.1 Effect of sintering time on density and shrinkage volume of calcium phosphate

Table 6.7 Volume shrinkage of calcium phosphate for difference sintering time (10 data for each formulation).

Sample	Volume Shrinkage (%)				
	RT1	RT2	RT3	RT4	RT5
CPP-50A	4	5	4	4	4
CPP-70A	3	5	5	5	5
CPP-100A	4	3	4	4	4
CPP-50B	3	5	5	3	3
CPP-70B	3	5	3	3	3
CPP-100B	4	5	4	3	4
CAPS-50	5	5	3	3	2
CAPS-70	5	5	3	4	3
CAPS-100	5	5	4	4	5

As the decomposition continued to 1250 °C, the crystals present within the ceramic matrix grow and the pores within the crystals decrease, which affects the shrinkage volume in the ceramic. However, increasing the sintering time does not give significant effect on the volume of shrinkage of the calcium phosphate, as shown in Table 6.6. This could be attributed to the appearance of a β-TCP peak as the sintering time increases, as shown in Figure 6.5.

On the other hand, Figure 6.9 shows a linear relationship between the true density and an increase in sintering temperature. True density is the mass of particle divided by its volume and it this work it was measured by Pycnometer. Changing the loading of the ceramic ratio also significantly affects the density, as the sintering time is increased. For instance, the density of the green body CPP-100A increases by 80% after sintering for 5 hours. In addition, increasing the sintering time from 5-20 hours also increases the density of CPP-100A to 45%.

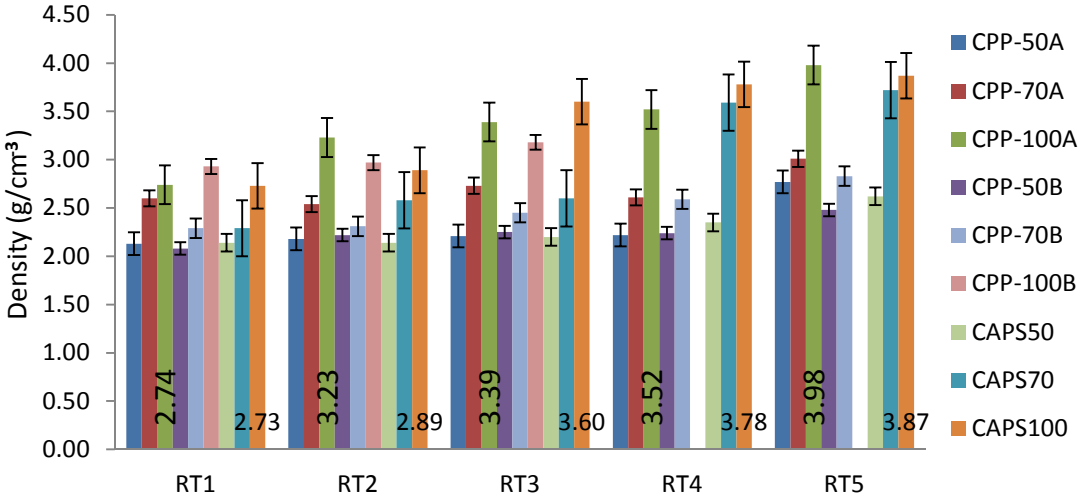

Figure 6.9 Density of different ratio of CPP-A, CPP-B and CAP for different heating profile. The error bars is the standard deviation of five data obtained for each samples. The numbers in the green bar chart are the density for CPP-100A, whereas the orange in colours are for CAPS100.

The porosity in Table 6.8 was quantified by GM methods and is reported as a function of the sintering time. The results show that with an increase in sintering time the ceramic porosity is increased. As the sintering time is increased, the neck formations become apparent as more particles become diffused to the neighbouring powder particles. The necks then merge and shrink resulting in a change of grain shape and formation of interconnected pores along the particle junctions [241].

Table 6.8 Effect of sintering time on the porosity of the ceramic composite.

Sintering Time	Porosity (%)								
	CPP-A			CPP-B			CAPS		
	50	70	100	50	70	100	50	70	100
RT1 (5 hours)	47	48	51	57	59	63	22	18	23
RT2 (7hours)	49	51	53	63	65	66	25	27	28
RT3(10 hours)	55	56	61	66	64	71	31	29	33
RT4 (15 hours5	61	63	66	71	74	76	33	35	37
hours)	73	73	78	76	78	78	34	37	41
RT5 (20 hours)									
	Standard deviation								
	CPP-A			CPP-B			CAPS		
	50	70	100	50	70	100	50	70	100
RT1 (5 hours)	3	2	3	2	3	3	2	3	2
RT2 (7hours)	2	2	3	3	2	1	1	3	2
RT3(10 hours)	3	3	2	3	2	1	1	2	3
RT4 (15 hours5	1	1	1	3	2	1	3	1	1
hours)	3	3	1	1	2	2	1	1	2
RT5 (20 hours)									

The pores interconnectivity is well defined and consequently affects the microstructure of the composite (Figure 6.10). By increasing the sintering time from 5 to 20 hours, the grain size increases greatly to 7.99 μm from 5.52 μm whereas the density increases to 3.98 g/cm^{-3} from 2.74 g/cm^{-3} as shown in Figure 6.11.

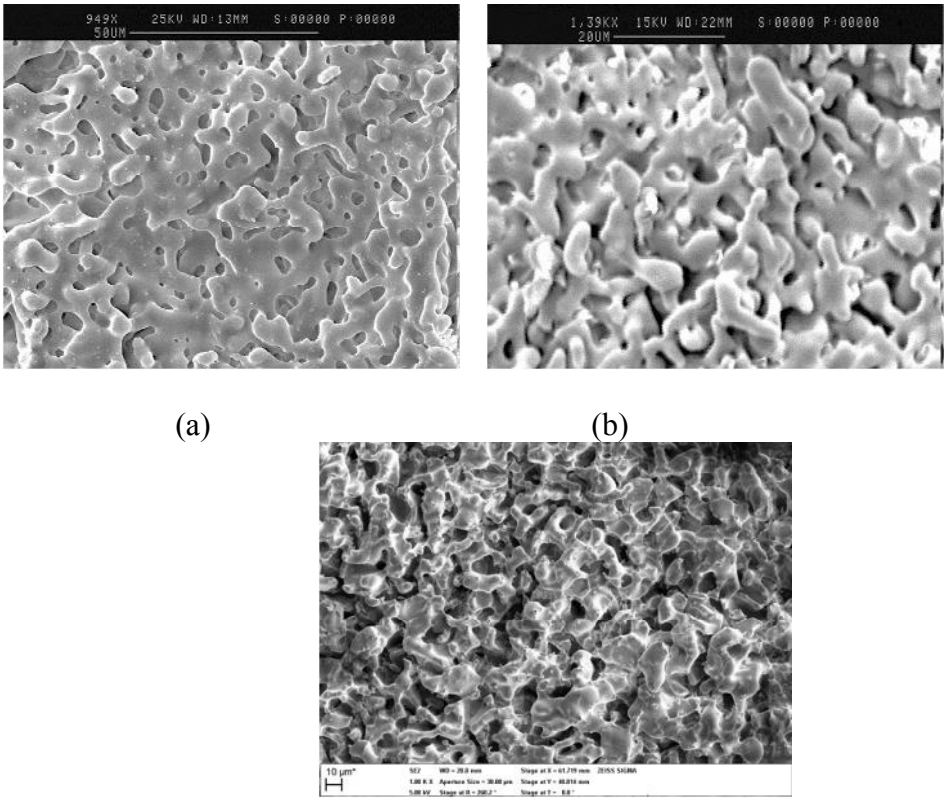

(a) (b)

(c)

Figure 6.10 Surface morphology for CPP-A after sintering for (a) 5 hours, (b), 12 hours and (c) 20 hours (1000x magnification).

Grain growth can be expressed by equation 6.13 [242]:

$$G^a - G_o^a = K_o t \exp\left(-\frac{Q}{RT}\right) \qquad (6.13);$$

where G and G_0 are the average grain size after and before sintering, a is the kinetic grain growth exponent, T is the sintering temperature, t is the sintering time, Q is the apparent activation energy for grain growth, K_o and R are constants. According to this grain-growth model, CPP grains have more time to grow with a longer sintering time. These results coincide with the increase in average grain size and density of CPP as sintering time increased.

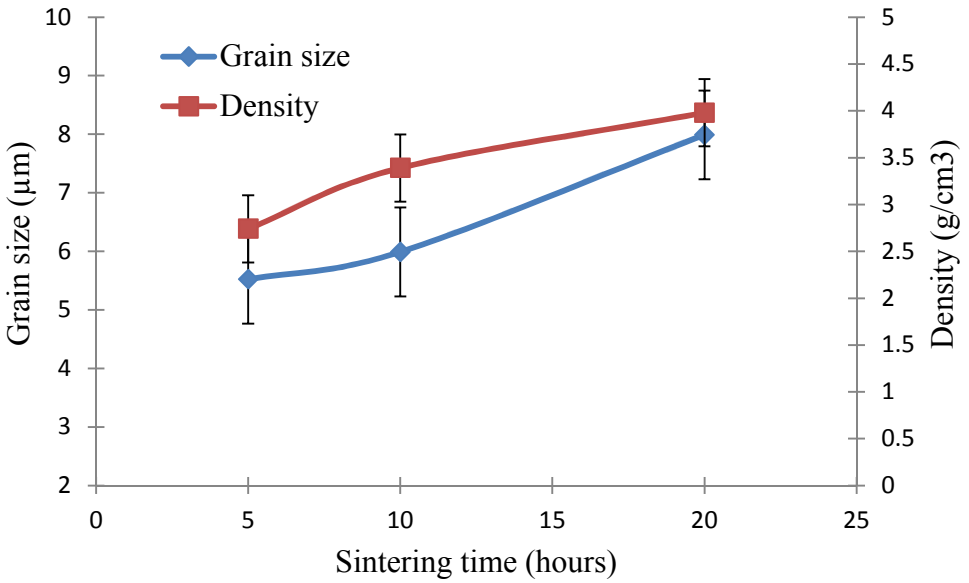

Figure 6.11 The grain size and density of CPP-A with different sintering times. The error bars is the standard deviation of three data obtained at each sintering time.

Figure 6.12 shows the XRD pattern for CPP-A sintered at 1250℃ for different times. After increasing the sintering time to 5 hours, the XRD peak for the α-$Ca_2P_2O_7$ phase change and intensify especially at the range of 26 – 30℃ and 42-47℃. The synthesised CPP-A was amorphous at 27.5℃, and then the peak becomes sharper to reflect the phase transformation to crystalline α-$Ca_2P_2O_7$. In addition, after 5 hours sintering time, the appearance of β-TCP, has increased the density of the polymer ceramic and this is in good agreement with the increase in density, as discussed above. Figure 6.11 shows that as the sintering time was increased, the crystals become denser and the particle size increases.

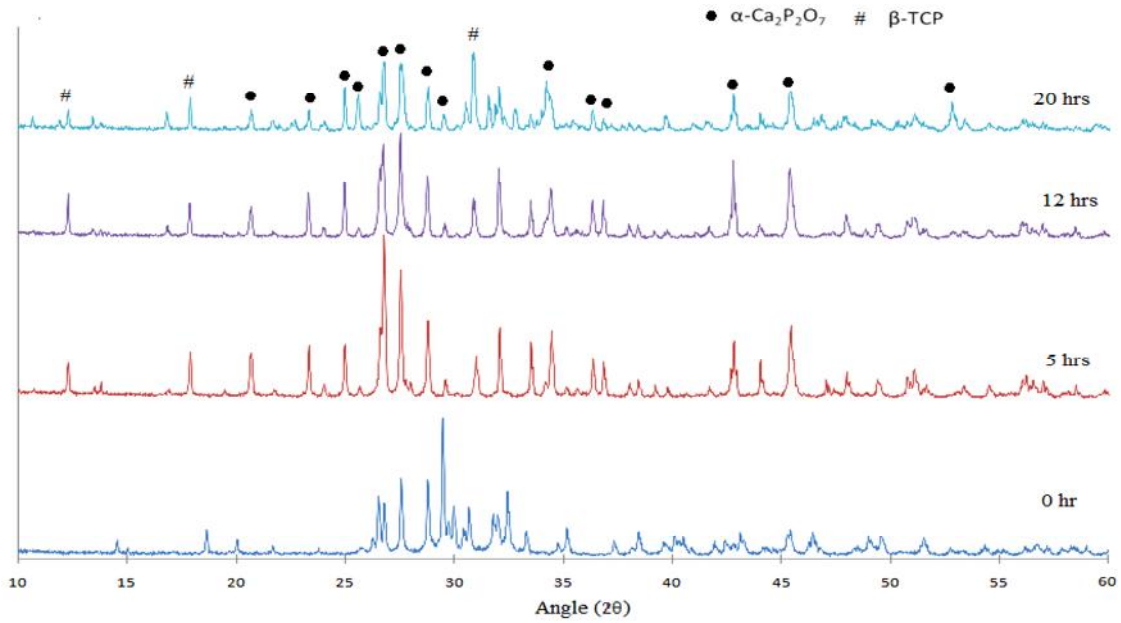

Figure 6.12 XRD pattern for CPP-A at different sintering time.

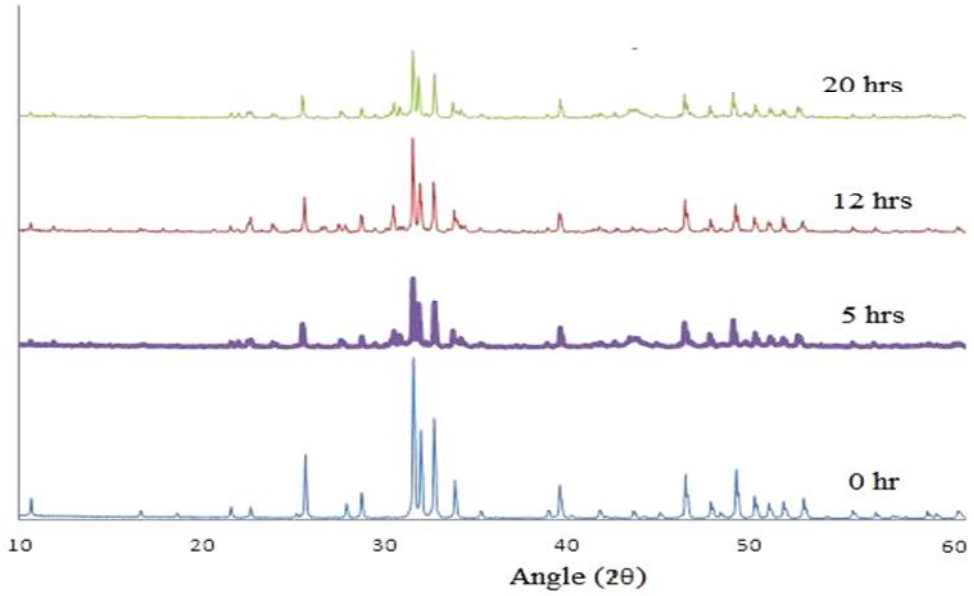

Figure 6.13 XRD pattern for HAP at different sintering time.

In comparison to this, Figure 6.13 shows no changes in diffraction pattern for HAP suggesting that there is no change in crystalline composition, or in the structure of the calcium phosphate. This shows that the compound is still calcium phosphate as the sintering time is increased at 1250℃.

6.4.3.2 Effect of sintering time on compressive strength and young's modulus of calcium phosphate

The compressive strength and elastic modules were determined from the stress–strain relationship. Figure 6.14 shows the effect of increasing sintering time on the compressive strength and Young's modulus for various compositions of calcium phosphate. The compressive strength increases as the density increases, which is in agreement with the increase of density, as shown Figure 6.9. It can be observed that for CPP-100A, the true density increased from 31% to 91% when the sintering time increased from 5 to 20 hours. As a consequence, the compressive strength of CPP sintered for 20 hours is higher than that of samples sintered for 5 hours. The volumetric shrinkage could also be linked to the ceramic densification, which also could influence the compressive strength of the sintered ceramic.

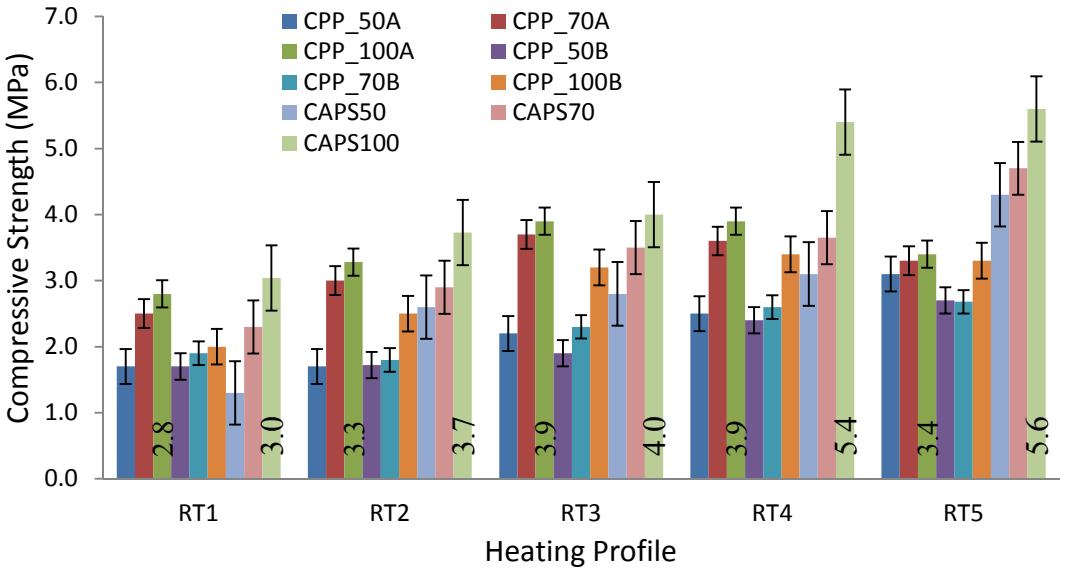

(a)

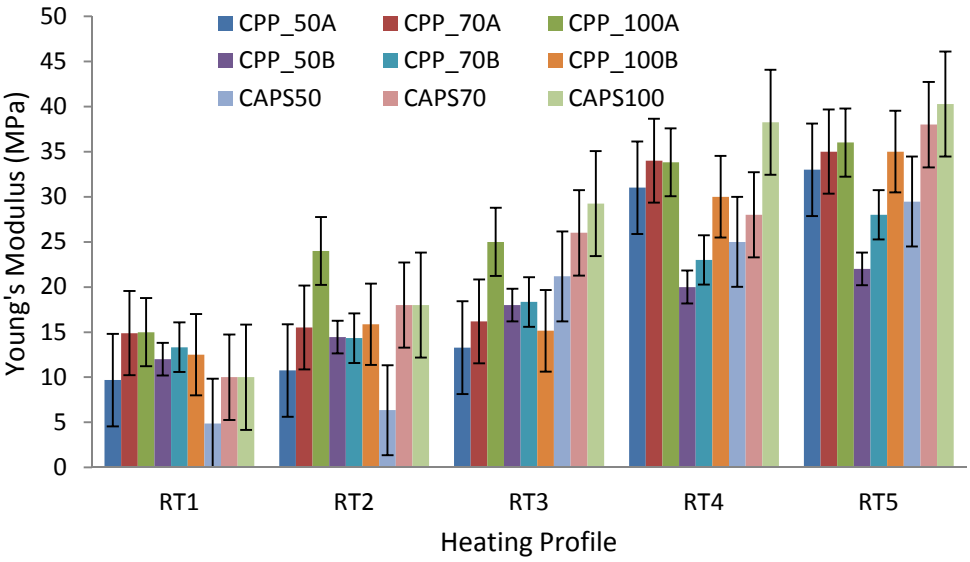

(b)

Figure 6.14 Effect of sintering time on the (a) compressive strength and (b) Young's modulus of different ratio of calcium phosphate ceramic composites. The error bars is the standard deviation of ten data obtained at each sintering time.

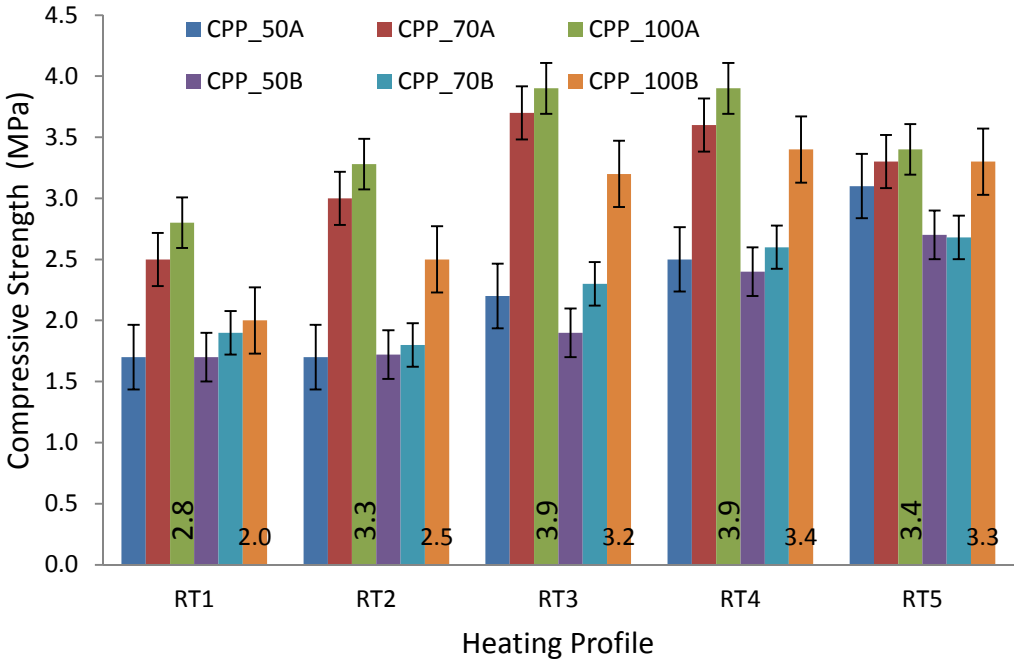

Figure 6.15 Effect of sintering time on the compressive strength of different ratio of synthesised calcium pyrophosphate (CPP-A) and as-received calcium pyrophosphate (CPP-B) composites. The error bars is the standard deviation of ten data obtained at each sintering time.

Figure 6.15 represents the effect of sintering time on the compressive strength for different ratios of synthesised calcium pyrophosphate (CPP-A) and as-received calcium pyrophosphate (CPP-B) composite. With extending the sintering time from 5 to 10 hours, the compressive strength increases significantly for both types of CPP, with an increase in CPP loading. For instance, the compressive strength for CPP-100A with 100 wt% ceramic loading has increased to 39% of strength after sintered from 5 hours to 10 hours, whereas for CPP-100B it has increased to 70% of strength.

Furthermore, increasing the sintering time from 10 to 20 hours resulted in the compressive strength reducing to 3.4 ± 1.0 MPa. This decrease is believed to be associated with the presence of micro-cracks in the surface morphology of samples sintered between 12 and 20 hours. Tetragonal to monoclinic phase transformation occurs at 1200℃, but in this study the transformation may only occur after sintering

for 12 to 20 hours at 1250℃. Figure 6.16 (a) and (b) shows the apparent micro-cracks for both samples respectively. As the sintering time is increased, the neck formation becomes apparent as more particles become diffused, resulting in crystallite growth. Higher porosity could also contribute to the reduction the integrity of the composites.

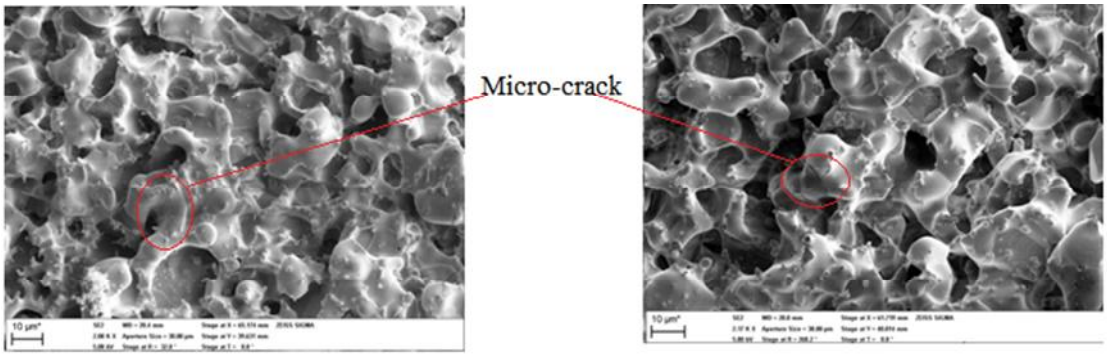

(a) (b)

Figure 6.16 Surface morphology of the polymer composite after sintered for 12 and 20 hours respectively show the apparent present of the micro-cracks (magnification 2000x).

From this work we can observe that CPP-A exhibits a higher compressive strength than CPP-B. This is due to differences in particles size and distribution, as CPP-A has a higher mean volume of smaller particle sizes as compare to CPP-B. The bigger particle size distribution for CPP-B (Figure 6.2 (b)) has resulted in agglomeration, as the ceramic loading increased during preparation of the ceramic suspension and subsequent fabrication. Consequently, this contributes to the lower compressive strength. Backscattered secondary electron (BSE) analysis on the composition of CPP-A and CPP-B has shown the difference in distribution of both calcium phosphate powders, in the polymer matrix, of the green body structures (Figure 6.17). BSE is used to detect a contrast between areas with different chemicals and is used here to identify the difference between calcium and polymer matrix.

These results are in strong agreement with the viscosity measurements of the ceramic suspension.

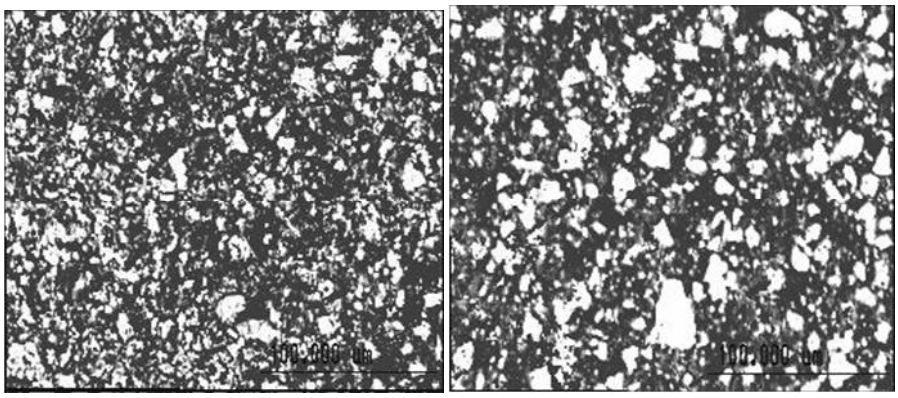

(a) (b)

Figure 6.17 Comparison of backscattered electron analysis of CPP-A (a) and CPP-B (b).

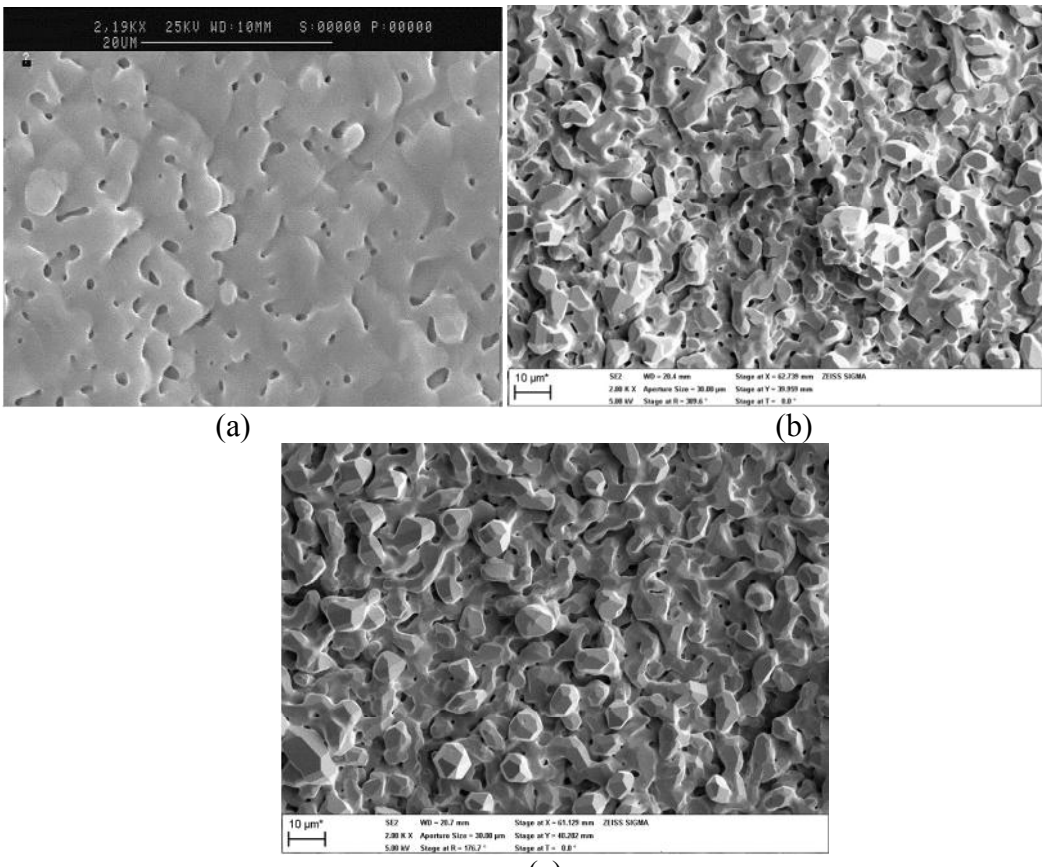

(a) (b)

(c)

Figure 6.18 Surface morphology for polymer ceramic at different sintering time; (a) 5 hours, (b) 12 hours and (c) 20 hours prepared from HAP suspension.

The surface morphology of the polymer ceramic HAP, has shown the most apparent transformation as the sintering time increases from 5 hours to 20 hours (Figure 6.18). HAP is well known to have a higher surface energy. The high diffusion rate resulting from this high surface energy gives rise to better inter particle contact and increases the elastic modulus of the composite [243]. At 5 hours (Figure 6.18 (a)), the surface of HAP is mostly closed, with the surface showing a rounding of particles and early stage neck formation. And as the time increases pores start to interconnect and the angular-necking shape become highly visible. At 20 hours of sintering, the interconnected pores evolve to pore closure and further crystal densification, which contributes to the increased of mechanical properties

Any new biomaterial developed as a bone replacement should have mechanical strength similar to the natural bone, to maintain integrity until the new tissue regenerates. The compressive strength and Young's modulus of cancellous bone has been reported over a wide range between 4-12 and 20-500 MPa respectively [116]. In this study, the compressive strength of all CPP ceramic composite and HAP ranged from 1.7 MPa to 6.7 MPa and Young's modulus between 10 MPa and 45 MPa. The results suggest that it may be possible that different types of calcium phosphate could meet the mechanical requirements and support new bone tissue regeneration when implanted in the body, especially if the patient is not putting significant burden on the scaffold. Therefore in order to provide a clinical application for the formulated ceramic composite, a study on the vitro degradation of the composite was performed.

The addition of calcium phosphate coupled with a high temperature sintering and a longer sintering time has a significant effect on the mechanical properties exhibited by the bioceramic. The successful fabrication of a novel bioceramic

polymer composite with μSL technique offers the possibility of designing complex tissue scaffolds with optimum mechanical properties for specific tissue engineering applications.

6.4.3.3 Bioactivity of polymer ceramic

SEM analysis demonstrates the strong influence of sintering time on the microstructure and morphology of the ceramic composites, as discussed previously. It can be seen that as the sintering time increases, the formation of microporosity becomes prominent and their connectivity offers good potential for cell attachment and proliferation. The variation of pH value relative to soaking times in simulated body fluid (SBF) of composite is shown in Table 6.9.

Table 6.9 Variation of pH value in SBF for CPP-70A sintered at RT3 (10 hours). The standard deviation was obtained from three data at each sintering time.

Soaking time (days)	pH reading (±0.01)
0	7.43
1	7.51
4	7.54
8	7.61

The increasing pH value during the first day is believed to be due to the partial dissolution at the surface level, indicating the high reactivity of these materials. These shows the interchange between Ca^{2+} and H_3O^+ during the formation of the apatite [244]. This interchange increases the pH level as the immersion time increased, consequently encouraging the formation of apatite nuclei on the CPP and HAP surfaces. Figure 6.19 shows that the gradual development of apatite formation on the

surface of CPP-70A for RT3 (sintering of 10 hours) as a result of increasing the number of days of immersion in SBF to 1, 4, and 8 days respectively.

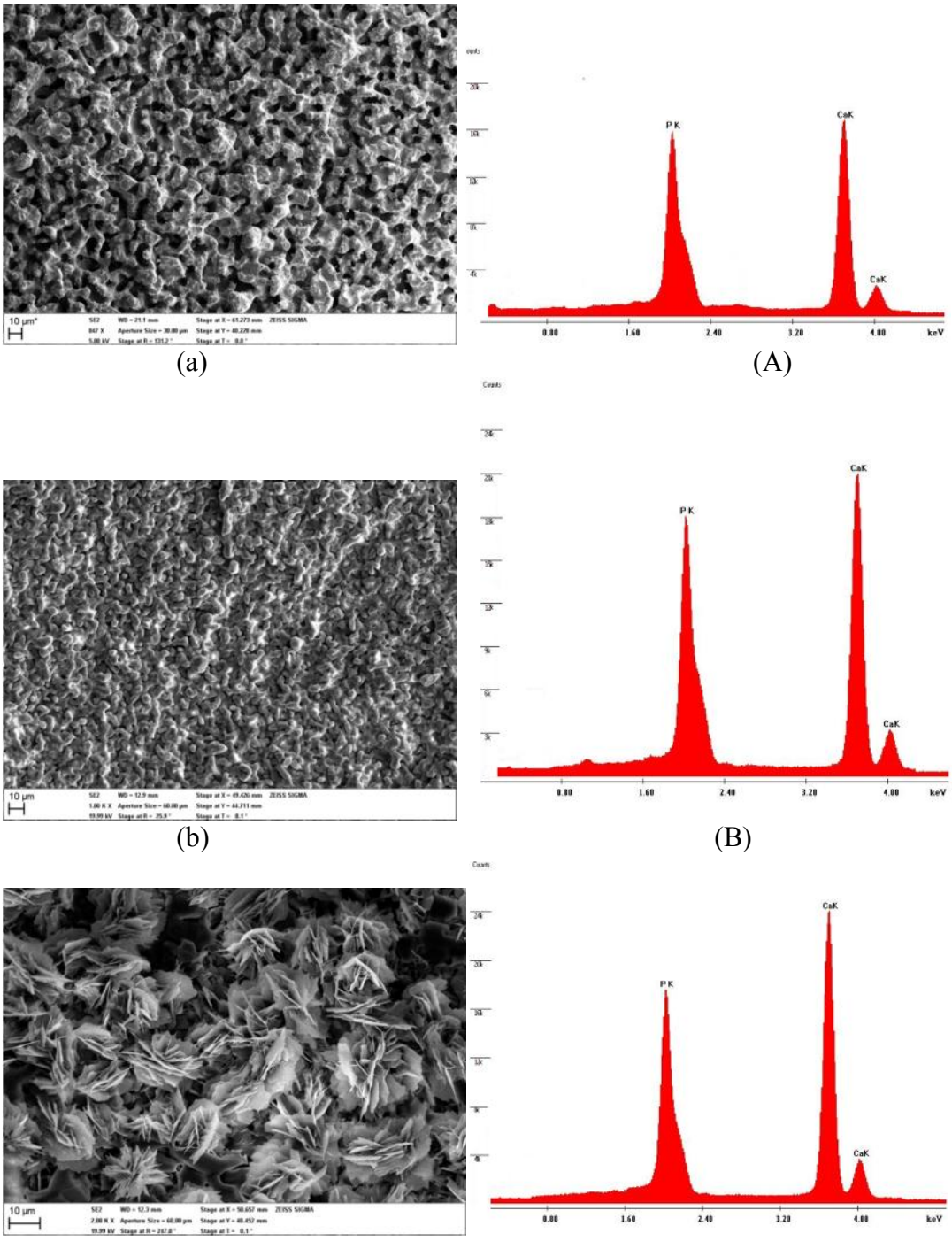

Figure 6.19 SEM micrograph of CPP-70A after soaking for (a) 1, (b) 4 and (c) 8 days. A, B and C represent their EDAX analysis respectively.

Figure 6.19 shows that as the soaking time increases, there were distinguishable changes on the surface morphology of the samples. After soaking the CPP-70A in SBF for 8 days, there was an abundance of leaf-like depositions with lengths of ~ 10 μm. These were evenly distributed over the surface of the samples, proving nucleation of apatite layer. The presence of large pores amongst the leaf-like crystallite indicates the effect of immersion and corrosion. The calculated Ca/P ratio is about 1.76, which is close to the theoretical value of stoichiometric HA (Ca/P=1.67), and Ca/P ratio of the human bone, as it ranges between 1.6 and 1.7 depending on the age of the person.

Table 6.9 shows that the value of Ca/P ratio has increased from 1.20 before immersion to 1.30 after immersion confirming growth of an apatite layer on the surface, which is confirmed by the EDAX analysis in Figure 6.19. The higher peak intensity of Ca after 8 days, explained the higher ratio Ca/P, as Ca ions are used for the re-precipitation process of HAP large particles [245]. These results were in agreement with the increase in sample weight, as the immersion period was raised (Figure 6.20), which can be attributed to the formation of apatite. On the other hand, the decrease in peak intensity of phosphorous, as shown in Figure 6.19(A), (B) and (C), is believed to be due to the loss of phosphorous during sintering, as phosphorous could be escaping from the surface of the sample as gaseous oxides, when being sintered in air [246].

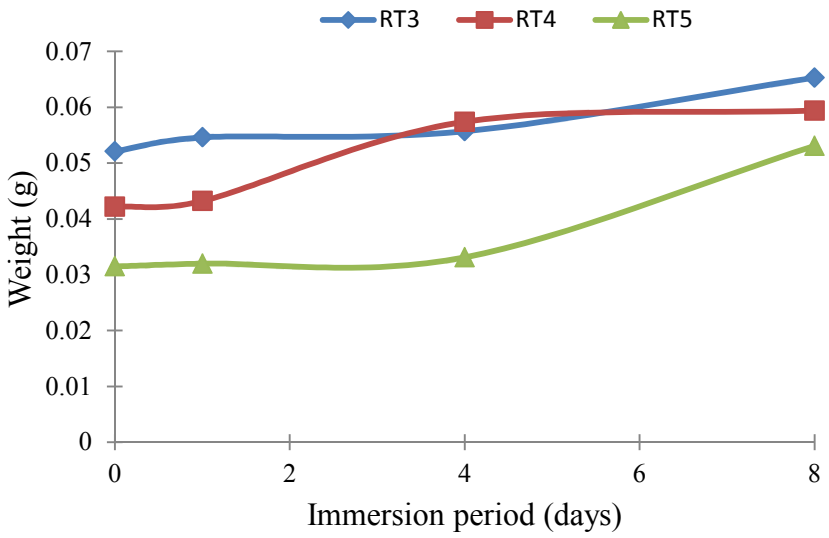

Figure 6.20 Weight of the RT3-CPP-70A after immersion in the SBF solution for 1, 4 and 8 days. Three data was obtained at each period.

Table 6.10 Spectral calcium and phosphorous concentrations with their corresponding Ca/P ratios.

Day	Sintering time					
	10 hr			20 hr		
	Ca (wt %)	P (wt %)	Ca/P	Ca (wt %)	P (wt %)	Ca/P
1st	57.14	42.86	1.33	52.89	47.11	1.12
4th	63.26	36.74	1.53	55.45	44.55	1.24
8th	64.81	35.19	1.76	57.43	42.57	1.31

Table 6.10 shows the spectrum of calcium and phosphorous concentrations, with their corresponding Ca/P ratios for 10 and 20 hours sintering time. This table shows that the Ca/P values for 20 hours are less when compare to 10 hours sintering time. The EDAX analysis has shown the low peak intensity of Ca and P, as shown in Figure 6.19(C). The small ratio of Ca/P has resulted in less formation of apatite on the composite surface. After 8 days in SBF medium, the apatite deposited on the surface of composite (RT5 CPP-70A) appeared as sub-micrometer crystals. The composite structure showed signs of immersion and corrosion, as were indicated by

the reduction in pore size and shrinkage of composite surface area, as shown in Figure 6.21(b).

A distinct difference of apatite formation, for both sintering times, could be seen in Figure 6.21(a) and Figure 6.19(c). At 10 hours of sintering time, the leaf-like particle formed on the sample morphology whereas after 20 hours, the morphology appeared to be granule-like. This has shown the significant effect of sintering time on the ceramic morphology.

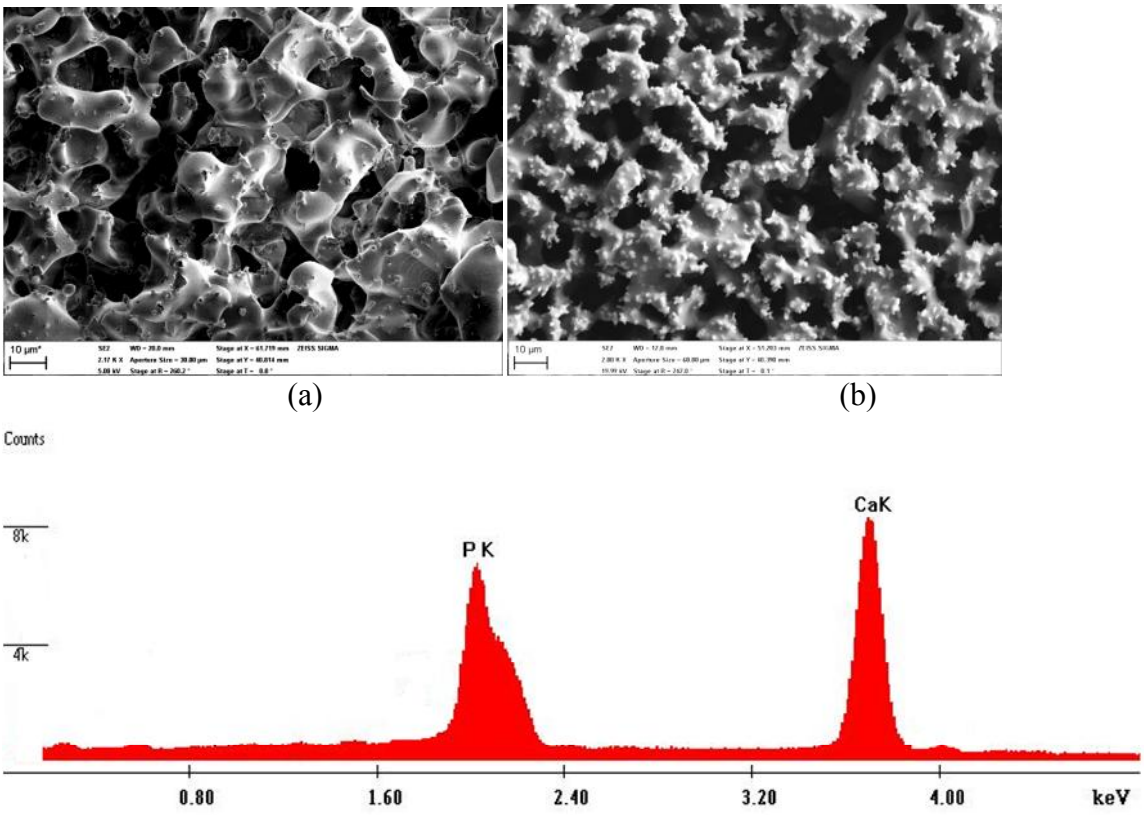

Figure 6.21 Surface morphology of RT5-CPP-70A for (a) pre-immersion and (b) post immersion and (c) EDAX analysis for post immersion of the composite sample after 8 days in SBF solution.

By comparison, the surface morphology of RT5-CPP-70A (Figure 6.21 (b)) has similarities to RT3-CPP-70A (Figure 6.19 (a)), which was immersed in SBF medium for 1 day. This suggests that for longer sintering times; the formation of apatite presumably only could occur if the immersion time was longer. Based on SEM and EDAX analysis on the composite samples, increasing the sintering time has a significant effect on the bioactivity of the samples, which contributes to the mechanical properties of each of the composites.

6.5 Conclusion

In this study it was shown that it was possible to synthesize a new photopolymer resin filled with calcium phosphate powder and to fabricate calcium pyrophosphate ceramics of defined architecture via a microstereolithography technique. The formation of $Ca_2P_2O_7$ ceramic was confirmed using XRD, TGA and DTA analysis. Different sintering times were designed in order to study its effect on the mechanical properties and microstructure of the composites. With low sintering times of 5 to 10 hours, the compressive strength increases significantly for both types of CPP as well as with increasing the CPP loading. However, further sintering time for 12 hours induced micro-cracks on the particles surface, which was responsible for decreasing the mechanical properties of the composites. Nevertheless, the compressive properties of the heat treated composite were quite close to those of cancellous bone (2–17 MPa).

In addition, XRD and SEM-EDAX confirmed the occurrence of apatite on the surface of ceramic composites. A study on sintering times has provided significant insight into the re-precipitation and microstructure of apatite formation, which coincided with the surface morphology shown in the SEM images. Increasing the

sintering time was expected to enhance the apatite nucleation onto the composite surface. Finally, novel ceramic composites prepared from calcium phosphate have bioactivity properties that could be used in bone substitutes and tissue engineering applications.

CHAPTER 7

Polymer Ceramic Structure Fabricated via 3D Extruder .

7.1 Introduction

To date the fabrication of three dimensional tissue scaffolds has attracted a lot of attention from the science community. This is due to their ability to manufacture and then seed the resultant structure, which combined can make the creation of an natural artificial organ a reality. There is also a significant demand for synthetic tissue or bone replacement materials used for tissue engineering due to limited numbers and the side effect arising from autograft or allograft transplant. Direct manufacturing, such as microstereolithography and 3D printing are amongst the techniques that are capable of producing complex and high resolution microstructures, via an additive layer-by-layer process. It allows the material scientists and physicians to design and rapidly produce custom-made scaffolds or implants by taking anatomical information of the patient's target defect (e.g. scan, MRI images) and created on a CAD machine [247].

Currently, synthetic bone replacement materials, based on calcium phosphates, are widely explored due to its similarity with natural bone. Furthermore, their material properties can be engineered to suit the mechanical and physiologic demands of the host tissue by controlling the volume fraction, morphology and arrangement of the reinforcing phase [151]. Calcium phosphates, such as HAP, is interesting to study because of its stoichiometric similarity to the inorganic part of natural bone [1-3]. A composite, for a bone tissue replacement, should have high initial strength and tailored initial elastic modulus close to the elastic modulus of bone. Polymer on its

own are low in mechanical strength and stiffness, whereas ceramics are brittle and ductile. Biomaterials with combination of polymer and ceramic could confer favourable mechanical properties, toughness and plasticity via the polymer phase and inherent higher stiffness and strength of the ceramic phase. Detailed information on polymer composites has been discussed in Chapter 3.

The advancement and versatility of 3D printing has opened up abundant opportunity for the researchers to fully utilise the technology in tissue engineering applications. 3D printing technology is based on additive layer manufacturing (ALM) methods is an alternative process to microstereolithography. The base materials could be powder, synthetic polymer or polymer composite. 3D parts are created by a layered printing process according to sliced cross-sectional computer-assisted design (CAD) and extruded through a nozzle as molten plastic. The process is repeated layer by layer until the part is complete [248]. Figure 7.1 shows the schematic diagram of a 3D Extruder nozzle moving in x-y direction to create outlines of each layer according to a CAD file.

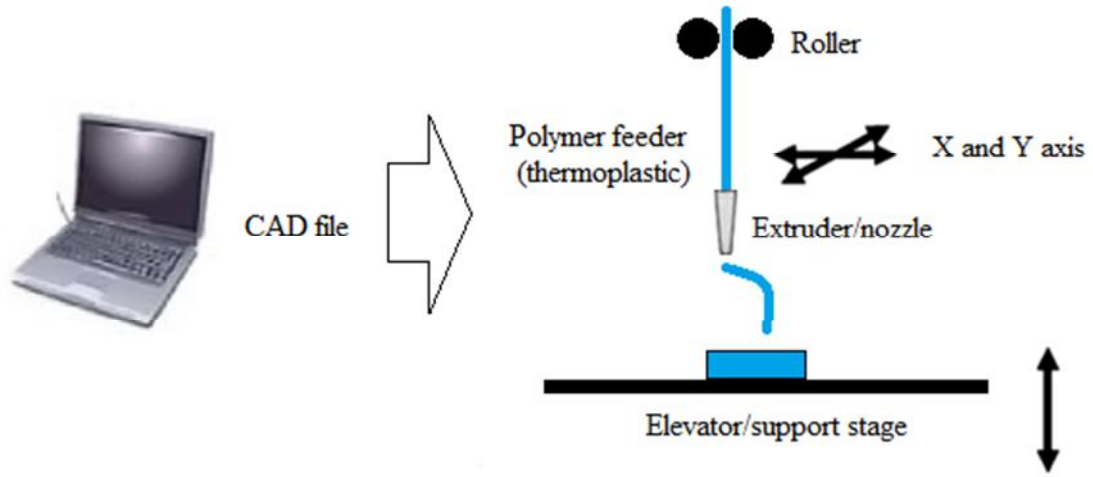

Figure 7.1 Schematic diagram of the 3D Extruder technique.

This chapter is dedicated as a preliminary study and to explore hydroxyapatite (HAP) as a candidate precursor in 3D printing. A 3D Extruder manufactured by Bits from Bytes, UK was purchased and polycaprolactone (PCL)/ hydroxyapatite (HAP) was prepared and fabricated on the 3D Extruder for further investigation. Commercially, BFB 3000 3D Extruders (Figure 7.2) use thermoplastics such as acrylonitrile butadiene styrene (ABS) and polylactic acid (PLA) as a precursor or polymer feeder. It is one of the most convenient and versatile extruding machines due to its user friendly operation conditions, wide choices of polymer feeder and the ability to produce scaffolds without any binders. Figure 7.3 shows the wide choice of polymer feeder offer by the manufacturer. In addition, the cost for single head printer machine is less than £ 2 000; which give it an advantage when compared to other type of rapid prototyping techniques such as envisionTEC Desktop; which cost more than £ 10 000.

In Chapter 6, envisioTEC Desktop machine successfully fabricated ceramic composite up to 100wt% of ceramic loading. However, the composite has had reproducibility problem and suffered stress-post curing which affect the properties of the composites. This preliminary study was undertaken to assess the feasibility of the machine to fabricate photopolymer resin with higher loading of ceramic particles. This could open up the possibility or its potential as a fabricating tool for tissue engineering applications.

Figure 7.2 BFB 3000 3D Extruder from Bit by Bytes, UK

Figure 7.3 Wide selection of polymers feeder as starting materials for BFB 3000 3D Extruder such as acrylonitrile butadiene styrene (ABS) and polylactic acid (PLA) (http://www.bitsfrombytes.com).

7.2 Materials and Methods

7.2.1 BFB 3000 3D Extruder

BFB 3000 3D Extruder was purchased from Bit by Bytes, UK and shown in Figure 7.2. The machine offers a simple and direct fabricating method, where it heats the biopolymer above its glass transition temperature to give the material a paste-like

consistency and applying pressure through the extruder or print head. The extruder then pushes out a very fine plastic thread which is applied layer by layer according to x and y co-ordinates, building a solid, 3D object. It is important to maintain shear-stress on the material while it is being layered to ensure continuity of the process. Table 7.1 represent the specification of the machine.

Table 7.1 BFB 3000 3D Extruder specification provided by manufacture Bit by Bytes, UK.

Maximum built size X axis Y axis Z axis Z axis resolution	 275 mm 275 mm 210 mm 0.125 mm (125 µm)
Print tolerance X and Y axis Z axis	 ±0-1% of object dimension or ± 0.2 mm (whichever is greater) ± half the processed Z resolution
Print speed extruded volume	Maximum 15mm^3 per second print and polymer dependent
Maximum operating temperature at extruder tip	280°C

7.2.2 Composite filament preparation

Composite filament was prepared by a researcher at Microelectronic and Biosensor Laboratory, University of Warwick. HAP was dispersed in dichloromethane (DCM), (Sigma Aldrich, UK) and stirred for 1 hour. Polycaprolactone (PCL) was then dissolved in the HAP suspension and stirring continued at 80 °C. After 1 hour, the DCM was evaporated from the mixture on a glass plate and the resultant HAP/PCL composite film was placed into a water bath at 100°C. At regular intervals, the HAP/PCL composite was removed from the water bath and rolled between two glass plates. The procedure was repeated until a solid composite filament of 3 mm diameter

was achieved (Figure 7.4). 100 and 200wt% of HAP were prepared as for a preliminary study.

Figure 7.4 Composite filament of 100wt%HAP/PCL with 3 mm in diameter.

7.2.3 Ceramic composite printing

The 3 mm filament of the HAP/PCL composite was placed into the extruder of the BFB 3000 3D Extruder. The head temperature was set to 200°C and printing was commenced without any modification to the Extruder. Upon completion of printing, the printed objects were allowed to cool to room temperature and removed from the build platform with a scalpel. To investigate the feasibility of the machine, a dumb-bell shape structure was printed. The dumb-bell was characterised with thermogravimetrical analysis (TGA) under a flow of air with heating rate of 10°C/min using a Pyris Diamond, Perkin Elmer (UK) in order to find the decomposition temperature of the composite. The sintering process was performed in a furnace, Lanton Thermal Designs Limited (LTD, UK).

7.3 Results and Discussion

A dumb-bell shape composite with 100wt% HAP was successfully fabricated with the BFB 3000 3D Extruder as shown in Figure 7.5. This shows the feasibility of the machine to fabricate a 3D structure of polymer ceramic. Figure 7.6 represent the TGA for the composite.

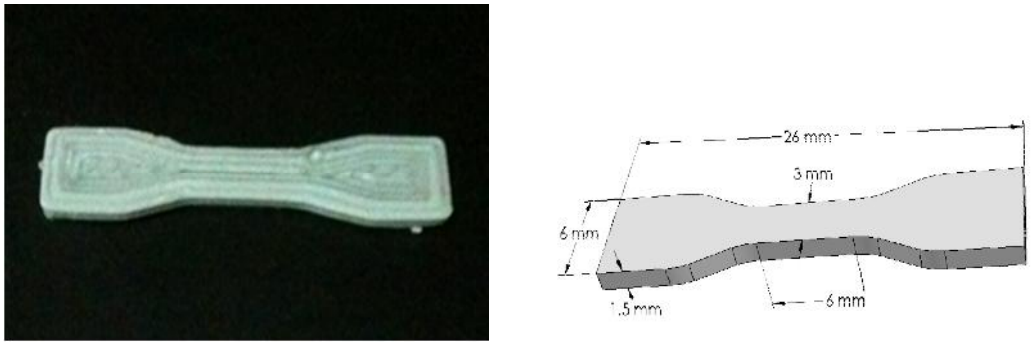

(a) (b)

Figure 7.5 (a) Green body of 100wt%HAP/PCL in dumb-bell shape is an exact replica of the dumbbell-shape's drawing .

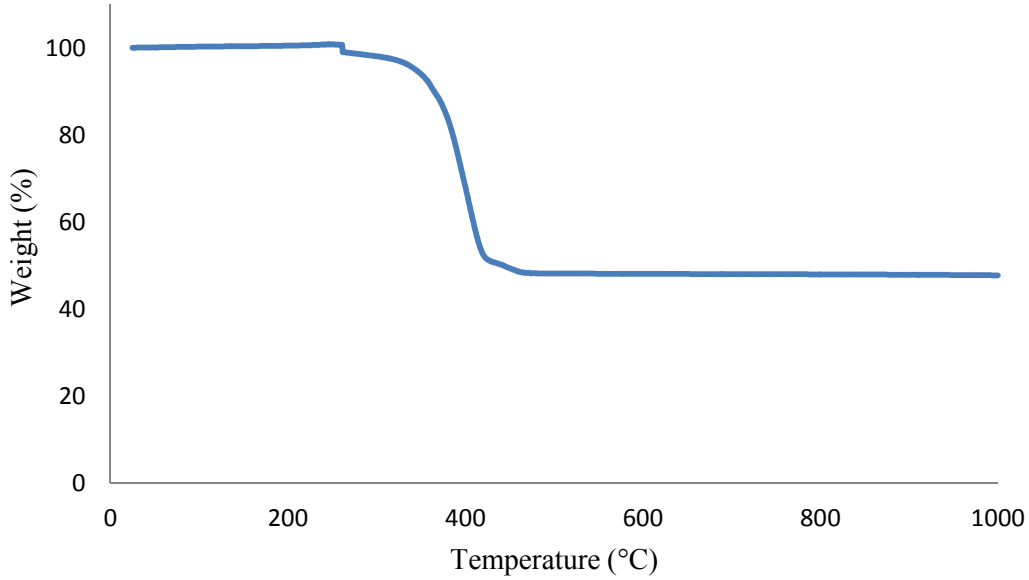

Figure 7.6 Thermogravimetrical analysis (TGA) of 100wt%HAP/PCL composite

The onset decomposition temperature for the composite was found at 350°C with 50% of residue. The decomposition temperature for HAP/PCL composite was

found to be at the same range of calcium pyrophosphate (CPP-B/HDeDA) composite at 370°C as discovered in Chapter 6. Therefore, the same heating profile used for CPP-B composite was used for the new composite fabricated via the 3D Extruder as shown below:

Room temperature $\xrightarrow{10°C/min}$ 300°C (1 hr) $\xrightarrow{2°C/min}$ 500°C (1hr) $\xrightarrow{2°C/min}$ 1250°C (10hours)

After sintering at 1250°C for 10 hours, the structure of dumb-bell test pieces were disintegrated and brittle. Figure 7.7 clearly shows the failure structure of the sample.

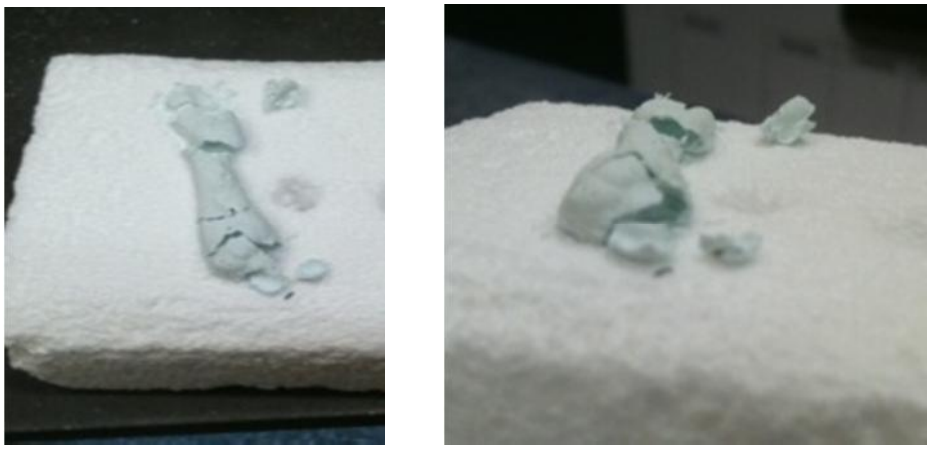

(a) (b)

Figure 7.7 The disintegrated dumb-bell structure after sintered for 10 hours at 1250°C; (a) top view and (b) side view.

The unsatisfactory result on the sintered structure is presumably due to the air trapped between layered fabrications. Based on the machine specification in Table 7.1, the maximum print speed of extruded volume is 15mm^3/sec and it depends on the type of polymer feeder. Presumably, for polymer composite, the print speed could have been reduced due to higher shear stress in the nozzle cause by the ceramic filler.

The slower printing speed has allowed more air to trap between layers and consequently affect the ability of the composite to hold the structure after sintering.

A bulk composite filament was prepared to test the hypothesis. After preparing the 3 mm composite filament, it was diced with cutter about 5mm to produce a bulk cylinder shape sample as shown in Figure 7.8.

Figure 7.8 The cylinder structure of composite filament.

The diced filaments were then sintered to a ‘gentler’ heating profile in order to see the ability of the sample to hold its structure. The new heating profile was as follows:

Room temperature $\xrightarrow{1°C/min}$ 240°C $\xrightarrow{0.2°C/min}$ 550°C $\xrightarrow{5°C/min\ (10hours)}$ 1250°C

Figure 7.9 Composite of bulk filament samples

The samples were unable to hold the integrity of the shape even under gentler heating rate as shown in Figure 7.9. At slower heating rate, the degradation of polymer phase also occurred at slower rate and eventually collapsed and lost the shape. At the same time; according to grain-growth model, HAP grains have more time to growth in the collapsing structure of the composite and as a result; an odd shape of sintered composite was produced.

Due time constraint, the author could not continue the investigation to further characterise the ceramic composite. It is interesting to characterise the scanning electron micrograph (SEM) of grain growth and the structure of the ceramic with XRD analysis in order to study the affect of using 'gentler' heating rate. Heating profile for the sintering process could be improved by performing a faster heating rate (1°C/min) at the range of polymer decomposition temperature (300-500°C) in order to give the ideal time for the grain growth of ceramic to hold the structure whilst polymer phase slowly degrade. The mechanism of grain growth and the mechanism of degradation can be further investigated.

As an alternative, process ability of the polymer ceramic during extrusion could be improve by optimising the formulation of polymer ceramics. This is to reduce the shear stress during extrusion, which gives significant effect on the green body of the composite during sintering. One way to overcome the stress is to produce nano-size ceramic particle and induce chemical treatment on the ceramic particle to homogenise the size of the ceramic particles and optimise the viscous-elasticity of the polymer ceramic. Figure 7.10 shows the capability of BFB 3000 3D Extruder to fabricate custom-made tissue scaffold from 100wt%HAP/PCL. This shows the feasibility of the machine to fabricate new biopolymer materials and also offering a

better alternative approach in designing tissue scaffold for specific tissue engineering applications.

Figure 7.10 A layer by layer structure of polymer ceramic (100wt% HAP/PCL) fabricated via BFB 3000 3D Extruder.

7.4 Conclusion

Unlike microstereolithography technique, BFB 3000 3D is low in cost and there are varieties of polymer feeders available from the manufacturer; which are suitable for wide field of application. In addition, the simpler operation and more robust machine has had attracted the author to develop novel materials specifically for tissue engineering application. A bulk composite filament was prepared from 100 and 200wt% HAP and 3D structure of polymer ceramic composite was successfully fabricated with BFB 3000 3D extruder. However, obtaining a ceramic composite after sintering the green body was not possible even though a much gentler heating rate was performed. Nevertheless, the author believe with further optimisation of the polymer ceramic formulation; coupled with ideal heating rate, a custom-made 3D structure of tissue scaffold is achievable in the near future.

CHAPTER 8

Conclusion and Further Work

8.1 Overview

Research in the field of tissue engineering has been exciting and fascinating due to the dramatic advances in the fields of biochemistry, cell and molecular biology, genetics, biomedical engineering and materials science over the past decades. Amongst the objectives of this work is to improve the health and quality of life for millions of people worldwide by restoring, maintaining, or enhancing tissue and organ function. One of the key ways that this is being achieved is through the combination of material science, engineering and cell therapy. The advancements in direct manufacture has compliment this revolution in tissue engineering.

Microstereolithography has been one of the direct manufacture techniques that have attracted a lot of attention, due to its precision in fabricating complex 3-D microstructures with high-aspect ratio. The limited supply of biomaterial resins for microstereolithography has driven researchers to find novel materials and to improve the performance of this technique.

8.2 Project Objective

In this study, a range of new bio-compatible/degradable materials that are compatible with a commercial 3D direct manufacture system has been explored. There were three stages involved in this project (as presented in Chapter 1) and the conclusion for each stage is summarised:

8.2.1 The development of a stereolithography system for the optimal formulation of biodegradable photopolymer resin to fabricate 3D scaffolds with controlled microstructures specifically for soft tissue engineering applications such as hydrogels.

In this study, two types of equipment were developed in order to allow some understanding on the techniques and process involved in microstereolithography. A light projector was developed from a decommissioned Envisiontec Perfactory® Mini and UV light engine was built from high power ultra-bright LED array.

Commercial resin (envisionTec's R11) was successfully cured on the Light Projector but the layer-by-layer formation was limited due to the presence of a photoinhibitor in R11. On the other hand, the Enfis light engine system was specifically designed to fabricate a 3D structure from formulated photo-curable ceramic suspensions. A 3D structure was successfully fabricated from 70wt% hydroxyapatite (HAP)/1, 6 hexanediol diacrylate (HDDA) suspension. The development of both systems was limited due to the absence of a Z-stage. For future work, the addition of a Z-stage into these systems (especially the Enfis system) could produce a promising system. Nevertheless, the decommissioned Light projector and Light engine have given abundance of knowledge and clear understanding on the principle of microstereolithography techniques.

An important finding in this study was the optimisation of dumb-bell sample size and dimension for materials characterisation on the Deben Microtensile machine, which was used for all measurement in this project, in order to obtain reliable and precise measurements.

8.2.2 The development of a range of new bio-compatible/degradable materials for soft tissue application that is compatible with a commercial 3D direct manufacture system (Envisiontec Desktop).

The objective of this section was to investigate the feasibility of the commercial machine to fabricate novel biomaterials. In this study, a new photopolymer resin with different types of multifunctional acrylate polymer was successfully fabricated on a commercial 3D direct manufacture system, envisionTEC Desktop. Table 8.1 shows the formulated photopolymer resin.

Table 8.1 Formulation of multifunctional acrylate for photopolymer resin.

Monomer/polymer	Ratio (%)
Diethylene glycol diacrylate (DEDGA)	90
Dipentaerythritol penta-/hexa-acrylate (HDPA)	10
Trietyleneglycol diacrylate (TEGDA)	90
Dipentaerythritol penta-/hexa-acrylate (HDPA)	10
Polyethylene glycol diacrylate (PEGDA)	80
Dipentaerythritol penta-/hexa-acrylate (HDPA)	20

Photoinnitiator and dye for each formulation: 3.75 wt% and 0.15 wt% of the polymer weight respectively.

Mechanical characterisation was performed on the fabricated hydrogels to investigate the properties and their possible application. The polymerised formulation hydrogels exhibited degradation properties, which is a vital requirement for a biomaterial that promise potential for the use of this resin for soft tissue scaffold applications. However, the hydrogels suffered with stress post-curing, which promote delamination and warping of the sample.

Even though the hydrogels faced the problems mentioned above, the formulated photopolymer resin allowed the exploration/functionalization of these resins by investigating the addition of a carbohydrate groups to the polymer system

for biomedical application of hydrogels. This is to explore the feasibility of the microstereolithography technique to fabricate new photopolymer resin for further enhance its diversity. The formulation of new photopolymer resin is shown as in Table 8.2.

Table 8.2Formulation of glycopolymers photopolymer resin

Sample	Ratio (%)		
	PEGDA	HDPA	*GlcAc
Control	70.0	30.0	-
2.5Glc	72.5	25.0	2.5
5.0Glc	70.0	25.0	5.0

*: 1,2,3,4,6-Penta-O-acetyl-beta-D-glucopyranose; Acetyl 2,3,4,6-tetra-o-acetyl-beta-D-glucopyranoside

The glycopolymer resin was successfully fabricated on the machine and was characterised to study the effect of carbohydrate group to the formulation. The modification and increases of GlcAc has increased the molecular weight of the polymer mixture and as a result increased the swelling ratio of the cured polymer. The addition of GlcAc also assists in the erosion process during degradation. However, sugar-based glycopolymers has no significant effect on the tensile strength of the cured polymers due to reoccurring stress post-curing on the samples.

8.2.3 The optimal formulation of polymer ceramic resin compatible with a commercial 3D direct manufacture system (envisionTEC Desktop) specifically for hard tissue engineering applications such as bone.

In this study, three types of calcium phosphate have been used; synthesised calcium pyrophosphate (CPP-A), as-received calcium phosphate (CPP-B) and hydroxyapatite (HAP), as part of a new synthesized photopolymer resin. It was shown that a 3 dimensional ceramic composite structure can be fabricated on an EnvisionTEC Desktop machine. It has been shown that particle size, composition, and viscosity of calcium phosphate within the photopolymer resin have a significant effect on the decomposition temperature and porosity of the polymer composite. Table 8.3 represent the polymer ceramic resin prepared in this study.

Table 8.3 Formulation of photopolymer ceramic resin for fabrication on envisionTEC Desktop.

Calcium Phosphate	Weight % (wt%) [i]	Abbreviation	Photopolymer Resin	Ratio (%)[ii]
CPP-A	50	50A		
	70	70A		
	100	100A	*HDeDA	70
CPP-B	50	50A	*DPA	20
	70	70A	*BPA	10
	100	100A	PI	3[a]
HAP	50	HAP50	Dye	0.15[b]
	70	HAP70		
	100	HAP100		

[i] : weight percent of total weight of prepolymer (*)
[ii]: ratio based on total volume of prepolymer (*)
[a] : weight percent of PI based on the total weight of prepolymer (*)

Different sintering times were designed in order to study its effect on the mechanical properties and microstructure of the composites. The mechanical strength of both type of CPP ceramic were found to increase with increasing sintering times from 5 to 10 hours at 1250°C. Generally as sintering temperature is increased the

compressive strength was increased but after 12 hours, micro-cracks were induced on the particles surface. On the other hand, the elastic modulus of the HAP-based composite increased as the sintering time increased. This is due to the small particles size and high diffusion rate between particle contacts during the sintering process. Nevertheless, the compressive properties of the heat treated composite were quite close to those of cancellous bone (2–17 MPa) [116].

In bioactivity study, increasing the sintering time has enhanced the apatite nucleation onto the composite surface. A study on sintering times has provided significant insight into the re-precipitation and microstructure of apatite formation that could be used in bone substitutes and tissue engineering applications.

As a preliminary study, a 3D extruder machine (BFB 3000 3D extruder) was used to study the feasibility and the potential of the machine as a tool for manufacturing a 3D polymer composite for tissue engineering application. A composite filament of polycaprolactone (PCL)/ hydroxyapatite (HAP) was successfully fabricated on the machine. However, further study on the sintering temperature has to explore in order to obtain a 3D ceramic composite for tissue engineering application.

8.3 Future Work

For future work in the development of biodegradable photopolymer resin for soft tissue application, the temperature during photopolymerisation should be taken into account. An increasing in temperature could affect the gel formation of the photopolymer resin due to increased polymer chain termination. Early crosslinking of the polymer network could occur at certain temperatures and as results a cured layer is formed. The thickness of the cured layer could affect the penetration depth of light

into the photopolymer resin. If a layer is not cured deep enough, the interlayer bonding fails and delamination occurs [136].

Another possible area for future study is to enhance the mechanical properties of the biodegradable biopolymer. One way to address this is increasing the crosslinking density of the polymer by increasing the macromer concentration or decreasing the macromer molecular weight. In addition, higher density of crosslinking network could also increase the time for network degradation, as it decreases the water diffusion and increases the number of bonds that must be cleaved to break the network into water-soluble components [249].

For development of polymer ceramic resin, characterisation on particles size and dimension of calcium phosphate can be further investigated in order to overcome the agglomerate during preparation of the ceramic suspension. Backscattered secondary electron (BSE) analysis on the composition of CPP has shown that the difference in distribution of particle size in the polymer ceramic. Surface modification or treatment on the ceramic particles should be explored in order to produce uniform particles size and distribution in ceramic suspension. Ribeiro et. al has successfully prepared porous ceramic microspheres as injectable bone-filling materials and drug delivery matrices [163]. It would be interesting to investigate the possibility to prepare microsphere calcium phosphate as filler in a photopolymer resin for microstereolithography fabrication.

The effect of sintering temperature on the mass loss and volumetric shrinkage of the sintered ceramic must be explored further in other to determine the shape of the final ceramic. An extensive study between sintering temperature, ceramic porosity and pore connectivity is important in the degradation of the material, which will affect

the apatite formation of the sintered composite. Progressively, *in vivo* behaviour of the tissue scaffold should be further investigated to learn the viability, proliferation, and extracellular matrix production.

References

[1] B. Baroli, “From Natural Bone Grafts to Tissue Engineering Therapeutics : Brainstorming on Pharmaceutical Formulative Requirements and Challenges,” *Blood*, vol. 98, no. 4, pp. 1317-1375, 2009.

[2] L. B. Connelly, A. Woolf, and P. Brooks, “Cost-Effectiveness of Interventions for Musculoskeletal Conditions.,” in *Disease Control Priorities in Development Countries*, 2nd ed., no. May, D. T. Jamison et al., Eds. Luke B. Connelly, Anthony Woolf, and Peter Brooks. 2006. “Cost-Effectiveness of Interventions for Musculoskeletal Conditions.” In Disease Control Priorities in Development Countries, 2nd ed. D. T. Jamison, J. G. Breman, A. R. Measham, G. Alleyne, M. Claes: Oxford University Press., 2006, pp. 963-980.

[3] “What is osteoarthritis ? www.arthritisreserachuk.org. [Accessed on 21 Jan 2010].,” *Bone*.

[4] *Annual prevalence report 2006. http://www.rcgp.org.uk/clinical_and_research/rsc/annual_prevalence.aspx. [Accessed on 21 Feb 2011]*. .

[5] “Health and Safety Executive. Musculoskeletal disorders.” .

[6] D. M. Lanyon P, Muir K, Doherty S, “Age and sex differences in hip joint space among asymptomatic subjects without structural change: implications for epidemiologic studies.,” *Arthritis Rheum*, vol. 48, no. 4, pp. 1041-1046, 2003.

[7] S. R. Pye, D. M. Reid, J. E. Adams, a J. Silman, and T. W. O’Neill, “Radiographic features of lumbar disc degeneration and bone mineral density in men and women.,” *Annals of the rheumatic diseases*, vol. 65, no. 2, pp. 234-8, Feb. 2006.

[8] D. Ellams, C. Newell, M. Swanson, and L. Copley, *National Joint Registry for England and Wales, 7th Annual Report*, vol. 1450, no. 2009. 2010.

[9] D. Symmons et al., “The prevalence of rheumatoid arthritis in the United Kingdom: new estimates for a new century.,” *Rheumatology (Oxford, England)*, vol. 41, no. 7, pp. 793-800, Jul. 2002.

[10] “Health and Safety Executive. Musculoskeletal disorders – Why tackle them? whytackle.htm.” [Online]. Available: http://www.hse.gov.uk/ healthservices/msd/whytackle.htm [Date accessed:13-04-2011]. . [Accessed: 21-Feb-2011].

[11] R. D. Verteuil et al., “Total hip replacement approaches in the management of arthritic disease of the hip,” *Business*, vol. 12, no. 26, 2008.

[12] *Health and Safety Executive. Estimated days (full-day equivalent) off work and associated average days lost per (full-time equivalent) worker and per case due to a self-reported work-related illness or workplace injury. //www.hse.gov.uk/statistics/tables/*. .

[13] J. Vacanti and A. C. Vacanti, "the History and Scope of Tissue Engineering," in *Principles of Tissue Engineering*, 3rd ed., J. P. V. (Editor) Robert Lanza (Editor), Robert Langer (Editor), Ed. 2007, p. 4.

[14] J. Panno, *Stem Cell Research: Medical Applications and Ethical Controversy*. Facts on File Inc; Library Binding edition, 2004, p. 59.

[15] *OVERVIEW OF ORGAN DONATION AND TRANSPLANTATION. http://www.organdonation.nhs.uk/ukt/statistics/transplant_activity_report/transplant_activity_report.jsp [Date assessed 13-04-2011]*, no. March. 2010, pp. 2008-2011.

[16] D. F. Williams, "To engineer is to create: the link between engineering and regeneration.," *Trends in biotechnology*, vol. 24, no. 1, pp. 4-8, Jan. 2006.

[17] C. P. Barnes, S. A. Sell, E. D. Boland, D. G. Simpson, and G. L. Bowlin, "Nanofiber technology: Designing the next generation of tissue engineering scaffolds," *Advanced Drug Delivery Reviews*, vol. 59, no. 14, pp. 1413-1433, 2007.

[18] T. J. Webster, *Nanotechnology For The Regeneration Of Hard And Soft Tissues*, 1st ed. World Scientific Publishing; 1 edition (3 Nov 2007), 2007, p. 12.

[19] P. A. Gunatillake and R. Adhikari, "Biodegradable synthetic polymers for tissue engineering.," *European Cells & Materials*, vol. 5, pp. 1-16; discussion 16, May. 2003.

[20] C.-Y. Hsieh, S.-P. Tsai, D.-M. Wang, Y.-N. Chang, and H.-J. Hsieh, "Preparation of [gamma]-PGA/chitosan composite tissue engineering matrices," *Biomaterials*, vol. 26, no. 28, pp. 5617-5623, 2005.

[21] H. R. R. Ramay and M. Zhang, "Biphasic calcium phosphate nanocomposite porous scaffolds for load-bearing bone tissue engineering.," *Biomaterials*, vol. 25, no. 21, pp. 5171-80, Sep. 2004.

[22] F. Tamimi et al., "Brushite-collagen composites for bone regeneration," *Acta Biomaterialia*, vol. 4, no. 5, pp. 1315-1321, 2008.

[23] J. P. Fisher, "Polymeric Scaffolds for Tissue Engineering Applications 37.1," *Design*, 2006.

[24] T. R. Kyriakides, T. Hartzel, G. Huynh, and P. Bornstein, "Regulation of angiogenesis and matrix remodeling by localized, matrix-mediated antisense

gene delivery.," *Molecular Therapy : The Journal of The American Society of Gene Therapy*, vol. 3, no. 6, pp. 842-9, Jun. 2001.

[25] U. Klammert, T. Reuther, C. Jahn, B. Kraski, A. C. Kübler, and U. Gbureck, "Cytocompatibility of brushite and monetite cell culture scaffolds made by three-dimensional powder printing," *Acta Biomaterialia*, vol. 5, no. 2, pp. 727-734, 2009.

[26] F. Barrère, C. a van Blitterswijk, and K. de Groot, "Bone regeneration: molecular and cellular interactions with calcium phosphate ceramics.," *International Journal of Nanomedicine*, vol. 1, no. 3, pp. 317-32, Jan. 2006.

[27] J. Chevalier and L. Gremillard, "Ceramics for medical applications : A picture for the next 20 years," *Journal of the European Ceramic Society*, vol. 29, pp. 1245-1255, 2009.

[28] M. P. Ferraz, F. J. Monteiro, and C. M. Manuel, "Hydroxyapatite nanoparticles: A review of preparation methodologies.," *Journal of Applied Biomaterials & Biomechanics : JABB*, vol. 2, no. 2, pp. 74-80, 2004.

[29] S. V. Dorozhkin, "Calcium Orthophosphates as Bioceramics: State of the Art," *Journal of Functional Biomaterials*, vol. 1, no. 1, pp. 22-107, Nov. 2010.

[30] T. M. G. Chu, D. G. Orton, S. J. Hollister, S. E. Feinberg, and J. W. Halloran, "Mechanical and in vivo performance of hydroxyapatite implants with controlled architectures," *Biomaterials*, vol. 23, no. 5, pp. 1283-1293, 2002.

[31] E. Ebaretonbofa and J. R. G. Evans, "High Porosity Hydroxyapatite Foam Scaffolds for Bone Substitute," *Journal of Porous Materials*, vol. 9, no. 4, pp. 257-263, 2002.

[32] T. M. Chu, J. W. Halloran, S. J. Hollister, and S. E. Feinberg, "Hydroxyapatite implants with designed internal architecture.," *Journal of Materials Science. Materials in Medicine*, vol. 12, no. 6, pp. 471-8, Jun. 2001.

[33] R. Detsch, F. Uhl, U. Deisinger, and G. Ziegler, "3D-Cultivation of bone marrow stromal cells on hydroxyapatite scaffolds fabricated by dispense-plotting and negative mould technique," *Materials inMedicine*, vol. 19, no. 4, pp. 1491-1496, 2008.

[34] C. Heiss et al., "Development of a bioresorbable self-hardening bone adhesive based on a composite consisting of polylactide methacrylates and beta-tricalcium phosphate," *Journal of Biomedical Materials Research.B. Applied Biomaterials,*, vol. 90, no. 1, pp. 55-66, 2009.

[35] X. Li, D. Li, L. Wang, B. Lu, and Z. Wang, "Osteoblast cell response to β-tricalcium phosphate scaffolds with controlled architecture in flow perfusion culture system," *Journal of Materials Science. Materials in Medicine*, vol. 19, no. 7, pp. 2691-2697, 2008.

[36] R. Jewad, C. Bentham, B. Hancock, W. Bonfield, and S. M. Best, "Dispersant selection for aqueous medium pressure injection moulding of anhydrous dicalcium phosphate," *Journal of the European Ceramic Society*, vol. 28, no. 3, pp. 547-553, 2008.

[37] L. M. Grover, U. Gbureck, A. J. Wright, and J. E. Barralet, "Cement Formulations in the Calcium Phosphate H2O-H3PO4-H4P2O7 System," *Journal of the American Ceramic Society*, vol. 88, no. 11, pp. 3096-3103, Nov. 2005.

[38] W. J. E. M. Habraken, J. G. C. Wolke, and J. a Jansen, "Ceramic composites as matrices and scaffolds for drug delivery in tissue engineering.," *Advanced drug delivery reviews*, vol. 59, no. 4-5, pp. 234-48, May. 2007.

[39] W. Y. Zhou, M. Wang, W. L. Cheung, and W. Y. Ip, "Selective Laser Sintering of Poly (L -Lactide)/ Carbonated Hydroxyapatite Nanocomposite Porous Scaffolds for Bone Tissue Engineering," *Tissue Engineering*, pp. 179-204, 2005.

[40] B. S. Chang et al., "Osteoconduction at porous hydroxyapatite with various pore configurations.," *Biomaterials*, vol. 21, no. 12, pp. 1291-8, Jun. 2000.

[41] E. a Botchwey, M. a Dupree, S. R. Pollack, E. M. Levine, and C. T. Laurencin, "Tissue engineered bone: measurement of nutrient transport in three-dimensional matrices.," *Journal of Biomedical Materials Research. Part A*, vol. 67, no. 1, pp. 357-67, Oct. 2003.

[42] B. Geun Chung, L. Kang, and A. Khademhosseini, "Micro-and nanoscale technologies for tissue engineering and drug discovery applications.," *Experts Opinion*, vol. 2, no. 12, pp. 1-16, 2007.

[43] A. A. Chen, V. L. Tsang, D. R. Albrecht, and S. N. Bhatia, "3-D Fabrication Technology for Tissue Engineering," *Biomems and Biomedical Nanotechnology.*, vol. I, pp. 23-38, 2007.

[44] S. Q. Liu, P. L. R. Ee, C. Y. Ke, J. L. Hedrick, and Y. Y. Yang, "Biodegradable poly(ethylene glycol)-peptide hydrogels with well-defined structure and properties for cell delivery.," *Biomaterials*, vol. 30, no. 8, pp. 1453-61, Mar. 2009.

[45] E. Sachlos and J. T. Czernuszka, "Making tissue engineering scaffolds work. Review: the application of solid freeform fabrication technology to the production of tissue engineering scaffolds.," *European Cells & Materials*, vol. 5, pp. 29-39; discussion 39-40, Jun. 2003.

[46] V. Tsang and S. Bhatia, "Fabrication of Three-Dimensional Tissues," *Tissue Engineering II*, vol. 103, pp. 189-205, 2007.

[47] Y. S. Nam, J. J. Yoon, and T. G. Park, "A novel fabrication method of macroporous biodegradable polymer scaffolds using gas foaming salt as a

porogen additive.," *Journal of Biomedical Materials Research*, vol. 53, no. 1, pp. 1-7, Jan. 2000.

[48] J. Yoon, "Dexamethasone-releasing biodegradable polymer scaffolds fabricated by a gas-foaming/salt-leaching method," *Biomaterials*, vol. 24, no. 13, pp. 2323-2329, Jun. 2003.

[49] Q. Fu, M. N. Rahaman, F. Dogan, and B. S. Bal, "Freeze-cast hydroxyapatite scaffolds for bone tissue engineering applications.," *Biomedical Materials (Bristol, England)*, vol. 3, no. 2, p. 025005, Jun. 2008.

[50] F. O'Brien, "Influence of freezing rate on pore structure in freeze-dried collagen-GAG scaffolds," *Biomaterials*, vol. 25, no. 6, pp. 1077-1086, Mar. 2004.

[51] W.-Y. Yeong, C.-K. Chua, K.-F. Leong, and M. Chandrasekaran, "Rapid prototyping in tissue engineering: challenges and potential.," *Trends in Biotechnology*, vol. 22, no. 12, pp. 643-52, Dec. 2004.

[52] S. Yang, K.-F. Leong, Z. Du, and C.-K. Chua, "The Design of Scaffolds for Use in Tissue Engineering. Part II. Rapid Prototyping Techniques," *Tissue Engineering*, vol. 8, no. 1, pp. 1-11, 2002.

[53] G. Vozzi, C. Flaim, A. Ahluwalia, and S. Bhatia, "Fabrication of PLGA scaffolds using soft lithography and microsyringe deposition," *Biomaterials*, vol. 24, no. 14, pp. 2533-2540, 2003.

[54] S. Park, G. Kim, Y. C. Jeon, Y. Koh, and W. Kim, "3D polycaprolactone scaffolds with controlled pore structure using a rapid prototyping system.," *Journal of Materials Science. Materials in Medicine*, vol. 20, no. 1, pp. 229-34, Jan. 2009.

[55] D. J. Mooney, D. F. Baldwin, N. P. Suh, J. P. Vacanti, and R. Langer, "Novel approach to fabricate porous sponges of poly(D,L-lactic-co-glycolic acid) without the use of organic solvents.," *Biomaterials*, vol. 17, no. 14, pp. 1417-22, Jul. 1996.

[56] P. Gu, X. Zhang, Y. Zeng, Ferguson, and B., "Quality analysis and optimization of solid Ground Curing process," *Journal of Manufacturing Systems*, vol. 20, no. 4, pp. 250-263, 2001.

[57] S. Jyoti, S. Bose, H. L. Hosick, and A. Bandyopadhyay, "Development of controlled porosity polymer-ceramic composite scaffolds via fused deposition modeling," *Processing*, vol. 23, pp. 611 - 620, 2003.

[58] S. Limpanuphap and B. Derby, "Manufacture of biomaterials by a novel printing process," *Journal of Materials Science: Materials in Medicine*, vol. 13, no. 12, pp. 1163-1166, 2002.

[59] A. Khalyfa et al., “Development of a new calcium phosphate powder-binder system for the 3D printing of patient specific implants,” *Journal of Materials Science: Materials in Medicine*, vol. 18, no. 5, pp. 909-916, 2007.

[60] I. V. Shishkovsky, L. T. Volova, M. V. Kuznetsov, Y. G. Morozov, and I. P. Parkin, “Porous biocompatible implants and tissue scaffolds synthesized by selective laser sintering from Ti and NiTi,” *Journal of Materials Chemistry*, vol. 18, no. 12, p. 1309, 2008.

[61] L. Lin, A. Tong, H. Zhang, Q. Hu, and M. Fang, “The Mechanical Properties of Bone Tissue Engineering Scaffold Fabricating Via Selective Laser Sintering,” *Life System Modeling and Simulation,*, vol. 4689, pp. 146-152, 2007.

[62] K.-ke Yang, X.-li Wang, and Y.-zhong Wang, “Progress in Nanocomposite of Biodegradable Polymer,” *Review Literature And Arts Of The Americas*, vol. 13, no. 4, pp. 485-500, 2007.

[63] H. J. Choi, J. Kim, and M. S. Jhon, “Viscoelastic characterization of biodegradable poly (3-hydroxybutyrate-co-3-hydroxyvalerate) 1,” *Polymer*, vol. 40, pp. 4135-4138, 1999.

[64] S. Sinharay and M. Bousmina, “Biodegradable polymers and their layered silicate nanocomposites: In greening the 21st century materials world,” *Progress in Materials Science*, vol. 50, no. 8, pp. 962-1079, Nov. 2005.

[65] M. Wang, “Composite scaffolds for bone tissue engineering.,” *American Journal of Biochemistry and Biotechnology*, vol. 2, no. 2, pp. 80-84, 2006.

[66] D. C. Rui L. Reis, *Polymer based systems on tissue engineering, replacement and regeneration. 2002 Kluwer Academic*, NATO Scien. Kluwer Academic Publishers., 2002, p. 55.

[67] Z. Li, H. R. Ramay, K. D. Hauch, D. Xiao, and M. Zhang, “Chitosan-alginate hybrid scaffolds for bone tissue engineering.,” *Biomaterials*, vol. 26, no. 18, pp. 3919-28, Jun. 2005.

[68] Y. Wan, H. Wu, X. Cao, and S. Dalai, “Compressive mechanical properties and biodegradability of porous poly(caprolactone)/chitosan scaffolds,” *Polymer Degradation and Stability*, vol. 93, no. 10, pp. 1736-1741, 2008.

[69] X. Mo, Z. Chen, and H. Weber, “Electrospun nanofibers of collagen-chitosan and P(LLA-CL) for tissue engineering,” *Frontiers of Materials Science in China*, vol. 1, no. 1, pp. 20-23, 2007.

[70] N. J. Chang, M. L. Yeh, and Y. R. Jhung, “Fabricating PLGA sponge scaffold integrated with gelatin/hyaluronic acid for engineering cartilage,” *2009 IEEE 35th Annual Northeast Bioengineering Conference*, no. 1, pp. 1-2, Apr. 2009.

[71] P. Bulpitt and D. Aeschlimann, “New strategy for chemical modification of hyaluronic acid: preparation of functionalized derivatives and their use in the

formation of novel biocompatible hydrogels.," *Journal of Biomedical Materials Research*, vol. 47, no. 2, pp. 152-69, Nov. 1999.

[72] N. Bhattarai, Z. Li, D. Edmondson, and M. Zhang, "Alginate-Based Nanofibrous Scaffolds: Structural, Mechanical, and Biological Properties," *Advanced Materials*, vol. 18, no. 11, pp. 1463-1467, Jun. 2006.

[73] I. M. van der Lubben, G. Kersten, M. M. Fretz, C. Beuvery, J. Coos Verhoef, and H. E. Junginger, "Chitosan microparticles for mucosal vaccination against diphtheria: oral and nasal efficacy studies in mice.," *Vaccine*, vol. 21, no. 13-14, pp. 1400-8, Mar. 2003.

[74] J. L. Drury and D. J. Mooney, "Hydrogels for tissue engineering: scaffold design variables and applications," *Biomaterials*, vol. 24, no. 24, pp. 4337-4351, 2003.

[75] C. M. Jain SK, Jain NK, Gupta Y, Jain A, Jain D, "Mucoadhesive chitosan microspheres for non-invasive and improved nasal delivery of insulin.," *Indian Journal of Pharmacy Science*, vol. 69, pp. 498-504, 2007.

[76] M. Liu, J. Dong, Y. Yang, X. Yang, and H. Xu, "Anti-inflammatory effects of triptolide loaded poly(D,L-lactic acid) nanoparticles on adjuvant-induced arthritis in rats.," *Journal of Ethnopharmacology*, vol. 97, no. 2, pp. 219-25, Feb. 2005.

[77] A. Mikos et al., "Preparation and characterization of poly(l-lactic acid) foams," *Polymer*, vol. 35, no. 5, pp. 1068-1077, Mar. 1994.

[78] F. P. W. Melchels, J. Feijen, and D. W. Grijpma, "A poly(d,l-lactide) resin for the preparation of tissue engineering scaffolds by stereolithography," *Biomaterials*, vol. 30, no. 23-24, pp. 3801-3809, 2009.

[79] S. He, M. J. Yaszemski, A. W. Yasko, P. S. Engel, and A. G. Mikos, "Injectable biodegradable polymer composites based on poly(propylene fumarate) crosslinked with poly(ethylene glycol)-dimethacrylate," *Biomaterials*, vol. 21, no. 23, pp. 2389-2394, 2000.

[80] M. V. Badiger, M. E. McNeill, and N. B. Graham, "Porogens in the preparation of microporous hydrogels based on poly(ethylene oxides).," *Biomaterials*, vol. 14, no. 14, pp. 1059-63, Nov. 1993.

[81] J. Elisseeff, W. McIntosh, K. Anseth, S. Riley, P. Ragan, and R. Langer, "Photoencapsulation of chondrocytes in poly(ethylene oxide)-based semi-interpenetrating networks.," *Journal of Biomedical Materials Research*, vol. 51, no. 2, pp. 164-71, Aug. 2000.

[82] I. K. Kwon and T. Matsuda, "Photo-polymerized microarchitectural constructs prepared by microstereolithography (muSL) using liquid acrylate-end-capped trimethylene carbonate-based prepolymers.," *Biomaterials*, vol. 26, no. 14, pp. 1675-84, May. 2005.

[83] S. P. Nalawade, D. Westerman, G. Leeke, R. C. D. Santos, D. W. Grijpma, and J. Feijen, "Preparation of porous poly(trimethylene carbonate) structures for controlled release applications using high pressure CO2," *Journal of Controlled Release*, vol. 132, no. 3, p. e73-e75, 2008.

[84] R. Stoop, "Smart biomaterials for tissue engineering of cartilage," *Injury, Int. J. Care Injured*, vol. 39, no. 1, Supplement 1, pp. 77-87, 2008.

[85] H. S. Azevedo and R. L. Reis, "the 12 Understanding Enzymatic Degradation of Biodegradable Polymers and Strategies to Control Their Degradation Rate," *In Vitro*, pp. 177-202, 2005.

[86] a Göpferich, "Mechanisms of polymer degradation and erosion.," *Biomaterials*, vol. 17, no. 2, pp. 103-14, Jan. 1996.

[87] L. Weng, N. D. Ivanova, J. Zakhaleva, and W. Chen, "In vitro and in vivo suppression of cellular activity by guanidinoethyl disulfide released from hydrogel microspheres composed of partially oxidized hyaluronan and gelatin.," *Biomaterials*, vol. 29, no. 31, pp. 4149-56, Nov. 2008.

[88] R. S. Labow, D. Sa, L. a Matheson, D. L. M. Dinnes, and J. P. Santerre, "The human macrophage response during differentiation and biodegradation on polycarbonate-based polyurethanes: dependence on hard segment chemistry.," *Biomaterials*, vol. 26, no. 35, pp. 7357-66, Dec. 2005.

[89] V. Hasirci, K. Lewandrowski, J. D. Gresser, D. L. Wise, and D. J. Trantolo, "Versatility of biodegradable biopolymers: degradability and an in vivo application.," *Journal of Biotechnology*, vol. 86, no. 2, pp. 135-50, Mar. 2001.

[90] R. Mahadevan and L. Smith, "A Mechanistic Model Describing the Degradation of Polymers," *Journal of Polymers and the Environment*, vol. 15, no. 2, pp. 75-80, Apr. 2007.

[91] L. Schedl, "Why degradable polymers undergo surface erosion or bulk erosion," *Biomaterials*, vol. 23, pp. 4221-4231, 2002.

[92] A. Go, "Polymer Bulk Erosion," *Society*, vol. 9297, no. 96, pp. 2598-2604, 1997.

[93] M. Husmann, S. Schenderlein, and M. Lu, "Polymer erosion in PLGA microparticles produced by phase separation method," *International Journal of Pharmaceutics*, vol. 242, pp. 277- 280, 2002.

[94] P. J. Martens, C. N. Bowman, and K. S. Anseth, "Degradable networks formed from multi-functional poly(vinyl alcohol) macromers: comparison of results from a generalized bulk-degradation model for polymer networks and experimental data," *Polymer*, vol. 45, no. 10, pp. 3377-3387, May. 2004.

[95] R. Chandra and R. Rustgi, "Biodegradable Polymer," *Progress in Polymer Science*, vol. 23, no. 97, pp. 1273-1335, 1998.

[96] R. G.H., "Biomedical Polymers.," in *Biomaterials, artificial organs and tissue engineering.*, Larry L.H and Julian R.J. Woodhead, Ed. Publishing in Materials, Cambridge England., 2005, pp. 107-115.

[97] A. Huhtala, T. Pohjonen, L. Salminen, A. Salminen, K. Kaarniranta, and H. Uusitalo, "In vitro biocompatibility of degradable biopolymers in cell line cultures from various ocular tissues: extraction studies," *Journal of Materials Science: Materials in Medicine*, vol. 19, no. 2, pp. 645-649, 2008.

[98] K. F. Leong, C. M. Cheah, and C. K. Chua, "Solid freeform fabrication of three-dimensional scaffolds for engineering replacement tissues and organs," *Biomaterials*, vol. 24, no. 13, pp. 2363-2378, 2003.

[99] J. S. Murday, R. W. Siegel, J. Stein, and J. F. Wright, "Translational nanomedicine : status assessment and opportunities," *Nanotechnology*, vol. 5, pp. 251 - 273, 2009.

[100] H. Nishikawa, R. Hatanaka, M. Kusunoki, T. Hayami, and S. Hontsu, "Preparation of Freestanding Hydroxyapatite Membranes with Excellent Biocompatibility and Flexibility," *Applied Physics Express*, vol. 1, p. 088001, Jul. 2008.

[101] S. Hontsu, M. Nakamori, H. Tabata, J. Ishii, and T. Kawai, "Pulsed laser deposition of bioceramic hydroxyapatite thin films on polymer materials.," *Jppn. J. Appl. Phys*, vol. 35, pp. 1208-1210, 1996.

[102] S. J. Hollister, "Porous scaffold design for tissue engineering," *Nature Materials*, vol. 4, no. 7, pp. 518-524, 2005.

[103] M. Schieker, H. Seitz, I. Drosse, S. Seitz, and W. Mutschler, "Biomaterials as Scaffold for Bone Tissue Engineering," *European Journal of Trauma*, vol. 32, no. 2, pp. 114-124, 2006.

[104] D. W. Hutmacher, M. Sittinger, and M. V. Risbud, "Scaffold-based tissue engineering: rationale for computer-aided design and solid free-form fabrication systems," *Trends in Biotechnology*, vol. 22, no. 7, pp. 354-362, 2004.

[105] Z. Li, H. R. Ramay, K. D. Hauchb, D. Xiao, and M. Zhang, "Chitosan–alginate hybrid scaffolds for bone tissue engineering," *Biomaterials*, vol. 26, pp. 3919-3928, Jan. 2005.

[106] B. K. Mann and J. L. West, "Cell adhesion peptides alter smooth muscle cell adhesion , proliferation , migration , and matrix protein synthesis on modified surfaces and in polymer scaffolds," *Journal of Biomedical Materials Research*, vol. 60, no. 1, pp. 86-93, 2002.

[107] B. K. Mann, A. S. Gobin, A. T. Tsai, R. H. Schmedlen, and J. L. West, "Smooth muscle cell growth in photopolymerized hydrogels with cell adhesive

and proteolytically degradable domains : synthetic ECM analogs for tissue engineering," *Cell*, vol. 22, pp. 3045-3051, 2001.

[108] C. M. Agrawal and R. B. Ray, "Biodegradable polymeric scaffolds for musculoskeletal tissue engineering.," *Journal of Biomedical Materials Research*, vol. 55, no. 2, pp. 141-50, May. 2001.

[109] C. T. Buckley, "Chapter v regular scaffold fabrication techniques for investigations in tissue engineering," *Biomedical Engineering*, pp. 147-166.

[110] S. L. Ishaug-Riley, G. M. Crane-Kruger, M. J. Yaszemski, and a G. Mikos, "Three-dimensional culture of rat calvarial osteoblasts in porous biodegradable polymers.," *Biomaterials*, vol. 19, no. 15, pp. 1405-12, Aug. 1998.

[111] M. Martina and D. W. Hutmacher, "Biodegradable polymers applied in tissue engineering research: a review," *Polymer International*, vol. 56, no. 2, pp. 145-157, 2007.

[112] J. H. Brauker, V. E. Carr-Brendel, L. A. Martinson, J. Crudele, W. D. Johnston, and R. C. Johnson, "Neovascularization of synthetic membranes directed by membrane microarchitecture," *Journal Biomedical Materials Research.*, vol. 29, no. 15, pp. 17-24, 1995.

[113] L. T.C, B. C.P, C. K.S, and K. F. Leong, "Development of cryogenic prototyping for tissue engineering," *Virtual Phys Prototyping*, vol. 3, no. 25-31, 2008.

[114] B. D. Boyan, T. W. Hummert, D. D. Dean, and Z. Schwartz, "Role of material surfaces in regulating bone and cartilage cell response.," *Biomaterials*, vol. 17, no. 2, pp. 137-46, Jan. 1996.

[115] P. A. N. Aurelio Salerno, Daniela Guarnieri, Maria Iannone, Stefania Zeppetelli, "No TitleEffect of Micro- and Macroporosity of Bone Tissue Three-Dimensional-Poly(ε-Caprolactone) Scaffold on Human Mesenchymal Stem Cells Invasion, Proliferation, and Differentiation In Vitro," *Tissue Engineering Part A*, vol. 16, no. 8, pp. 2661-2673, 2010.

[116] V. Karageorgiou and D. Kaplan, "Porosity of 3D biomaterial scaffolds and osteogenesis.," *Biomaterials*, vol. 26, no. 27, pp. 5474-91, Sep. 2005.

[117] J. M. Taboas, R. D. Maddox, P. H. Krebsbach, and S. J. Hollister, "Indirect solid free form fabrication of local and global porous, biomimetic and composite 3D polymer-ceramic scaffolds.," *Biomaterials*, vol. 24, no. 1, pp. 181-94, Jan. 2003.

[118] X. Li, D. Li, B. Lu, and C. Wang, "Fabrication of bioceramic scaffolds with pre-designed internal architecture by gel casting and indirect stereolithography techniques," *Journal of Porous Materials*, vol. 15, no. 6, pp. 667-671, 2008.

[119] K. Hayashi, “Tensile Properties and Local Stiffness of Cells,” in *Mechanics of Biological Tissue*, R. W. O. (Editor Gerhard A. Holzapfel (Editor), Ed. New York: Springer, 2003, pp. 137-152.

[120] F. P. W. Melchels, D. W. Grijpma, and J. Feijen, “Properties of porous structures prepared by stereolithography using a polylactide resin,” *Journal of Controlled Release*, vol. 132, no. 3, p. e71-e73, Dec. 2008.

[121] K. T. Nguyen and J. L. West, “Photopolymerizable hydrogels for tissue engineering applications.,” *Biomaterials*, vol. 23, no. 22, pp. 4307-14, Nov. 2002.

[122] J.-W. Choi, R. Wicker, S.-H. Lee, K.-H. Choi, C.-S. Ha, and I. Chung, “Fabrication of 3D biocompatible/biodegradable micro-scaffolds using dynamic mask projection microstereolithography,” *Journal of Materials Processing Technology*, vol. 209, no. 15-16, pp. 5494-5503, Aug. 2009.

[123] N. Loboutin and E. Garcia, *Mechanics of Microelectromechanical System. Springer 2004. pg 360*. Springer, 2004, p. 360.

[124] B. Arnaud, J. Bastien, and R. Philippe, “Microfabrication of ceramic components by microstereolithography,” *Journal Microelectronics and Microengineering*, vol. 14, no. 2, p. 197, 2004.

[125] T. Takagi and N. Nakajima, “Photoforming applied to fine machining,” *[1993] Proceedings IEEE Micro Electro Mechanical Systems*, pp. 173-178, 1993.

[126] K. Ikuta and K. Hirowatari, “Real three dimensional micro fabrication using stereo lithography and metal molding,” *[1993] Proceedings IEEE Micro Electro Mechanical Systems*, pp. 42-47, 1993.

[127] A. Bertsch, S. Jiguet, P. Bernhard, and P. Renaud, “Microstereolithography: A Review,” in *Materials Research Society Symposium Proceedings*, vol. 758, A. Piqu, A. S. Holmes, and D. B. Dimos, Eds. 2003, pp. 3-15.

[128] I. B. Park, Y. M. Ha, and S. H. Lee, “Cross-section segmentation for improving the shape accuracy of microstructure array in projection microstereolithography,” *The International Journal of Advanced Manufacturing Technology*, vol. 46, no. 1-4, pp. 151-161, May. 2009.

[129] C. Sun, N. Fang, D. M. Wu, and X. Zhang, “Projection micro-stereolithography using digital micro-mirror dynamic mask,” *Sensors and Actuators A: Physical*, vol. 121, no. 1, pp. 113-120, May. 2005.

[130] A. Bertsch, S. Jiguet, and P. Renaud, “Microfabrication of ceramic components by microstereolithography,” *Journal of Micromechanics and Microengineering*, vol. 14, no. 2, pp. 197-203, Feb. 2004.

[131] L.-chia Chen, C.-nan Chen, and Y.-wei Chang, “Development of a new multi-wavelength confocal surface profilometer for in-situ automatic optical

inspection (AOI),” *Asian Symposium for Precision Engineering and Nanotechnology*, 2009.

[132] B. Baroli, “Photopolymerization of biomaterials: issues and potentialities in drug delivery, tissue engineering, and cell encapsulation applications,” *Journal of Chemical Technology & Biotechnology*, vol. 81, no. 4, pp. 491-499, Apr. 2006.

[133] K. S. Anseth, V. R. Shastri, and R. Langer, “Photopolymerizable degradable polyanhydrides with osteocompatibility.,” *Nature Biotechnology*, vol. 17, no. 2, pp. 156-9, Feb. 1999.

[134] K. S. Anseth, A. T. Metters, S. J. Bryant, P. J. Martens, J. H. Elisseeff, and C. N. Bowman, “In situ forming degradable networks and their application in tissue engineering and drug delivery.,” *Journal of Controlled Release : Official Journal of the Controlled Release Society*, vol. 78, no. 1-3, pp. 199-209, Jan. 2002.

[135] J. W. Lee, P. X. Lan, B. Kim, G. Lim, and D.-W. Cho, “3D scaffold fabrication with PPF/DEF using micro-stereolithography,” *Microelectronic Engineering*, vol. 84, no. 5-8, pp. 1702-1705, 2007.

[136] T. M. Seck, F. P. W. Melchels, J. Feijen, and D. W. Grijpma, “Designed biodegradable hydrogel structures prepared by stereolithography using poly(ethylene glycol)/poly(d,l-lactide)-based resins.,” *Journal of Controlled Release : Official Journal of the Controlled Release Society*, vol. 148, pp. 34-41, Jul. 2010.

[137] B. Karina, A., Brenda, K.M, and Ryan, “Stereolithography of three-dimensional bioactive poly(ethylene glycol) constructs with encapsulated cells.,” *Annals of biomedical Engineering*, vol. 34, no. 9, pp. 1429-1441, 2006.

[138] V. Chan, P. Zorlutuna, J. H. Jeong, H. Kong, and R. Bashir, “Three-dimensional photopatterning of hydrogels using stereolithography for long-term cell encapsulation.,” *Lab on a Chip*, vol. 197, no. 207890, Jul. 2010.

[139] T. Yamaoka, Y. Tabata, and Y. Ikada, “Distribution and tissue uptake of poly(ethylene glycol) with different molecular weights after intravenous administration to mice,” *Journal of Pharmaceutical Sciences*, vol. 83, no. 4, pp. 601-606, 1994.

[140] D. M. Cullinane and T. A. Einhorn, “Biomechanics of bone.,” in *Principles of Bone Biology.*, J. P. Bilezikian, L. Raisz, and G. Rodan, Eds. San Diego, USA: Academic Press, 2002, pp. 17-32.

[141] S. van Gaalen et al., “Tissue Engineering of Bone,” in *Tissue Engineering*, 1st ed., C. van Blitterswijk, Ed. Academic Press, 2008, pp. 559-610.

[142] “Mechanical properties of bone:http://www.feppd.org/ICB-Dent/campus/biomechanics_in_dentistry/ldv_data/mech/basic_bone.htm). [Date assessed 13-04-2011], 2010.” .

[143] “Renal failure and bone disease [Assessed on 24 April 2008].” [Online]. Available: http://www.kidneydialysis.org.uk/renal-failure-and-bone-disease.htm.

[144] X. E. Guo, *Mechanical Properties of Cortical Bone and Cancellous Bone Tissue. Bone Mechanics Handbook. Second Edition.* Informa Healthcare, 2001, pp. 10.1-10.23.

[145] “Bone remodelling [Assesed on 24 April 2009].” [Online]. Available: (http://depts.washington.edu/bonebio/bonAbout/histo/histo.html, http://www.medes.fr/home_fr/applications_sante/osteoporose/eristo/osteoporosis/Bone_Remodeling.html.

[146] S. C. Cowin, *Bone Mechanics Handbook, S. C. Cowin.*, 2nd ed. Boca Raton: CRC Press, 2001.

[147] B. van Rietbergen et al., “Assessment of cancellous bone mechanical properties from micro-FE models based on micro-CT, pQCT and MR images.,” *Technology and Health Care : Official Journal of the European Society for Engineering and Medicine*, vol. 6, no. 5-6, pp. 413-20, Dec. 1998.

[148] F. Linde and I. Hvid, “The Effect of Constraint on The Mechanical Behaviour of Trabecular Bone Specimens,” *Biomechanics*, vol. 22, no. 5, 1989.

[149] H. Yuan and K. De Groot, “Calcium PhosphateBiomaterials: An Overview,” in *Learning from Nature How to Design New Implantable Biomaterials: From Biomineralization Fundamentals to Biomimetic Materials and Processing Routes: ... II: Mathematics, Physics and Chemistry)*, First edit., S. Reis, Rui L; Weiner, Ed. Springer Netherlands, 2004, pp. 37-57.

[150] S. Ramakrishna, J. Mayer, E. Wintermantel, and K. W. Leong, “Biomedical applications of polymer-composite materials: a review,” *Composites Science and Technology*, vol. 61, no. 9, pp. 1189-1224, 2001.

[151] D. Mohamad Yunos, O. Bretcanu, and A. Boccaccini, “Polymer-bioceramic composites for tissue engineering scaffolds,” *Journal of Materials Science*, vol. 43, no. 13, pp. 4433-4442, 2008.

[152] S. Ramakrishna, J. Mayer, E. Wintermantel, and K. W. Leong, “Biomedical applications of polymer-composite materials: a review,” *Composites Science and Technology*, vol. 61, no. 9, pp. 1189-1224, 2001.

[153] S. M. Rabiee et al., “Mechanical behavior of a new biphasic calcium phosphate bone graft,” *Biotechnology and Bioprocess Engineering*, vol. 13, no. 2, pp. 204-209, May. 2008.

[154] L. Jeng and F. Livingston, “Bone Tissue Scaffold in PCL,” *Bone*, 2005. [Online]. Available: http://ebookbrowse.com/bone-tissue-scaffold-in-pcl-pdf-d89366776. [Accessed: 24-Mar-2010].

[155] M. I. Sabir, X. Xu, and L. Li, “A review on biodegradable polymeric materials for bone tissue engineering applications,” *Journal of Materials Science*, vol. 44, no. 21, pp. 5713-5724, Aug. 2009.

[156] E. Alsberg, K. W. Anderson, a Albeiruti, R. T. Franceschi, and D. J. Mooney, “Cell-interactive Alginate Hydrogels for Bone Tissue Engineering,” *Journal of Dental Research*, vol. 80, no. 11, pp. 2025-2029, Nov. 2001.

[157] J. W. Lee, K. S. Kang, S. H. Lee, J.-Y. Kim, B.-K. Lee, and D.-W. Cho, “Bone regeneration using a microstereolithography-produced customized poly(propylene fumarate)/diethyl fumarate photopolymer 3D scaffold incorporating BMP-2 loaded PLGA microspheres.,” *Biomaterials*, vol. 32, no. 3, pp. 744-52, Jan. 2011.

[158] H. R. R. Ramay and M. Zhang, “Biphasic calcium phosphate nanocomposite porous scaffolds for load-bearing bone tissue engineering,” *Biomaterials*, vol. 25, no. 21, pp. 5171-5180, 2004.

[159] A. Woesz, “Rapid Prototyping to Produce Porous Scaffolds With Controlled Architecture for Possible Use in Bone Tissue Engineering,” in *Virtual Prototyping and Biomanufacturing in Medical Applications*, 2008, pp. 171-206.

[160] Y.-J. Seol, J. Y. Kim, E. K. Park, S.-Y. Kim, and D.-W. Cho, “Fabrication of a hydroxyapatite scaffold for bone tissue regeneration using microstereolithography and molding technology,” *Microelectronic Engineering*, vol. 86, no. 4-6, pp. 1443-1446, Apr. 2009.

[161] Y. Khan, M. J. Yaszemski, A. G. Mikos, and C. T. Laurencin, “Tissue Engineering of Bone: Material and Matrix Considerations,” *The Journal of Bone and Joint Surgery (American)*, vol. 90, pp. 36-42, 2008.

[162] S. E. Lobo and T. Livingston Arinzeh, “Biphasic Calcium Phosphate Ceramics for Bone Regeneration and Tissue Engineering Applications,” *Materials*, vol. 3, no. 2, pp. 815-826, Jan. 2010.

[163] C. C. Ribeiro, C. C. Barrias, and M. a Barbosa, “Preparation and characterisation of calcium-phosphate porous microspheres with a uniform size for biomedical applications.,” *Journal of Materials Science. Materials in Medicine*, vol. 17, no. 5, pp. 455-63, May. 2006.

[164] A. Krisanapiboon, B. Buranapanitkit, and K. Oungbho, “Biocompatability of hydroxyapatite composite as a local drug delivery system.,” *Journal of Orthopaedic Surgery (Hong Kong)*, vol. 14, no. 3, pp. 315-8, Dec. 2006.

[165] H. J. Chung and T. G. Park, “Surface engineered and drug releasing pre-fabricated scaffolds for tissue engineering.,” *Advanced Drug Delivery Reviews*, vol. 59, no. 4-5, pp. 249-62, May. 2007.

[166] C. J. Whitters et al., “Dental materials: 1997 literature review.,” *Journal of Dentistry*, vol. 27, no. 6, pp. 401-35, Aug. 1999.

[167] S. S. Taksali, J. N. Grauer, and A. R. Vaccaroand, “Material considerations for invertebral disc replacement implants,” *Spine Journal*, vol. 4, p. 231S-238S, 2004.

[168] A. F. Schilling et al., “Resorbability of bone substitute biomaterials by human osteoclasts,” *Biotechnology*, vol. 25, pp. 3963-3972, 2004.

[169] J. R. Jones, “New trends in bioactive scaffolds : The importance of nanostructure,” *Journal of the European Ceramic Society*, vol. 29, pp. 1275-1281, 2009.

[170] P. Sepulveda, a H. Bressiani, J. C. Bressiani, L. Meseguer, and B. König, “In vivo evaluation of hydroxyapatite foams.,” *Journal of Biomedical Materials Research*, vol. 62, no. 4, pp. 587-92, Dec. 2002.

[171] S. S.-S. M. V.-R. S. Padilla, “Bioactive glass as precursor of designed-architecture scaffolds for tissue engineering,” *Journal of Biomedical Materials Research Part A*, vol. 81, no. 1, pp. 224-232, 2007.

[172] W. den Hollander, P. Patka, C. P. Klein, and G. a Heidendal, “Macroporous calcium phosphate ceramics for bone substitution: a tracer study on biodegradation with 45Ca tracer.,” *Biomaterials*, vol. 12, no. 6, pp. 569-73, Aug. 1991.

[173] S. J. Kalita, S. Bose, H. L. Hosick, and A. Bandyopadhyay, “Development of controlled porosity polymer-ceramic composite scaffolds via fused deposition modeling,” *Materials Science and Engineering: C*, vol. 23, no. 5, pp. 611-620, 2003.

[174] M. A. Abu Bakar and V. David, “Microstructural Changes of Porous Hydroxyapatite Using Acrylamide and Polyvinyl Alcohol Source: http://www.shvoong.com/exact-sciences/706571-microstructural-changes-porous-hydroxyapatite-using/#ixzz1NrByBrkl [Assessed on 23 April 2008].” .

[175] J. Zhou, X. Zhang, and Y. Chen, “High temperature characteristics of synthetic hydroxyapatite,” *Journal of Materials Science in Medicine*, vol. 4, pp. 83-85, 1993.

[176] L. Hench and R. Jones, *Biomaterials, Artificial Organs and Tissue Engineering*. Cambridge: Woodhead Publishing, 2005.

[177] H. Yoshikawa and A. Myoui, “Bone tissue engineering with porous hydroxyapatite ceramics.,” *Journal of Artificial Organs : The Official Journal*

of the Japanese Society for Artificial Organs, vol. 8, no. 3, pp. 131-6, Jan. 2005.

[178] A. Uchida, N. Araki, Y. Shinto, H. Yoshikawa, E. Kurikas, and K. Ono, "The Use of Calcium Hydroxyapatite Ceramic in Bone Tumour Surgery," *The Journal of Bone and Joint Surgery*, vol. 72, no. 2, pp. 298-302, 1990.

[179] A. Matsumine et al., "Calcium hydroxyapatite ceramic implants in bone tumour surgery," *The Journal of Bone and Joint Surgery*, vol. 86, no. 5, pp. 719-725, Jul. 2004.

[180] L. L. Hench, "Bioceramics: From Concept to Clinic," *Journal of American Ceramics Society*, vol. 74, no. 7, pp. 1487-1510, 1991.

[181] D. C. Tancred, B. a McCormack, and a J. Carr, "A synthetic bone implant macroscopically identical to cancellous bone.," *Biomaterials*, vol. 19, no. 24, pp. 2303-11, Dec. 1998.

[182] T. Kitsugi, T. Yamamuro, T. Nakamura, S. Kotani, T. Kokubo, and H. Takeuchi, "Four calcium phosphate ceramics as bone substitutes for non-weight-bearing.," *Biomaterials*, vol. 14, no. 3, pp. 216-24, Feb. 1993.

[183] A. R. El-Ghannam, "Advanced bioceramic composite for bone tissue engineering: design principles and structure-bioactivity relationship.," *Journal of Biomedical Materials Research. Part A*, vol. 69, no. 3, pp. 490-501, Jun. 2004.

[184] H. Yuan, Z. Yang, Y. Li, X. Zhang, J. D. De Bruijn, and K. De Groot, "Osteoinduction by calcium phosphate biomaterials.," *Journal of Materials Science. Materials in Medicine*, vol. 9, no. 12, pp. 723-6, Dec. 1998.

[185] F.-huei Lin, C.-chang Lin, C.-ming Lu, H.-chang Liu, J.-sheng Sun, and C.-yi Wang, "Mechanical properties and histological evaluation of sintered Ca2P207 with 1 OH , addition," *Biomaterials*, vol. 16, no. 10, pp. 793-802, 1995.

[186] P. Ducheyne, "Bioceramics: material characteristics versus in vivo behavior," *Journal Biomedical Materials Research.*, vol. 21, no. 2, pp. 219-236, 1987.

[187] H. Perkins and P. G. Walker, "The occurence of pyrophosphate in bone," *Surgery*, vol. 40, no. 2, pp. 333-339, 1958.

[188] T. V. Safronova, V. I. Putlyaev, M. a Shekhirev, and a V. Kuznetsov, "Composite ceramic containing a bioresorbable phase," *Glass and Ceramics*, vol. 64, no. 3-4, pp. 102-106, Mar. 2007.

[189] J. S. Sun, Y. H. Tsuang, C. J. Liao, H. C. Liu, Y. S. Hang, and F. H. Lin, "The effect of sintered beta-dicalcium pyrophosphate particle size on newborn Wistar rat osteoblasts.," *Artificial Organs*, vol. 23, no. 4, pp. 331-8, Apr. 1999.

[190] A. C. Tas and S. B. Bhaduri, "Chemical Processing of CaHPO4.2H2O:Its Conversion to Hydroxyapatite," *Journal of American Ceramic Society*, vol. 87, no. 12, pp. 2195-2200, 2004.

[191] L. C. Chow, "Solubility of calcium phosphates.," *Monographs in Oral Science*, vol. 18, pp. 94-111, Jan. 2001.

[192] G. and Heness and B. Ben-Nissan, "G. Heness and B. Ben-Nissan. Source: Abstracted from 'Innovative Bioceramics' in Materials Forum, Vol. 27, 2004.Innovative Bioceramics. http://nariratih.wordpress.com/2007/11/05/calcium-phosphate-and-hydroxyapatite-coatings/.[Accessed on 08/07/2009].," *Materials Forum*, vol. 27, 2004.

[193] F.-H. Lin, J.-R. Liaw, M.-H. Hon, and C.-Y. Wang, "The effects of Na4P2O7 · 10H2O addition on the mechanical properties of sintered Ca2P2O7 bioceramic," *Materials Chemistry and Physics*, vol. 41, no. 2, pp. 110-116, Jul. 1995.

[194] J. S. Sun, Y. C. Huang, Y. H. Tsuang, L. T. Chen, and F. H. and Lin, "Sintered dicalcium pyrophosphate increases bone mass in ovariectomized rats.," *Journal of Biomedical Materials Research*, vol. 59, pp. 246-253, 2002.

[195] D. W. Hutmacher, "Scaffolds in tissue engineering bone and cartilage.," *Biomaterials*, vol. 21, no. 24, pp. 2529-43, Dec. 2000.

[196] C. Muzzarelli and R. a a Muzzarelli, "Natural and artificial chitosan-inorganic composites.," *Journal of Inorganic Biochemistry*, vol. 92, no. 2, pp. 89-94, Nov. 2002.

[197] A. C. Lawson and J. T. Czernuszka, "Collagen–calcium phosphate composites.," *Proc. Inst. Mech. Eng., H J. Eng. Med.*, vol. 212, no. 6, pp. 413-425, 1998.

[198] K. Miyazaki, T. Horibe, J. M. Antonucci, S. Takagi, and L. C. Chow, "Polymeric calcium phosphate cements: analysis of reaction products and properties.," *Dental Materials : Official Publication of The Academy of Dental Materials*, vol. 9, no. 1, pp. 41-5, Jan. 1993.

[199] S.-hoon Rhee and J. Tanaka, "Synthesis of a Hydroxyapatite / Collagen / Chondroitin Sulfate Nanocomposite by a Novel Precipitation Method," *Journal of American Ceramic Society*, vol. 84, no. 2, pp. 459-461, 2001.

[200] A. M. E. Kady, K. R. Mohamed, and G. T. El-bassyouni, "Fabrication , characterization and bioactivity evaluation of calcium pyrophosphate / polymeric biocomposites," *Ceramics International*, vol. 35, pp. 2933-2942, 2009.

[201] C. Sun and X. Zhang, "Experimental and numerical investigations on microstereolithography of ceramics," *Journal of Applied Physics*, vol. 92, no. 8, p. 4796, 2002.

[202] M. L. Griffith and J. W. Halloran, "Freeform fabrication of ceramics via stereolithography," *Journal of American Ceramic Society.*, vol. 79, no. 10, pp. 2601-2608, 1996.

[203] C. Sun and X. Zhang, "The influences of the material properties on ceramic micro-stereolithography," *Sensors and Actuators A: Physical*, vol. 101, no. 3, pp. 364-370, Oct. 2002.

[204] C. Sun, "The influences of the material properties on ceramic micro-stereolithography," *Sensors and Actuators A: Physical*, vol. 101, no. 3, pp. 364-370, Oct. 2002.

[205] Q. B. Wang, Q. G. Wang, and C. X. Wan, "Effect of sintering time on the microstructure and properties of inorganic polyphosphate bioceramics," *Science of Sintering*, vol. 42, no. 3, pp. 337-343, 2010.

[206] Q. Wang, Q. Wang, X. Zhang, X. Yu, and C. Wan, "The Effect Of Sintering Temperature on The Structure and Degradability of Strontium-Doped Calcium Polyphosphate Bioceramic," *Ceramics-Silikaty*, vol. 54, no. 2, pp. 97-102, 2010.

[207] A. O. McIntosh and W. L. Jablonski, "X-Ray Diffraction Powder Patterns of Calcium Phosphates," *Analytical Chemistry*, vol. 28, no. 9, pp. 1424-1427, Sep. 1956.

[208] L. Guo, H. Li, and X. Gao, "Phase transformations and structure characterization of calcium polyphosphate during sintering process," *Journal of Materials Science*, vol. 39, no. 23, pp. 7041-7047, Dec. 2004.

[209] L. E. Jackson, B. M. Kariuki, M. E. Smith, J. E. Barralet, and A. J. Wright, "Synthesis and Structure of a Calcium Polyphosphate with a Unique Criss-Cross Arrangement of Helical Phosphate Chains," *Chemistry of Materials*, vol. 17, no. 18, pp. 4642-4646, Sep. 2005.

[210] T. Chartier, "UV Curable Systems for Tape Casting," *Journal of the European Ceramic Society*, vol. 19, no. 1, pp. 67-74, Jan. 1999.

[211] H. Y. Yang et al., "Sintering behaviour of calcium phosphate filaments for use as hard tissue scaffolds," *Journal of the European Ceramic Society*, vol. 28, no. 1, pp. 159-167, 2008.

[212] M. S. Hahn, L. J. Taite, J. J. Moon, M. C. Rowland, K. a Ruffino, and J. L. West, "Photolithographic patterning of polyethylene glycol hydrogels.," *Biomaterials*, vol. 27, no. 12, pp. 2519-24, Apr. 2006.

[213] C. J. Soares, P. V. Soares, P. C. F. Santos-Filho, and S. R. Armstrong, "Microtensile Specimen Attachment and Shape--Finite Element Analysis," *Journal of Dental Research*, vol. 87, no. 1, pp. 89-93, Jan. 2008.

[214] "PERFACTORY Rapid Manufacturing System Rapid Prototyping System Buyers ´ Guide. envisionTEC Germany - V.2008-04-18. [http://www.envisiontec.de/fileadmin/pdf/BuyersGuide_en.pdf. Accessed on 23 April 2009]."

[215] EnvisionTEC, "Material safety data sheet: Photopolymers R4, R5 and R11 for Perfactory® (according to directive 91/155/EWG). [Accessed at http://www.envisiontec.de/fileadmin/pdf/MatSheet_R05R11_en.pdf]."

[216] "Technical Data for envisionTEC R 05 / R 11." .

[217] *Technical Data ® of envisionTEC R05/R11. [Accessed on 25 april 2009 at http://www.envisiontec.de/fileadmin/pdf/MatSheet_R05R11_en.pdf]*. pp. 48220-48220.

[218] "Technical Data for Desktop Digital Shell Printer (DDSP). [Accessed on 25 April 2009 at http://www.envisiontec.de/fileadmin/pdf/MachineDatasheet_DDSP.pdf)," *System*, no. March, pp. 48220-48220, 2009.

[219] U. S. B. Connection and N. White, "ENFIS UNO Air Cooled Light Engine Technical Specification. [Accessed on 8 May 2009 at http://www.enfis.com/files/Uno%20Air%20Cooled%20Light%20Engine%20General.pdf]." .

[220] M. Schuster, R. Inführ, C. Turecek, J. Stampfl, F. Varga, and R. Liska, "Photopolymers for Rapid Prototyping of Soluble Mold Materials and Molding of Cellular Biomaterials," *Monatshefte für Chemie - Chemical Monthly*, vol. 137, no. 7, pp. 843-853, Jun. 2006.

[221] M. Schuster, C. Turecek, F. Varga, H. Lichtenegger, J. Stampfl, and R. Liska, "3D-shaping of biodegradable photopolymers for hard tissue replacement," *Applied Surface Science*, vol. 254, no. 4, pp. 1131-1134, Dec. 2007.

[222] K. Pal, a K. Banthia, and D. K. Majumdar, "Polymeric Hydrogels: Characterization and Biomedical Applications," *Designed Monomers & Polymers*, vol. 12, no. 3, pp. 197-220, May. 2009.

[223] "Applications : Free Radical Initiators Applications : Applications : Free Radical Initiators [http://www.sigmaaldrich.com/etc/medialib/docs/Aldrich/General_Information/photoinitiators.Par.0001.File.tmp/photoinitiators.pdf. Accessed on 27/09/10].," *Spectroscopy*, no. 1. pp. 5-19.

[224] H. Park et al., “Effect of swelling ratio of injectable hydrogel composites on chondrogenic differentiation of encapsulated rabbit marrow mesenchymal stem cells in vitro.,” *Biomacromolecules*, vol. 10, no. 3, pp. 541-6, Mar. 2009.

[225] A. Borzacchiello and L. Ambrosio, “Structure-Property Relationship in Hydrogel,” in *Hydrogels: Biological Properties and Applications*, R. Barbucci, Ed. Springer, 2009, p. 17.

[226] F. Poirier and S. Kimber, “Cell surface carbohydrates and lectins in early development,” *Molecular Human Reproduction*, vol. 3, no. 10, pp. 907-918, Oct. 1997.

[227] A. A. Mateescu and M. VAMVAKAKI, “Glycosurfaces,” in *Glycosurfaces,” In Engineered Carbohydrate-Based Materials For Biomedical Applications. Polymers, Surfaces, Dendrimers, Nanoparticles, and Hydrogel*, R. Narain, Ed. John Wiley & Sons, Inc., Publication, 2011, pp. 308-329.

[228] S. Pearson, G. Chen, and M. H. Stenzel, “SYNTHESIS OF GLYCOPOLYMERS,” in *Synthesis Of Glycopolymers,” In Engineered Carbohydrate-Based Materials For Biomedical Applications Polymers, Surfaces, Dendrimers, Nanoparticles, and Hydrogels*, R. Narain, Ed. John Wiley & Sons, Inc., Publication, 2011, pp. 2-104.

[229] C. F. Goochee, \ Gramer, M.J., and D. C. Andersen, “The oligosaccharides of glycoproteins: bioprocess factors affecting oligosaccharide structure and their effect on glycoprotein properties.,” in *Biotechnology*, New Yorks, 1991, pp. 1347-1355.

[230] T. Ouchi, S. Jokei, and H. Chikashita, “Synthesis of 1,2:5,6-Di-O-isopropylidene-3-O-[3-(uracil-1-yl)propionoyl]-α-D-glucofuranose and 1,2-Mono-O-isopropylidene-6-O-[3-(uracil-1-yl)propionoyl]-α-D-glucofuranose.,” *Journal of Heterocyclic Chemistry*, vol. 19, no. 4, pp. 935-936, 1982.

[231] P. J. Bártolo, H. A. Almeida, R. A. Rezende, T. Laoui, and B. Bidanda, “Advanced Processes to Fabricate Scaffolds for Tissue Engineering,” in *Virtual Prototyping and Biomanufacturing in Medical Applications*, 2008, pp. 149-170.

[232] A. Bolarinwa, U. Gbureck, P. Purnell, M. Bold, and M. Grover, L., “Cement casting of calcium pyrophosphate based bioceramics,” *Advances in Applied Ceramics*, vol. 109, no. 5, pp. 291-295, 2009.

[233] “Technical Brief 101: Calculation of Viscometer Constants for Cannon-Fenske and Cannon-Fenske Opaque Viscometers. Technical Brief from Cannon Instrument Company. http://ww.cannoninstrument.com/TechBrief101.pdf. [Accessed on 16 Jan 2011].” .

[234] *Instructions for the use of The Cannon-Fenske Routine Viscometer. http://www.cannoninstrument.com/P10-0100%20CFR%20instructions.pdf. [Accessed on 16 Jan 2011].* .

[235] A. Ayral, J. Phalippou, and T. Woignier, "Skeletal density of silica aerogels determined by helium pycnometry," *Journal of Materials Science*, vol. 27, pp. 1166-1170, Jun. 1992.

[236] R. Asthana, A. Kumar, A., and N. Dahotre, "Powder Metallurgy and Ceramic Forming," in *Materials Processing and Manufacturing Science*, Butterworth-Heinemann, 2006, pp. 167-245.

[237] D. Parsch, T. Breitwieser, and S. J. Breusch, "Mechanical stability of structured bone grafts from the anterior iliac crest.," *Clinical Biomechanics (Bristol, Avon)*, vol. 23, no. 7, pp. 955-60, Aug. 2008.

[238] S. Pollington and R. van Noort, "An Update of Ceramics in Dentistry," *International Journal of Clinical Dentistry*, vol. 2, no. 4, 2011.

[239] T. Kokubo and H. Takadama, "How useful is SBF in predicting in vivo bone bioactivity?," *Biomaterials*, vol. 27, no. 15, pp. 2907-15, May. 2006.

[240] "ASTM E112-10: Standard Test Methods for Determining Average Grain Size [Accessesed at www.mse.iastate.edu on 01/10/2010].," .

[241] U. Gbureck, T. Hölzel, I. Biermann, J. E. Barralet, and L. M. Grover, "Preparation of tricalcium phosphate/calcium pyrophosphate structures via rapid prototyping.," *Journal of Materials Science. Materials in Medicine*, vol. 19, no. 4, pp. 1559-63, Apr. 2008.

[242] R. J. Brooks, "Treatise on Materials Science and Technology.," in *Ceramic Fabrication Processes. Vol 9*, F. F. Y. Wang, Ed. Academic Press, New York, 1976, p. 331.

[243] R. Luo, J. AU - Stevens, "The role of residual stress on the mechanical properties of Al2O3-5 vol% SiC nano-composites No Title," *Journal of the European Ceramic Society*, vol. 17, no. 13, p. 1565, 1997.

[244] Z. Zhi-hua et al., "Bioactivity of bioresorbable composite based on bioactive glass and," *Science*, no. 50174059, 2006.

[245] A. Bignon, J. Chevalier, and G. Fantozzi, "Effect of ball milling on the processing of bone substitutes with calcium phosphate powders.," *Journal of Biomedical Materials Research*, vol. 63, no. 5, pp. 619-26, Jan. 2002.

[246] D. K. Pattanayak, R. Dash, R. C. Prasad, B. T. Rao, and T. R. R. Mohan, "Synthesis and sintered properties evaluation of calcium phosphate ceramics," *Materials Science and Engineering: C*, vol. 27, no. 4, pp. 684-690, 2007.

[247] B. Leukers et al., "Hydroxyapatite scaffolds for bone tissue engineering made by 3D printing.," *Journal of Materials Science. Materials in Medicine*, vol. 16, no. 12, pp. 1121-4, Dec. 2005.

[248] C.-kai Chua, “Review The Design of Scaffolds for Use in Tissue Engineering. Part II. Rapid Prototyping Techniques,” *Tissue Engineering*, vol. 8, no. 1, pp. 1-11, 2002.

[249] J. L. Ifkovits and J. a Burdick, “Review: photopolymerizable and degradable biomaterials for tissue engineering applications.,” *Tissue Engineering*, vol. 13, no. 10, pp. 2369-85, Oct. 2007.